

Radiological strength assessment of the proximal femur


Rick R. van Rijn

ISBN 90-9011913-2

Vormgeving: R.J. van Rijn

Omslagontwerp: R.R. van Rijn

Illustraties: T. Rijsdijk en A.W. Zwamborn

Druk:  Ridderprint B.V. Ridderkerk

© 1998, R.R. van Rijn

All rights reserved. No part of this dissertation may be reproduced, stored in a retrieval system or transmitted in any other form or by any means, electronic, mechanical, photocopying, recording, or otherwise, without the prior written permission of the holder of the copyright.

Radiological strength assessment of the proximal femur

Radiologische sterkte bepaling van het proximale femur

Proefschrift

Ter verkrijging van de graad van doctor
aan de Erasmus Universiteit Rotterdam
op gezag van de Rector Magnificus
Prof. dr P.W.C. Akkermans M.A.
en volgens het besluit van het College voor Promoties

De openbare verdediging zal plaatsvinden op
woensdag 7 oktober 1998 om 13.45 uur

door
Rick Robert van Rijn
geboren te Leiden

Promotiecommissie

Promotores	Prof. dr H.E. Schütte Prof. dr ir C.J. Snijders
Co-promotor	Dr C. van Kuijk
Overige leden	Prof. dr J.C. Birkenhäger Prof. dr E.K.J. Pauwels Prof. dr J.A.N. Verhaar

Aan Melanie
 Mijn ouders

Science is rooted in creative interpretation. Numbers suggest, constrain, and refute; they do not, by themselves, specify the content of scientific theories. Theories are built upon the interpretation of numbers, and interpreters are often trapped by their own rhetoric. They believe in their own objectivity, and fail to discern the prejudice that leads them to the one interpretation among many consistent with their numbers.

S.J. Gould, The mismeasure of man

Contents

1	General introduction	
1.1	Introduction	9
1.2	Anatomy of bone	11
1.3	Anatomy of the hip joint	13
1.4	Aim of the study	15
1.5	Outline of the study	15
1.6	References	17

Radiological analysis

2	Classification of hip fractures	
2.1	The need for classification	23
2.2	Classification of hip fractures: a review	23
2.3	Discussion	27
	Appendix 2A: Fractures illustrated	28
2.4	References	34
3	Measurement of femoral geometry: Conventional versus direct magnification radiography	
3.1	Introduction	37
3.2	Materials and methods	40
3.3	Results	42
3.4	Discussion	44
3.5	References	45
4	Dual-energy X-ray absorptiometry	
4.1	Introduction	49
4.2	Materials and methods	52
4.3	Results	53
4.4	Discussion	53
	Appendix 4A: Mathematical considerations concerning DXA	55
4.5	References	57
5	Volumetric quantitative computed tomography	
5.1	Introduction	61
5.2	Materials and methods	63
5.3	Results	65
5.4	Discussion	66
5.5	References	69

Biomechanical analysis

6	Biomechanics of the hip	
6.1	Introduction	71
6.2	Basic biomechanical terms	71
6.3	Biomechanics of the hip during one-legged stance	75
6.4	Biomechanics of the hip during a fall	78
	Appendix 6A: Quantities and units	81
	Appendix 6B: Moment of inertia	81
6.5	References	84
7	Generating hip fractures in vitro	
7.1	Introduction	85
7.2	Theory	87
7.3	Design of the device	88
7.4	Discussion	91
7.5	References	92
8	Dynamic loading of the proximal femur	
8.1	Introduction	95
8.2	Materials and methods	95
8.3	Results	97
8.4	Discussion	102
	Appendix 8A: Calculated sensitivity and specificity for radiographic and densitometric parameters	104
8.5	References	105
9	Semi-static loading of the proximal femur	
9.1	Introduction	107
9.2	Materials and methods	108
9.3	Results	110
9.4	Discussion	116
9.5	References	118
10	General discussion	
10.1	Introduction	121
10.2	Study design	122
10.3	Main results	123
10.4	Discussion of main results	124
10.5	Suggestions for future research	127
10.6	References	128
	Summary	133
	Samenvatting (Summary in Dutch)	135
	Publications and presentations	137
	Dankwoord	139

Chapter 1

General introduction

The society which scorns excellence in plumbing because plumbing is a humble activity and allows shoddiness in philosophy because it is an exalted activity, will have neither good plumbing nor good philosophy. Neither its pipes nor its theories will hold water

J.W.Gardner

1.1 Introduction

To Ambroise Paré (1510-1590), the famous French surgeon, credit is given for first recognizing a fracture of the femoral neck ^{1,2}. A second step into understanding the pathology of the broken hip was taken by Sir Astley Paston Cooper (1768-1841), as he was the first to underline the importance of the vascularization of the femoral head, describing what is now known as avascular necrosis ³.

Until the 1930's, methods of treatment for hip fractures were mainly conservative. This changed when Smith-Peterson of Boston developed a special nail that could be inserted surgically, thus keeping fracture fragments together ⁴. Surgical results improved mainly by the brilliant work of John Charnley (1911-1982) in England ⁵. His work was followed by the development of numerous devices up to the point where the total joint, including the socket, could be replaced ^{1,6-14}.

The earliest reported case of an osteoporotic hip fracture, is that of a XIIth dynasty (1990 BC) Egyptian female ¹⁵. Using the Hamann-Todd collection, a collection of 936 skeletons collected between 1910 and 1940, it was possible to calculate the annual hip fracture incidence per 100.000 subjects ¹⁶. The fracture incidence (583 hip fractures per 100.000) of Caucasian female skeletons showed remarkable similarities with an equivalent modern day population (531 hip fractures per 100.000) as reported by Farmer et al. ¹⁷. This dissertation focusses on those fractures which are located at the proximal femur. In every day practice these fractures are called 'hip fractures'. Therefore this nomenclature will be used in this dissertation. The risk of hip fracture is related to gender; females being more susceptible to hip fractures than man, race, Caucasians being more susceptible than Negroids

but less than Asians, and age as bone mineral density (BMD), a predictor for hip fracture, decreases steadily with ageing¹⁸⁻³³. In 1994, osteoporosis was defined by the World Health Organization (WHO) as 'a disease characterised by low bone mass and micro-architectural deterioration of bone tissue, leading to enhanced bone fragility and a consequent increase in fracture risk'³⁴. In combination with an increased risk in elderly people for falling, the risk for a hip fracture increases with age^{29,35,36}. Research has shown that a Caucasian female, 50 years of age, has a lifetime risk of sustaining a hip fracture of about 17% and that over 90% of all hip fractures occur in Caucasian women aged 70 years and over^{26,29,37-46}. In 1990 there were an estimated 1.66 million osteoporosis related hip fractures worldwide, over 50% of these occurring in Western Europe and North America²⁹. With the increasing number of elderly in Asia, Latin America and the Middle East, 70% of the expected 6.26 million hip fractures in the year 2050 are estimated to occur in those regions²⁹.

Although, the therapy of the broken hip has improved dramatically in recent years it still carries a high degree of morbidity and mortality in an elderly population. Research has shown the mortality to be around 25 - 27% and the morbidity to be about 30%, the latter being higher in northern regions of the western hemisphere^{20,34,44,47-53}. The major concomitant causes of death in patients with hip fractures are bronchopneumonia (46%), cardiac failure/myocardial infarction (23%) and pulmonary embolism (14%)⁵⁴. Eiskjær et al. calculated that the expected potential loss of life years amounted to 9.2 years, a low estimate, since only 5-20% of all deaths after hip fracture are classified as caused by hip fractures⁵⁵.

Osteoporosis related hip fractures are a severe economic burden to society⁵⁶⁻⁵⁹. Melton III estimated the cost of osteoporotic hip fractures at \$8 billion per year in the early 90's in the United States²⁹. In 1993 the total cost for hip fractures in the Netherlands amounted to 362 million Dutch guilders⁶⁰. Randell et al. reported the total cost for each hip fracture to be approximately 16,000 Australian dollars⁶¹. These costs arise, among others, from hospitalisation and the increased dependency of the elderly after hip fracture^{21,53,62}.

Radiology plays an important role in the early detection of osteoporosis^{39,63-67}. However, a radiologist will detect osteoporosis only if the loss in BMD is at least 30%^{68,69}. Therefore, in the last decades, special techniques for early detection of osteoporosis have been developed. The most important of these techniques are: radiogrammetry, quantitative radiography, dual-energy X-ray absorptiometry (see chapter 4), quantitative computed tomography (see chapter 5) and quantitative ultrasound⁷⁰⁻⁸⁸.

Although considerable time and effort has been devoted to studies aimed at detection, prevention and treatment of hip fractures, relatively little is known about the biomechanical aspects of hip fractures. Many studies assume that a

fall from standing height is a minor trauma compared to high velocity traumas such as motoring accidents and falls from great heights⁸⁹. Until now, only a few studies correlate the kinetic energy available during a fall with the relevant radiological parameters and the type, i.e. localization and appearance of the fracture.

1.2 Anatomy of bone

This paragraph gives a brief description of the function and anatomy of bone. For further details the reader is referred to Kaplan's 'Osteoporosis' and Junqueira's 'Basic histology'^{90,91}.

Bone does not only provide strength and rigidity to the skeleton but it also functions as a major reservoir of amongst others, calcium and phosphor. It is a highly vascularized and mineralized connective tissue composed of organic (30%), e.g. collagen and mucopolysacharids, and inorganic components (70%), e.g. hydroxyapatite⁹⁰.

Mature bone can be classified into two groups, viz. cortical or compact and trabecular or cancellous bone (figure 1.1)^{91,92}. Cortical bone, about 80% of the total amount of bone, is found on the periphery of bones surrounding trabecular bone and marrow. It is capable of withstanding considerable amounts of bending moment and torque. Cortical bone is composed of Haversian systems, cylindrical units, running parallel to the outer surface of the bone. The centre of each Haversian system contains a neurovascular bundle. This bundle is surrounded by concentric layers of bony tissue. The Haversian systems are interconnected by means of the Volkmann canals or canaliculi. Trabecular bone, a sponge-like structure, is located in the centre of bones, especially in the vertebrae, pelvis, flat bones and at the ends of long bones. Trabecular bone compared to cortical bone has a high surface area to volume ratio and is metabolically more active.

Three important types of bone cells can be distinguished: osteoblasts, osteoclasts and osteocytes⁹¹. Osteoblasts, are found at the site

Figure 1.1 - Schematic representation of the anatomy of bone

1. Cortical bone
2. Trabecular bone
3. Outer circumferential lamellae
4. Inner circumferential lamellae
5. Haversian canal
6. Interstitial lamellae
7. Volkman's canal
8. Trabeculae

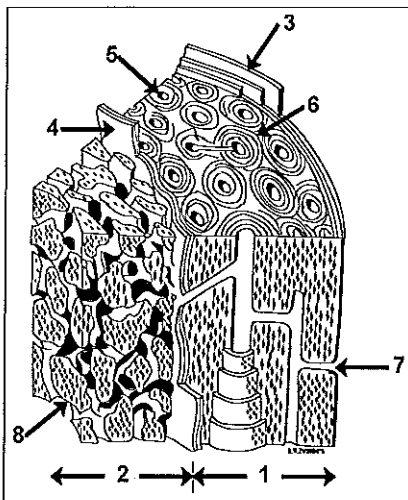
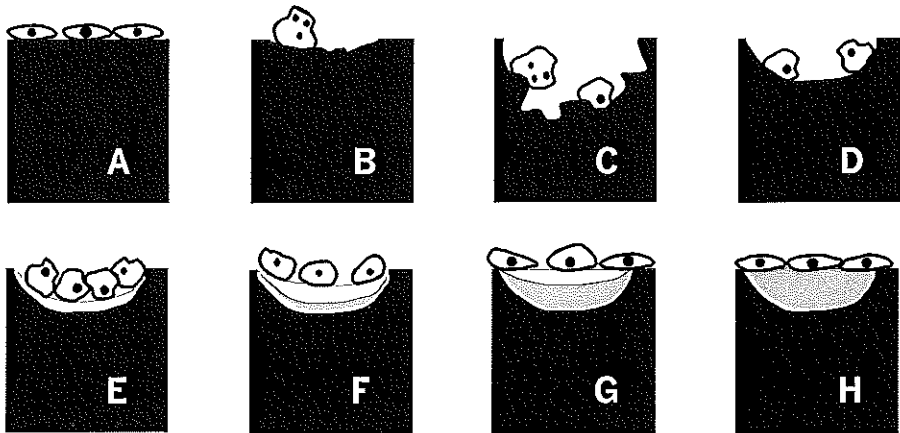


Figure 1.2 - Schematic representation of bone remodelling

- | | | | |
|----|---|----|--|
| A. | Quiescent bone surface. | E. | Differentiation of osteoblasts within the resorption cavity. |
| B. | Activation of bone resorption by the attraction of osteoclasts. | F. | Onset of matrix synthesis. |
| C. | Creation of a resorption cavity. | G. | Completion of matrix synthesis. |
| D. | Smoothing of the cavity. | H. | Completion of bone remodelling. |



of bone remodelling and/or bone formation. They are capable of secreting type-I-collagen, glycoproteins, and minor amounts of proteoglycans thus forming bone. Just underneath this layer of cells new, non-calcified, bone 'osteoid' can be observed. Osteoclasts are responsible for the resorption of bone and cartilage. They can be found in shallow excavations, known as Howship's lacunae, where bone resorption occurs. Finally, osteocytes are cells derived from osteoblasts, 'they result from osteoblasts "self-entombing" themselves by their own bone matrix secreting activity' (Stevenson, J., An atlas of osteoporosis) ⁹².

Remodelling of bone consists of six stages (figure 1.2) ⁹³. The first visible stage is the attraction of osteoclasts to the bone surface, this stage is called activation. This phase is followed by the resorption phase, during this phase the osteoclasts excavate an erosion of approximately 40-60 μ m in about 4-12 days. Thereafter, the multi-nucleated osteoclasts are replaced by mononuclear cells which are capable of smoothing the cavity. In the next 7-10 days a layer of cement, rich in proteoglycans, glycoproteins and acid phosphatase, is deposited. This phase, the time interval between osteoclastic and osteoblastic activity, is known as reversal. The next step is called the coupling phase, in which osteoblasts are attracted to the eroded surface. The osteoblasts form a sheet of cells within the resorption cavity and synthesize layers of osteoid matrix containing non-mineralized bone matrix. This phase

is known as formation. After a few days the newly deposited matrix undergoes mineralization. When this phase is completed the osteoblast become inactive completing the remodelling sequence. This sequence of activation, resorption, reversal, coupling, formation and mineralization occurs, at any one time, only at approximately 10% of the bone surface.

1.3 Anatomy of the hip joint

In this paragraph, a brief description of the skeletal anatomy of the hip is given^{94,95}. The hip joint is a typical example of a ball-and-socket joint, the acetabulum forming the socket and the caput femoris the ball (figure 1.3a and 1.3b)⁹⁶. This type of joint combines stability, in all normal positions, with a good range of movement.

Figure 1.3a, 1.3b - Plastinated slice of the pelvic region (a) and corresponding drawing (b).
Explanation of the numbers in figure 1.3b.

- | | | |
|------------------------|------------------------------------|------------------------------|
| 1. Vertebra lumbalis V | 10. Trochanter major | 19. M. obturatorius internus |
| 2. Vertebra sacralis I | 11. Trochanter minor | 20. M. rectus femoris |
| 3. Os ilium | 12. Corpus femoris | 21. M. obturatorius externus |
| 4. Acetabular lip | 13. Discus intervertebralis | 22. M. adductor longus |
| 5. Crista iliaca | 14. M. psoas major | 23. Zona orbicularis |
| 6. Fossa acetabuli | 15. M. iliacus | 24. Uterus |
| 7. Os ischium | 16. M. obliquus internus abdominis | 25. A. iliaca communis |
| 8. Caput femoris | 17. M. gluteus minimus | 26. A. iliaca interna |
| 9. Collum femoris | 18. M. gluteus medius | 27. Skin |

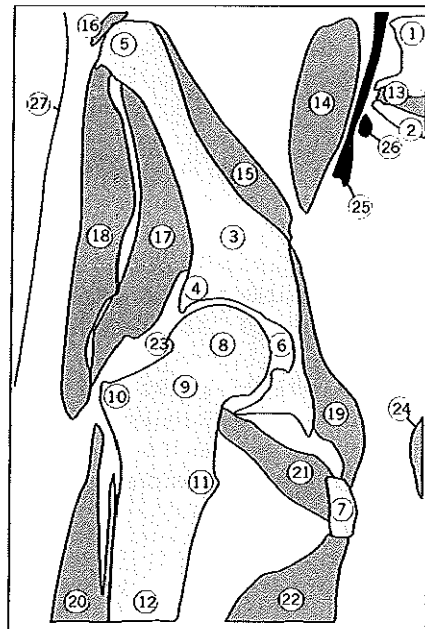
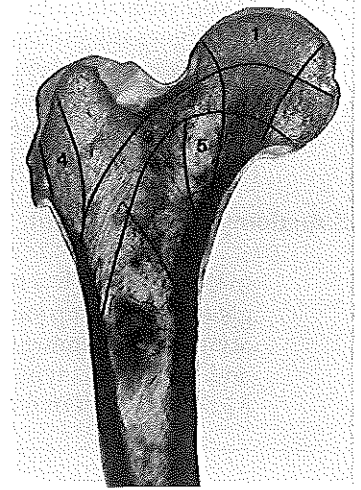


Figure 1.4 - Internal architecture of the proximal femur

1. Principal compressive group
2. Secondary compressive group
3. Principal tensile group
4. Trochanter major group
5. Ward's triangle



The acetabulum, named after a Roman vinegar (acetic acid) cup, is formed by the Os ilium, Os ischium and Os pubis. It is positioned on the anterior-inferior lateral side of the pelvis.

The inner aspect of the acetabulum is partially covered by a horse-shoe shaped hyaline cartilage articular surface, the facies lunata. The non-articular area is known as fossa acetabulum. Due to this construction, the femoral head only makes contact with a relatively small area of the acetabulum. The acetabulum protrudes slightly from the pelvis, forming a rim. The aperture, on the anterior inferior side of this rim, is called the acetabular notch. The femur is the longest bone in the human body, varying from one-fourth to one-third of the total body length. It can be divided into three parts; the proximal femur, the femoral shaft and the distal femur.

The proximal femur consists of the head, the neck and two trochanters. The head is covered with hyaline cartilage and forms a halve sphere. In the centre of the head lies the fovea, to which the ligamentum capitis femoris is attached. Embedded in this ligament runs the obturator artery which provides the blood supply for a part of the femoral head.

Looking at the proximal femur it is noted that the neck of the femur deviates anteriorly from the coronal plane. This is called anteversion (about 15° in the adult but it can be larger in childhood). Furthermore, the axes of the neck and of the shaft form an angle of inclination, of about 125° . When this angle is diminished ($<125^\circ$) one speaks of 'coxa vara', if on the other hand the angle is increased ($>125^\circ$) one speaks of 'coxa valga' ^{1,94,95,97-99}.

The internal architecture of the proximal femur is characterized by a distinct trabecular pattern (figure 1.4). This pattern consists of columnar groups of trabecular bone. It is commonly accepted that these columns act like struts and give the proximal femur its strength ¹⁰⁰⁻¹⁰².

1.4 Aim of the study

In light of the rapidly increasing global problem of osteoporotic fractures, as mentioned in paragraph 1.1, the selection of persons at high risk for hip fracture is becoming more and more important. Early detection of increased fracture risk enables the medical society to intervene at an early stage, either by medical intervention or by defining a set of rules to live by in order to reduce the risk of falling. In 1994 a WHO study group stated that 'The risk of fracture worldwide may be only partly explained by differences in bone density between communities. Data describing the relationship between fracture risk in specific sites and the distribution of BMD are required to clarify this' ³⁴.

One may postulate that in order to predict a hip fracture the basic mechanics of fracture must at least be understood. In order to gain more knowledge of the mechanics of fracture and the relation with radiological parameters a cadaver based study is undertaken. The aim of this study is to find the answers to the following questions:

1. What are the mechanics of a hip fracture ?
2. Can we design a model that simulates falls leading to fractures of the hip ?
3. Can we assess the strength of the proximal femur with radiographic and densitometric procedures ?

1.5 Outline of the study

After the introduction, this dissertation is divided into two main sections: a radiological and a biomechanical section. The radiological section consists of four chapters:

- In chapter two we discuss the diagnosis and classification of proximal femur fractures.
- Chapter three describes conventional and direct magnification (DIMA) radiography and the measurements obtained with these techniques.
- Chapter four describes dual-energy X-ray absorptiometry (DXA) and all subsequent measurements made with this technique.
- Chapter five discusses the basics of quantitative computed tomography (QCT) and the measurements resulting from this technique.

The biomechanical section consists of four chapters:

- Chapter six discusses the basic biomechanical terms and formulas, focussing on biomechanics of the hip.
- In chapter seven we present a device, designed to produce fractures in a realistic way. Furthermore, the theory behind this design is discussed.
- Chapter eight presents the correlation between geometrical,

densitometric and biomechanical data obtained, the latter with the new device.

- Chapter nine presents the correlation between geometrical, densitometric and biomechanical data obtained, now obtained by a previously published semi-static method.

This dissertation will be concluded by a chapter in which the presented data will be analysed and conclusions will be drawn (chapter 10).

1.6 References

1. Delee JC 1991 Fractures and dislocations of the hip. In: Rockwood Jr CA, Green DP, Buchholz RW (eds.) *Rockwood and Green's Fractures in adults*, Third ed., vol. 2. J.B. Lippincott Comp, Philadelphia, pp 1481-1652.
2. Lowell JD 1966 Fractures of the hip. *New Eng J Med* 274(25):1418-25.
3. Cooper AP 1973 A treatise on dislocations and on fractures of the joints: Fractures of the neck of the thigh-bone (the classic). *Clin Orthop Rel Res* 92:3-5.
4. Bisla RS, Louis HJ 1975 Intertrochanteric fractures of the hip. *Ariz Med* 32(5):401-7.
5. Lyons AS, Petrucelli II RJ 1987 *Medicine, an illustrated history*. Abradale Press, New York, pp 599-600.
6. Zain Elabdien BS, Olerud S, Karlström G 1984 Subtrochanteric fractures. Classification and results of Ender nailing. *Arch Orthop Trauma Surg* 103(4):241-50.
7. Fielding JW, Cochran GV, Zickel RE 1974 Biomechanical characteristics and surgical management of subtrochanteric fractures (review). *Orthop Clin N Am* 5(3):629-50.
8. Fielding JW 1973 Subtrochanteric fractures. *Clin Orthop Rel Res* 92:86-99.
9. Hughston JC 1974 Intertrochanteric fractures of the femur. *Orthop Clin North Am* 5(3):585-600.
10. Mobach MJ, Warmenhoven PG 1993 Goede resultaten van behandeling van pertrochantaire femurfracturen met een gammapen bij 42 patiënten. *Ned Tijdschr Geneesk* 137(33):1662-7.
11. Walsh E 1984 Fractures of the proximal third of femur. *Radiography* 50(591):111-4.
12. Cleveland M, Bosworth DM, Thompson FR 1947 Intertrochanteric fractures of the femur. *J Bone Joint Surg* 29(4):1049-67.
13. Boyd HB, Griffin LL 1949 Classification and treatment of trochanteric fractures. *Arch Surg* 58:853-66.
14. Evans EM, Wales S 1951 Trochanteric fractures: A review of 110 cases treated by nailplate fixation. *J Bone Joint Surg* 33-B(2):192-204.
15. Dequeker J, Ortner DJ, Stix AI, Cheng X-C, Brys P, Boonen S 1997 Hip fracture and osteoporosis in a XIIth dynasty female skeleton from Lisht, upper Egypt. *J Bone Miner Res* 12(6):881-8.
16. Mensforth RP, Latimer BM 1989 Hamann-Todd Collection aging studies: Osteoporosis fracture syndrome. *Am J Phys Anthropol* 80(4):461-79.
17. Farmer ME, White LR, Brody JA, Bailey KR 1984 Race and sex differences in hip fracture incidence. *Am J Public Health* 74(12):1374-80.
18. Burger H, van Daele PLA, Hofman A, Schütte HE, Birkenhäger JC, Pols HAP 1995 Werveldeformaties en botdichtheid bij ouderen; het ERGO-onderzoek. *Ned Tijdschr Geneesk* 139(41):2092-6.
19. Burger H 1995 *Epidemiological studies on bone mineral density and fractures [dissertation]* Epidemiology, Erasmus University, Rotterdam, pp 111.
20. Cummings SR, Kelsey JL, Nevitt MC, O'Dowd KJ 1985 Epidemiology of osteoporosis and osteoporotic fractures. *Epidemiol Rev* 7:178-208.
21. Cummings SR 1987 Osteoporotic fractures: The magnitude of the problem. In: Christiansen C, Johansen JS, Riis BJ (eds.) *Osteoporosis 1987*. Osteopress, Copenhagen, Denmark, pp 1193-6.

22. Diaz Curel M, Carrasco de la Pena JL, Honorato Perez J, Perez Cano R, Rapado A, Ruiz Martinez I 1997 Study of bone mineral density in lumbar spine and femoral neck in a Spanish population. *Osteoporosis Int* 7(1):59-64.
23. Dinç H, Sadikoglu Y, Savci G, Demerci A, Tuncel E 1995 Bone mineral density measurement by quantitative computed tomography in a normal Turkish population. *Eur J Radiol* 21:79-83.
24. Francis RM, Peacock M, Marshall DH, Horsman A, Aaron JE 1989 Spinal osteoporosis in men. *Bone Miner* 5:347-57.
25. Fujii Y, Tsutsumi M, Tsunenari T, Fukase M, Yoshimoto Y, Fujita T, Genant HK 1989 Quantitative computed tomography of lumbar vertebrae in Japanese patients with osteoporosis. *Bone Miner* 6:87-94.
26. Kanis JA, Pitt FA 1992 Epidemiology of osteoporosis. *Bone* 13(suppl):S7-15.
27. Luckey MM, Meier DE, Madeli JP, DaCosta MC, Hubbard ML, Goldsmith SJ 1989 Radial and vertebral bone density in white and black women: Evidence for racial differences in premenopausal bone homeostasis. *J Clin Endocrinol Metab* 69(4):762-70.
28. Mattei JP, Arniaud D, Tonolli I, Roux H 1993 Aetiologies of male osteoporosis: Identification procedures (review). *Clin Rheumatol* 12(4):447-52.
29. Melton III LJ 1993 Hip fractures: A worldwide problem today and tomorrow. *Bone* 14(suppl):1-8.
30. Melton III JL 1995 How many women have osteoporosis now ? *J Bone Miner Res* 10(2):175-7.
31. Nelson DA, Kleerekoper M, Parfitt AM 1988 Bone mass, skin color, and body size among black and white women. *Bone Miner* 4:257-64.
32. Seeman E 1995 The dilemma of osteoporosis in men. *Am J Med* 98(suppl 2A):76-88.
33. Steiger P, Cummings SR, Black DM, Spencer NE, Genant HK 1992 Age-related decrements in bone mineral density in women over 65. *J Bone Miner Res* 7(6):625-32.
34. WHO study group 1994 Assessment of fracture risk and it's application to screening for postmenopausal osteoporosis. WHO Technical reports series, Geneva.
35. Greenspan SL, Myers ER, Maitland LA, Kido TH, Krasnow MB, Hayes WC 1994 Trochanteric bone mineral density is associated with type of hip fracture in the elderly. *J Bone Miner Res* 9(12):1889-94.
36. Greenspan SL, Maitland LA, Myers ER, Krasnow MB, Kido TH 1994 Femoral bone loss progresses with age: A longitudinal study in women over age 65. *J Bone Miner Res* 9(12):1959-65.
37. Boereboom FT, de Groot RR, Raymakers JA, Duursma SA 1991 The incidence of hip fractures in the Netherlands. *Neth J Med* 38(1-2):51-8.
38. Cooper C, Wickham C, Walsh K 1991 Appendicular skeletal status and hip fracture in the elderly: 14-year prospective data. *Bone* 12:361-4.
39. Cormier C 1994 Epidemiology, diagnosis, and treatment of osteoporosis. [Review]. *Curr Opin Rheumatol* 6(3):329-35.
40. Cummings SR 1991 Epidemiological studies of osteoporotic fractures: Methodological issues. *Calcif Tissue Int* 49(suppl):15-20.
41. Hinton RY, Lennox DW, Ebert FR, Jacobsen SJ, Smith GS 1995 Relative rates of fracture of the hip in the United States. *J Bone Joint Surg* 77-A(5):695-702.
42. Melton III LJ, Kan SH, Wahner HW, Riggs BL 1988 Lifetime fracture risk: An approach to hip fracture risk assessment based on bone mineral density and age. *J Clin Epidemiol* 41(10):985-994.

43. Melton III LJ, Chrischilles EA, Cooper C, Lane AW, Ridds BL 1992 How many women have osteoporosis? *J Bone Miner Res* 7(9):1005-10.
44. Spector TD 1994 Epidemiology of hip and appendicular fractures. In: Ring EJF, Elvins DM, Bhalke AK (eds.) Fourth Bath conference on osteoporosis and bone mineral measurement. British Institute of Radiology, Bath, pp 22-3.
45. Simonen O 1991 Incidence of femoral neck fractures: Senile osteoporosis in Finland in the years 1970-1985. *Calcif Tissue Int* 49:8-10.
46. Schroder HM, Andreassen MD, Villadsen I, Sorensen JG, Erlandsen M 1995 Increasing age specific incidence of hip fractures in a Danish municipality. *Dan Med Bul* 42:109-11.
47. Browner WS, Pressman AR, Nevitt MC, Cummings SR 1996 Mortality following fractures in older women: The study of osteoporotic fractures. *Arch Intern Med* 156:1521-5.
48. Heyse SP, Sartori L, Crepaldi G 1990 Epidemiology of osteoporosis: A study of fracture mortality in Italy. *Calcif Tissue Int* 46:289-93.
49. Magaziner J, Simonsick EM, Kashner TM, Hebel JR, Kenzora JE 1989 Survival experience of aged hip fracture patients. *Am J Public Health* 79(3):274-8.
50. Ross PD 1996 Osteoporosis - Frequency, consequences, and risk factors. *Arch Intern Med* 156:1399-1411.
51. Schürch MA, Rizolli R, Mermillod B, Vasey H, Michel JP, Bonjour JP 1996 A prospective study on socioeconomic aspects of fracture of the proximal femur. *J Bone Miner Res* 11(12):1935-42.
52. Sorbie C 1985 The broken hip. *Can J Surg* 28(5):385-6.
53. van Vugt AB, Touw CR 1994 Kwantificering van te langdurige ziekenhuisopname ('verkeerde-beddenproblematiek'); heupfracturen bij bejaarden. *Ned Tijdschr Geneesk* 138(36):1806-10.
54. Perez JV, Warwick DJ, Case CP, Bannister GC 1995 Death after proximal femoral fracture: An autopsy study. *Injury* 26(4):237-40.
55. Eiskjær S, Ostgård SE, Jakobsen BW, Jensen J, Lucht U 1992 Years of potential life lost after hip fracture among postmenopausal women. *Acta Orthop Scand* 63(3):293-6.
56. Schütte HE 1995 Social and economic impact of osteoporosis. A review of the literature. *Eur J Radiol* 20:165-9.
57. Zethraeus N, Strömberg L, Jönsson B, Svensson O, Öhlén G 1997 The cost of a hip fracture; estimates for 1,709 patients in Sweden. *Acta Orthop Scand* 68(1):13-7.
58. Barret-Connor E 1995 The economic and human cost of osteoporotic fracture. *Am J Med* 98(suppl 2A):3-8.
59. Lindsay R 1995 The burden of osteoporosis: Cost. *Am J Med* 98(suppl 2A):9-11.
60. de Laet CEDH, van Hout BA, Hofman A, Pols HAP 1996 Kosten wegens osteoporotische fracturen in Nederland; mogelijkheden voor kostenbeheersing. *Ned Tijdschr Geneesk* 140(33):1684-8.
61. Randell A, Sambrook PN, Nguyen TV, Lapsley H, Jones G, Kelly PJ, Eisman JA 1995 Direct clinical and welfare costs of osteoporotic fractures in elderly men and women. *Osteoporosis Int* 5:427-32.
62. Phillips S, Fox N, Jacobs J, Wright WE 1988 The direct medical costs of osteoporosis for American women aged 45 and older, 1986. *Bone* 9:271-9.
63. Williamson MR, Boyd CM, Williamson SL 1990 Osteoporosis: Diagnosis by plain chest film versus dual-photon bone densitometry. *Skeletal Radiol* 19:27-30.

64. Rizzolli R, Slosman D, Bonjour JP 1995 The role of dual energy X-ray absorptiometry of lumbar spine and proximal femur in the diagnosis and follow-up of osteoporosis. *Am J Med* 98 (suppl 2A):33-6.
65. Glüter CC, Jergas M, Engelke K, Grampp S, Genant HK 1993 Fortschritte in der Osteoporosedagnostik. *Radiologe* 33(8):444-51.
66. Kanis JA, Melton III LJ, Christiansen C, Johnston CC, Khaltaev N 1994 Perspective: The diagnosis of osteoporosis. *J Bone Miner Res* 9(8):1137-41.
67. van Kuijk C, Genant HK 1995 Radiological aspects. In: Riggs BL, Melton III LJ (eds.) *Osteoporosis: etiology, diagnosis, and management*, second ed. Lippincott-Raven, Philadelphia, pp 249-73.
68. Jergas M, Uffmann M, Escher H, Glüter CC, Young KC, Grampp S, Genant HK 1994 Interobserver variation in the detection of osteopenia by radiography and comparison with dual X-ray absorptiometry of the lumbar spine. *Skeletal Radiol* 23:195-9.
69. Lachmann E, Whelan M 1936 The roentgen diagnosis of osteoporosis and its limitations. *Radiology* 26:165-77.
70. Alhava EM 1991 Bone density measurement. *Calcif Tissue Int* 49(suppl):21-3.
71. Bentley HB 1989 Quantification of bone density and mineral content. *Radiogr Today* 55(62):16-8.
72. Bouxsein ML, Courtney AC, Hayes WC 1995 Ultrasound and densitometry of the calcaneus correlate with the failure loads of cadaveric femurs. *Calcif Tissue Int* 56:99-103.
73. Braillon P, Duboeuf F, Meary MF, Barret P, Demas PD, Meunier PJ 1989 Mesure du contenu minéral osseux par radiographie digitale quantitative: Premiers résultats au niveau vertébral lombaire. *Presse Med* 18(21):1062-5.
74. Editorial 1988 Bone densitometry and clinical decision making in osteoporosis. *Ann Int Med* 108(2):293-5.
75. Foldes AJ, Rimon A, Keinan DD, Popovitz MM 1995 Quantitative ultrasound of the tibia: A novel approach for assessment of bone status. *Bone* 17(4):363-7.
76. Funck C, Wüster C, Alenfeld FE, Pereira-Lima JFS, Meeder PJ, Götz M, Ziegler R 1996 Ultrasound velocity of the tibia in normal German women and hip fracture patients. *Calcif Tissue Int* 58:390-4.
77. Genant HK, Block JE, Steiger P, Glüter CC, Ettinger B, Harris ST 1989 Appropriate use of bone densitometry. *Radiology* 170:817-22.
78. Genant HK, Engelke K, Fuerst T, Glüter CC, Grampp S, Harris ST, Jergas M, Lang T, Majumdar S, Mathur A, Takada M 1996 Noninvasive assessment of bone mineral and structure: State of the art [review]. *J Bone Miner Res* 11(6):707-30.
79. Glüter CC, Cummings SR, Pressman A, Li J, Glüter K, Faulkner KG, Grampp S, Genant HK 1994 Prediction of hip fractures from pelvic radiographs: The study of osteoporotic fractures. *J Bone Miner Res* 9(5):671-7.
80. Huddleston AA 1988 *Quantitative methods in bone densitometry*, 1 ed. Kluwer Academic publishers, Boston, pp 217.
81. Laugier P, Fournier B, Berger G 1996 Ultrasound parametric imaging of the calcaneus: In-vivo results with a new device. *Calcif Tissue Int* 58:326-31.
82. Mazess RB, Barden H, Vetter J, Ettinger M 1989 Advances in noninvasive bone measurement. *Ann Biomed Eng* 17:177-81.
83. van Berkum FNR, Pols HAP, Birkenhäger JC 1988 Niet invasieve meting van de botmassa en osteoporose. *Ned Tijdschr Geneesk* 132(49):2233-7.
84. van Daele PLA, Burger H, Algra D, Hofman A, Grobbee DE, Birkenhäger JC, Pols

- HAP 1994 Age-associated changes in ultrasound measurements of the calcaneus in men and women: The Rotterdam study. *J Bone Miner Res* 9(11):1751-7.
85. van Kuijk C, Genant HK, Schütte HE 1992 Botdensitometrie en osteoporose. *Ned Tijdschr Geneesk* 136(25):1193-7.
 86. van Kuijk C, Genant HK 1994 Detection of osteopenia and osteoporosis. In: Lobo RA (ed.) *Treatment of postmenopausal women: basic and clinical aspects*. Raven Press, New York, pp 169-74.
 87. van Kuijk C, Genant HK 1997 Radiogrammetry and radiographic absorptiometry. In: Genant HK, Gugliemi G, Jergas M (eds.) *Bone densitometry and osteoporosis*. Springer verlag, New York, pp 281-94.
 88. van Rijn RR, Lequin MH, van Kuijk C 1998 Botdensitometrie; een overzicht voor de medicus practicus. *Patient Care* 25(1):9-16.
 89. Hayes WC, Meyers ER 1995 Biomechanics of fractures. In: Riggs BL, Melton III LJ (eds.) *Osteoporosis: etiology, diagnosis and management*, second ed. Lippincott-Raven, Philadelphia, pp 93-114.
 90. Kaplan FS 1987 Osteoporosis; pathophysiology and prevention. In: Erdélyi-Brown M (ed.) *Clinical Symposia*, vol. 39. Ciba Geigy, New Jersey, pp 32.
 91. Junqueira LC, Carneiro J, Long JA 1987 Beenweefsel. In: James J, Langevoort HL (eds.) *Functionele histologie (edited from 'Basic histology')*, 4e ed. Bunge, Utrecht, pp 162-88.
 92. Stevenson JC, Marsh MS 1992 An atlas of osteoporosis. *The encyclopedia of visual medicine series*, vol. 1. The Parthenon Publishing group, New Jersey, pp 104.
 93. Eriksen EF 1986 Normal and pathological remodelling of human trabecular bone: Three-dimensional reconstruction of the remodelling sequence in normals and in metabolic bone disease. *Endocr Reviews* 7(4):379-408.
 94. O'Rahilly R 1983 The lower limb. In: *Basic human anatomy; a regional study of human structure*. W.B. Saunders, Philadelphia, pp 107-75.
 95. Sobotta J, Becher H 1982 Thorax, abdomen, pelvis, lower extremities, skin. In: Ferner H, Staubesand J (eds.) *Sobotta atlas of human anatomy*, 10 ed., vol. 2. Urban & Schwarzenberg, Baltimore, pp 245-64.
 96. Entius CAC, van Rijn RR, Holstege JC, Stoeckart R, Zwamborn AW 1997 Correlating sheet plastinated slices, computed tomography images and magnetic resonance images of the pelvic girdle: A teaching tool. *Acta Anatomica* 158:44-7.
 97. Massie WK 1964 Fractures of the hip. *J Bone Joint Surg* 46-A(3):658-90.
 98. Meyers MH 1985 Anatomy of the hip. In: Ryan Jr. JD, Perveiler FM (eds.) *Fractures of the hip*. Year Book Medical Publishers, Inc., New York, pp 12-22.
 99. Feneis H 1983 Geïllustreerd anatomisch zakwoordenboek. Bohn, Scheltema & Holkema, Utrecht-Antwerpen, pp 42-7.
 100. Elke R, Marugg S 1992 Krafteinleitung auf die trabecularen Strukturen des proximalen Femurendes. *Orthopäde* 21:51-6.
 101. Singh M, Nagrath AR, Maini PS 1970 Changes in trabecular pattern of the upper end of the femur as an index of osteoporosis. *J Bone Joint Surg* 52-A(3):457-67.
 102. vander Sloten J, van der Perre G 1989 Trabecular structure compared to stress trajectories in the proximal femur and the calcaneus. *J Biomed Eng* 11:203-8.

Chapter 2

Classification of hip fractures

We come into the world under the brim of the pelvis
and go out by the neck of the femur.

M. Cleveland & J.W. Fielding

2.1 Introduction

Radiology plays an important role in today's medical care. It has become an indispensable tool in assessing the extent of trauma and/or disease. For the systematic description and comparison of nature and the type of hip fractures a number of classifications, most of them based on radiography, are used¹⁻¹¹.

The need for classification is twofold. First of all, clinicians want to use it as a tool to determine the best therapy for any given fracture and to predict the outcome of this therapy. Secondly, researchers need a classification to describe fractures in order to compare them with fractures previously described in the literature^{10,12-16}.

For a classification system to be acceptable for clinicians it should be fairly easy to use in every day practice. On the other hand, a classification system for researchers must be comprehensive and unambiguous. For clinical research a match of both would be perfect.

Since nearly all osteoporosis related hip fractures are those of the femoral neck (♀ 48%, ♂ 46%) and the trochanteric area (♀ 44%, ♂ 47%), only the classification of these groups of fractures will be discussed¹⁷.

2.2 Classification of hip fractures: a review

Historically fractures of the hip were described according to their anatomical position i.e. subcapital, transcervical, basal neck, trochanteric, and subtrochanteric or according to their relation with the joint capsule i.e. intra- and extracapsular^{12,15,18-20}. Because of the improved surgical procedures and the ability to treat complicated fractures, more elaborate descriptions of

fractures are needed. Descriptions should not only comprise the anatomical position of the fracture, as described above, but also include specific denominators, such as the angle or the degree of comminution. This makes a more specific classification of hip fractures possible. There are numerous ways to describe hip fractures, most of them are based on (a) the anatomical position of the fracture, (b) the angle of the fracture, and (c) the displacement of fracture fragments^{7,21}. The classifications will be described in two sections: femoral neck and trochanteric fractures. This differentiation is made since these two fracture locations require specific treatment and occur in different age groups. Research has shown that among Caucasian women below the age of 70 years, femoral neck fractures were more common, whereas in older women trochanteric fractures predominated. This difference was not found in a group of Caucasian men^{22,23}.

2.2.1 Femoral neck fractures

The oldest form of classification of fractures of the femoral neck is based on anatomical location i.e. subcapital and transcervical^{21,24}. The first more elaborate method of classification used for femoral neck fractures was that of Pauwels. He proposed to describe the fractures according to the inclination angle between the fracture line and the horizontal, as measured on an anterior posterior (AP) radiograph^{5,12,21,25-27}. Pauwels claimed that the angle of inclination coincided with the percentage of non-union. He discerned three types of femoral neck fractures. The rate of non-union increases from less than 10% in type I to 90% in type III (figures 1-3, appendix 2-A):

- I. An angle of inclination of 30°.
- II. An angle of inclination of 50°.
- III. An angle of inclination of 70°.

In the classification according to Pauwels, a fracture is described in two dimensions even though a fracture is three-dimensional. Therefore, Kahl proposed an additional lateral radiograph in combination with the AP radiograph, in order to obtain a three-dimensional representation of the fracture²⁶. In this modification each Pauwels type is subdivided into three separate groups depending on the lateral aspect of the fracture (figures 4-12, appendix A): KI transverse fracture line, KII oblique fracture line and KIII comminuted fracture. In combination with the classification according to Pauwels this results in 9 fracture types: PIKI, PIKII, PIKIII, PIIKI, etcetera (figures 4-12, appendix 2-A).

Garden proposed a different classification based on the degree of displacement⁵. This resulted in four fracture types (figures 13-16, appendix 2-A):

- I. Incomplete impacted fracture.
- II. Complete fractures without displacement.
- III. Complete fractures partially displaced, the two fragments retaining contact with each other.
- IV. Complete fractures with complete displacement.

The most recent classification is developed by the Swiss 'Arbeitsgemeinschaft für Osteosynthesefragen' (AO). This classification can be used to describe fractures of all long bones^{7,12,14,16,28}. Basically the AO classification codes each bone with a number and is then subdivided into, usually three, numbered segments. The first two digits represent the affected segment of a long bone. The segments are each divided into three sub-segments, which are each sub-classified into three groups, and then again into three subgroups. The AO classification is capable of classifying 783 different types of fractures, of which 39 are related to the proximal femur.

In the AO classification, the femur is given the number 3, the proximal part of the femur number 1, resulting in 31 for the proximal femur. The neck is given the digit B resulting in 31.B for the femoral neck. A further division is then made: 1. subcapital with slight displacement, 2. transcervical, and 3. subcapital with marked displacement. Finally the classification is completed by dividing these groups into three subgroups each (figures 17-25, appendix 2-A):

- | | | |
|-------|----|--|
| 31.B1 | .1 | Impacted in valgus 15°. |
| | .2 | Impacted in valgus < 15°. |
| | .3 | Non-impacted. |
| 31.B2 | .1 | Basicervical. |
| | .2 | Midcervical adduction. |
| | .3 | Midcervical shear. |
| 31.B3 | .1 | Moderate displacement in varus and external rotation. |
| | .2 | Moderate displacement with vertical translation and external rotation. |
| | .3 | Marked displacement. |

If a femoral neck fracture cannot be assigned to any of the above mentioned groups, it must be coded as 31.D1 (unclassifiable) and described in full.

2.2.2 Trochanteric fractures

Historically trochanteric fractures are divided into two classes: stable and unstable fractures^{21,29}. In 1949 Boyd and Griffin published a classification for intertrochanteric fractures, based on the relative ease or difficulty in securing and maintaining reduction. Four types were defined^{1,21,30} (figures 26-29, appendix 2-A):

- I. Fractures showing a more or less linear break extending along the general direction of the intertrochanteric line from major to minor trochanter. The reduction usually is simple and maintained with minimal difficulty.
- II. Fractures that are comminuted, with the main line of fracture along the intertrochanteric line, but with multiple cracks occurring in the cortex. Reduction is more difficult than in type I.
- III. Fractures that are essentially subtrochanteric, with at least one fracture line passing across the upper end of the shaft just below or in the region of the trochanter minor. Various degrees of comminution can be present with this type. Gaining and maintaining reduction generally is much more complicated.
- IV. Comminuted fractures that extend through the trochanteric region and usually into the femoral shaft, with fracture lines in at least two planes. These fractures require two plane fixation.

Tronzo and coworkers modified this classification in 1973. They divided type III into two separate types thereby creating five fracture types ^{6,9,31}:

- IIIa. Comminuted fractures involving the upper end of the femoral shaft with a large fragment of the trochanter minor.
- IIIb. Like type IIIa, but the trochanter major also shows a comminuted fracture.

Kyle and coworkers modified Boyd's classification again in 1979 ³². In their classification there are four fracture types (figures 30-33, appendix 2-A):

- I. Stable undisplaced fractures along the intertrochanteric line.
- II. Stable varus displaced fractures along the intertrochanteric line with a fracture of the trochanter minor.
- III. Unstable varus displaced fractures with posterior medial comminution and involvement of the trochanter major.
- IV. Unstable displaced posterior medial comminuted inter- subtrochanteric fractures with a fracture of the trochanter major.

Evans proposed a more simple classification, based on the stability of the fracture ^{3,21,33,34}. His classification consisted of five types of fractures (figures 34-38, appendix 2-A):

- I. Non-displaced two fragmentary fracture.
- II. Displaced fragmentary fracture.
- III. Three fragmentary fracture without posterolateral support due to dislocation of a trochanter major fragment.
- IV. Three fragmentary fracture without medial support due to dislocation of the lesser trochanter.
- V. Four fragmentary fracture without medial and posterolateral support. This is in fact a combination of type III and IV.

These fractures may also be classified using the AO classification^{7,35}. The trochanteric area, delimited cranially by the intertrochanteric line and lower edge of the lesser trochanter caudally, is coded 31.A. A further division into three groups is then made: 1. pertrochanteric simple, 2. pertrochanteric multi fragmentary, and 3. intertrochanteric. The classification is completed by dividing each group into three subgroups (figures 39-47, appendix 2-A):

- 31.A1 .1 Along the intertrochanteric line.
- .2 Through the trochanter major.
- .3 Below the lesser trochanter.
- 31.A2 .1 With one intermediate fragment.
- .2 With several intermediate fragments.
- .3 Extending more than one cm. below the lesser trochanter.
- 31.A3 .1 Simple, oblique.
- .2 Simple, transverse.
- .3 Multi fragmentary.

2.3 Discussion

Clinicians and researchers have different needs with regard to the classification of femoral neck fractures. One of the major problems with most classifications is that they are designed only to describe a small proportion of all fractures possible. For clinicians, a relatively simple classification will suffice, since they are mainly interested in individual cases. Researchers on the other hand have a need to compare different studies. This requires classification of large groups of different fractures, preferably along the lines of a comprehensive classification system.

In this study it we choose to classify all fractures according to the AO classification⁷. The rationale for this decision is twofold. In the first place the AO presents a systematic classification, coded with five digits/letters, with in theory less room for inter-observer variability. Second, it is the most complete classification system at the moment. However, we recognize that the AO classification is not widely accepted by clinicians, mainly because of the complexity of this system.

Appendix 2A
Fractures illustrated

Pauwels classification ²⁷

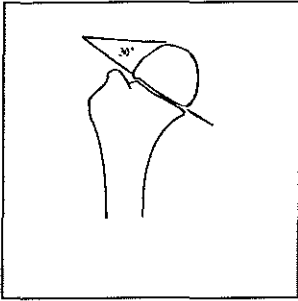


Figure 1: Type 1

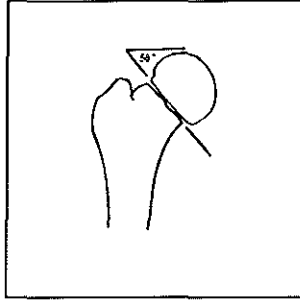


Figure 2: Type 2

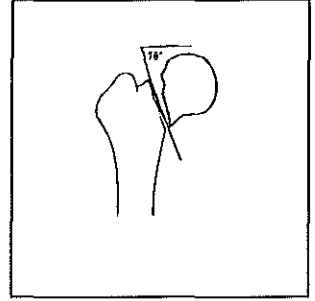


Figure 3: Type 3

Pauwel's - Kahl classification ²⁶

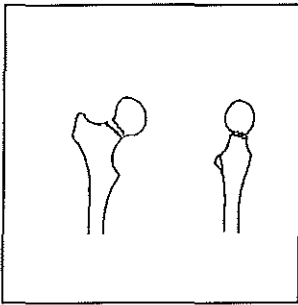


Figure 4: Type P1K1

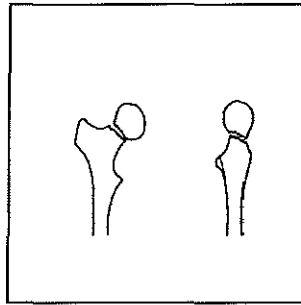


Figure 5: Type P1K2

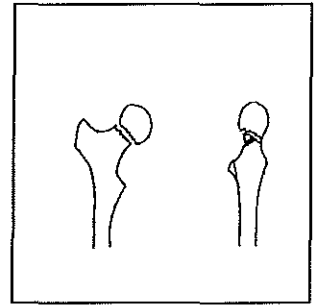


Figure 6: Type P1K3

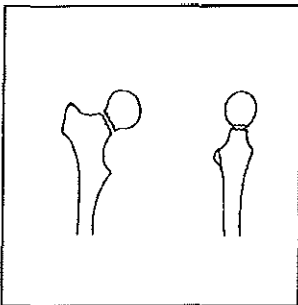


Figure 7: Type P2K1

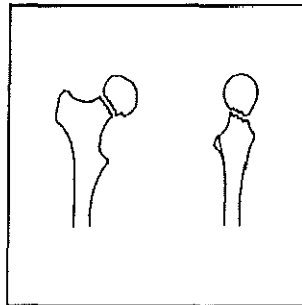


Figure 8: Type P2K2

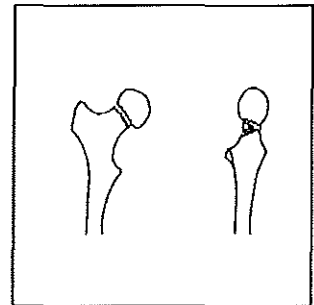


Figure 9: Type P2K3

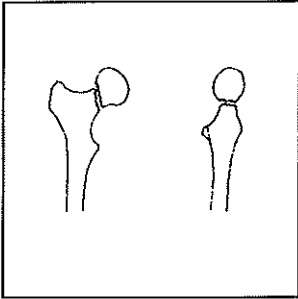


Figure 10: Type P3K1

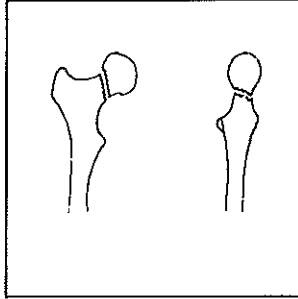


Figure 11: Type P3K2

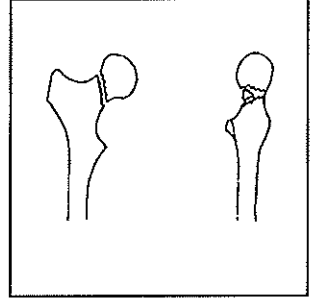


Figure 12: Type P3K3

Garden's classification ⁵

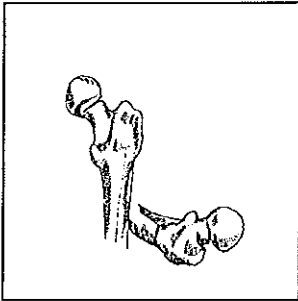


Figure 13: Type 1

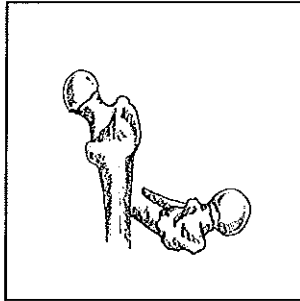


Figure 14: Type 2

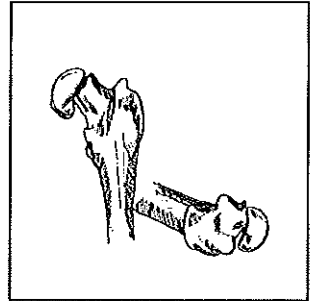


Figure 15: Type 3

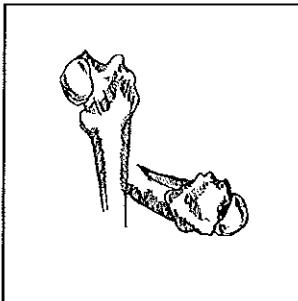


Figure 16: Type 4

AO classification ⁷

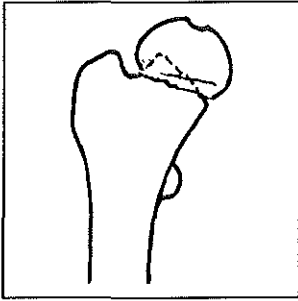


Figure 17: Type 31B11

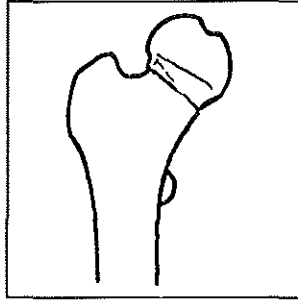


Figure 18: Type 31B12

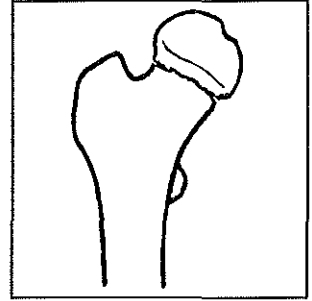


Figure 19: Type 31B13

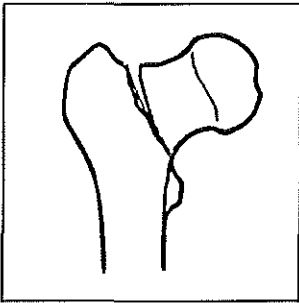


Figure 20: Type 31B21

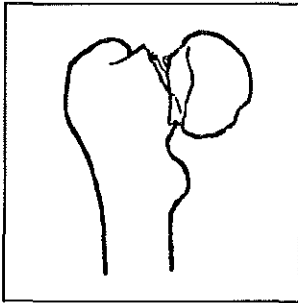


Figure 21: Type 31B22

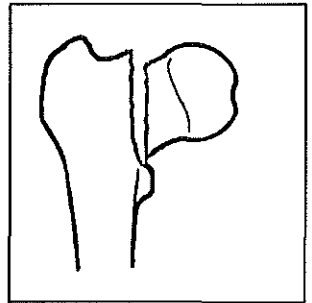


Figure 22: Type 31B23

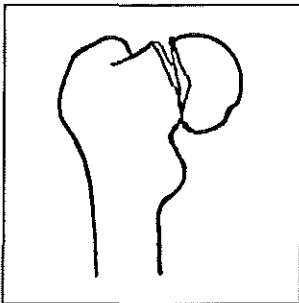


Figure 23: Type 31B31

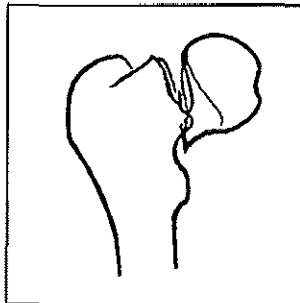


Figure 24: Type 31B32

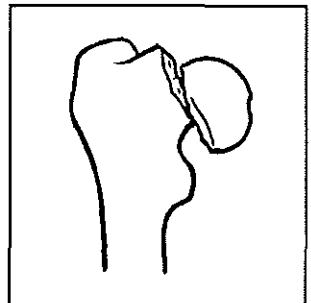


Figure 25: Type 31B33

Boyd's classification ¹

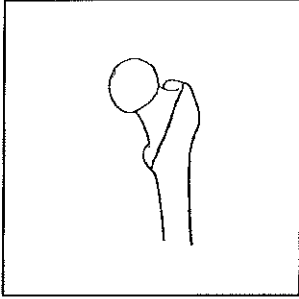


Figure 26: Type 1

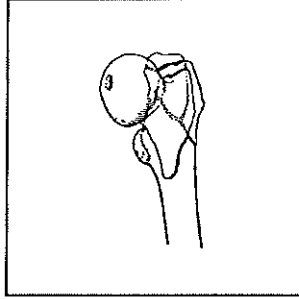


Figure 27: Type 2

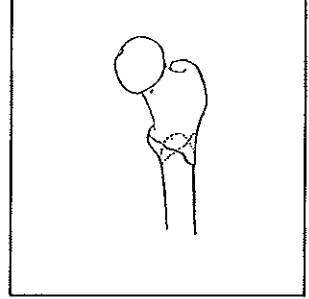


Figure 28: Type 3

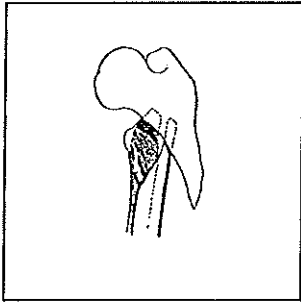


Figure 29: Type 4

Kyle's classification ³²

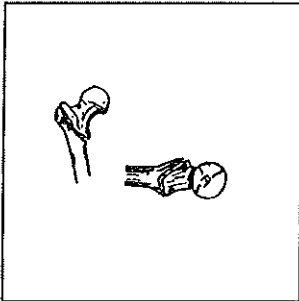


Figure 30: Type 1

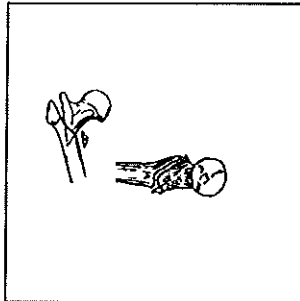


Figure 31: Type 2

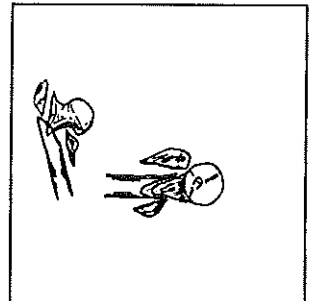


Figure 32: Type 3

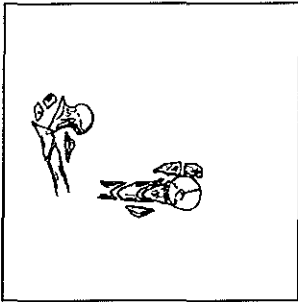


Figure 33: Type 4

Evans's classification, modified by Jensen ^{3,6}

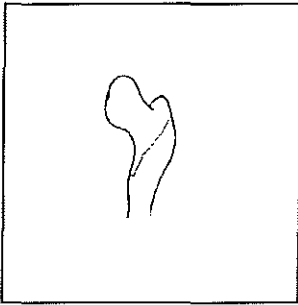


Figure 34: Type 1

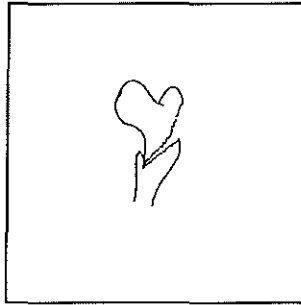


Figure 35: Type 2

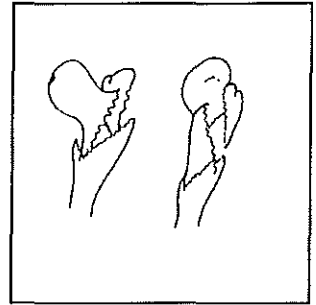


Figure 36: Type 3

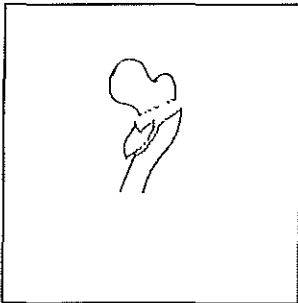


Figure 37: Type 4

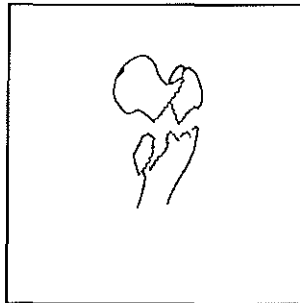


Figure 38: Type 5

AO classification ⁷

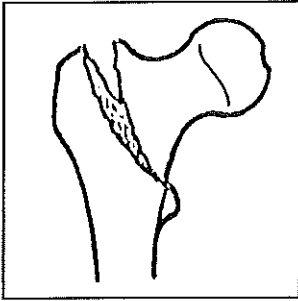


Figure 39: Type 31A11

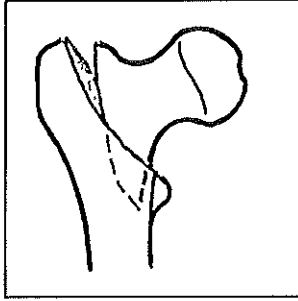


Figure 40: Type 31A12

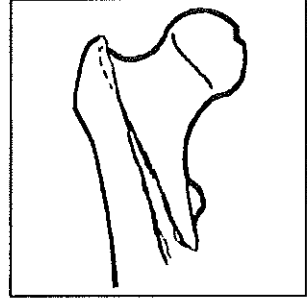


Figure 41: Type 31A13

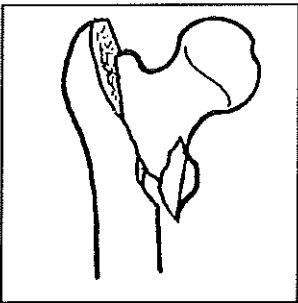


Figure 42: Type 31A21

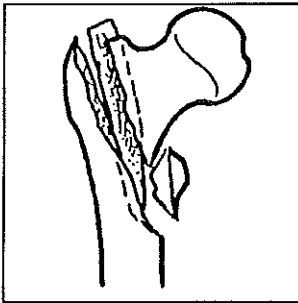


Figure 43: Type 31A22

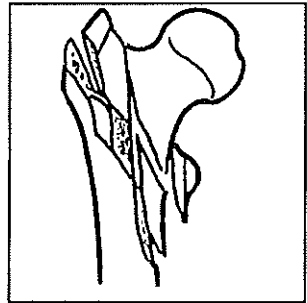


Figure 44: Type 31A23

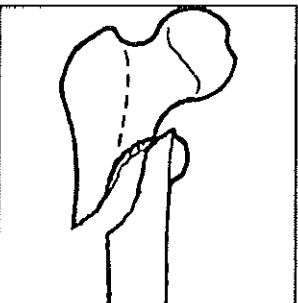


Figure 45: Type 31A31

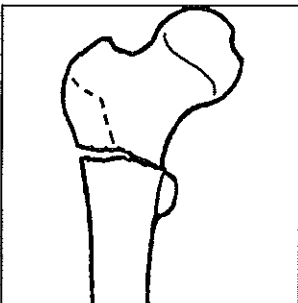


Figure 46: Type 31A32

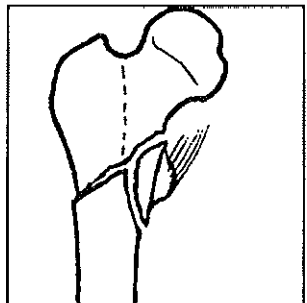


Figure 47: Type 31A33

2.4 References

1. Boyd HB, Griffin LL 1949 Classification and treatment of trochanteric fractures. *Arch Surg* 58:853-66.
2. Cleveland M, Bosworth DM, Thompson FR 1947 Intertrochanteric fractures of the femur. *J Bone Joint Surg* 29(4):1049-67.
3. Evans EM 1949 The treatment of trochanteric fractures of the femur. *J Bone Joint Surg* 31-B(2):190-203.
4. Fielding JW, Cochran GV, Zickel RE 1974 Biomechanical characteristics and surgical management of subtrochanteric fractures (review). *Orthop Clin N Am* 5(3):629-50.
5. Garden RS 1974 Reduction and fixation of subcapital fractures of the femur. *Orthop Clin N Am* 5(4):683-712.
6. Jensen JS 1980 Classification of trochanteric fractures. *Acta Orthop Scand* 51(5):803-10.
7. Müller ME, Nazarian S, Koch P, Schatzker J 1990 The comprehensive classification of fractures of long bones. Springer-Verlag, Berlin Heidelberg, pp 116-27.
8. Seinsheimer III F 1978 Subtrochanteric fractures of the femur. *J Bone Joint Surg* 60-A(3):300-6.
9. Tronzo RG 1974 Special considerations in management. *Orthop Clin North Am* 5(3):571-83.
10. Zain Elabdien BS, Olerud S, Karlström G 1984 Subtrochanteric fractures. Classification and results of Ender nailing. *Arch Orthop Trauma Surg* 103(4):241-50.
11. Zickel RE 1976 An intramedullary fixation device for the proximal part of the femur. *J Bone Joint Surg* 58-A(6):866-72.
12. de Boeck H 1994 Classification of hip fractures. *Acta Orthop Belg* 60(suppl 1):S106-9.
13. Frandsen PA, Andersen E, Madsen F, Skjodt T 1988 Garden's classification of femoral neck fractures. *J Bone Joint Surg* 70-B:588-90.
14. Johnstone DJ, Radford WJ, Parnell EJ 1993 Interobserver variation using the AO/ASIF classification of long bone fracture. *Injury* 24(3):163-5.
15. Lowell JD 1966 Fractures of the hip. *New Engl J Med* 274(25):1418-25.
16. Newey ML, Ricketts D, Roberts L 1993 The AO classification of long bone fractures: An early study of its use in clinical practice. *Injury* 24(5):309-12.
17. Hinton RY, Lennox DW, Ebert FR, Jacobsen SJ, Smith GS 1995 Relative rates of fracture of the hip in the United States. *J Bone Joint Surg* 77-A(5):695-702.
18. Bailey H 1980 The hip joint and the thigh. In: Clain A (ed.) *Hamilton Bailey's demonstrations of physical signs in clinical surgery*, 16 ed. Yearbook Medical Publishers Inc., Chicago, pp 486-502.
19. Friedenberg ZB, Baird D 1970 Fracture of the hip: A review of 200 consecutive fractures. *J Trauma* 10(1):51-6.
20. Walsh E 1984 Fractures of the proximal third of femur. *Radiography* 50(591):111-4.21. Delee JC 1991 Fractures and dislocations of the hip. In: Rockwood Jr CA, Green DP, Bucholz RW (eds.) *Rockwood and Green's Fractures in adults*, Third ed., vol. 2. J.B. Lippincott Comp, Philadelphia, pp 1481-1652.
22. Karagas MR, Lu-Yao GL, Barrett JA, Beach ML, Baron JA 1996 Heterogeneity of hip fracture: Age, race, sex, and geographic patterns of femoral neck and trochanter fractures among the US elderly. *Am J Epidemiol* 143:677-82.
23. Levy AR, Mayo NE, Grimard G 1995 Rates of transcervical and pertrochanteric hip fractures in the province of Quebec, Canada, 1981-1992. *Am J Epidemiol* 142(4):428-36.

24. Klenerman L, Marcuson RW 1970 Intracapsular fractures of the neck of the femur. *J Bone Joint Surg* 52-B(3):514-7.
25. Meyers MH 1985 Fractures of the hip. In: Ryan Jr. JD, Perveiler FM (eds.) *Fractures of the hip*. Year Book Medical Publishers, Inc., New York.
26. Kahl C 1986 Die mediale Schenkelhalsfraktur: Einteilung und Therapie. *Unfallchirurgie* 89:57-61.
27. Schüller NM, Marti RK, Raaymakers ELFB, Hoogbergen SHLJ 1988 Oprichtende osteotomie volgens Pauwels voor niet genezen(de) dijbeenhalsfractuur. *Ned Tijdschr Geneesk* 132(33):1532-6.
28. Schütz M, Bühler M 1992 Klassifikation der proximalen Femurfrakturen. *Helv Chir Acta* 59:947-54.
29. Arthorthurasook A 1982 Trochanteric fracture. *J Med Assoc Thai* 65(12):629-33.
30. Bisla RS, Louis HJ 1975 Intertrochanteric fractures of the hip. *Ariz Med* 32(5):401-7.
31. Hughston JC 1974 Intertrochanteric fractures of the femur. *Orthop Clin North Am* 5(3):585-600.
32. Kyle RF, Gustillo RB, Premer RF 1979 Analysis of six hundred and twenty-two intertrochanteric hip fractures. *J Bone Joint Surg* 61-A(2):216-21.
33. Evans EM, Wales S 1951 Trochanteric fractures: A review of 110 cases treated by nail plate fixation. *J Bone Joint Surg* 33-B(2):192-204.
34. Jensen JS, Rondevold E, Sonne-Holm S 1980 Stable trochanteric fractures. A comparative analysis of four methods of internal fixation. *Acta Orthop Scand* 51:811-6.
35. Mobach MJ, Warmenhoven PG 1993 Goede resultaten van behandeling van pertrochantaire femurfracturen met een gammapen bij 42 patiënten. *Ned Tijdschr Geneesk* 137(33):1662-7.

Chapter 3

Measurement of femoral geometry: Conventional versus direct magnification radiography

Und Hans Castorp sah, was zu sehen er hatte erwarten müssen, was aber eigentlich dem Menschen zu sehen nicht bestimmt ist und wovon auch er niemals gedacht hatte, daß ihm bestimmt sein könne, es zu sehen: er sah in sein eigenes Grab.

T. Mann, *Der Zauberberg*

3.1 Introduction

Since its discovery by Wilhelm Conrad Röntgen on November 8th 1895, the use of X-rays has become widespread in medicine¹⁴. X-rays are electromagnetic waves, of a certain wavelength range ($\lambda = 0.01\text{-}5 \cdot 10^{-10}$ m), generated by electrons striking a solid target, thereby forming photons⁵. If such an X-ray beam impinges on an object, part of the photons will be scattered on the surface, and will therefore not be visualized. The part penetrating, will be subject to scatter and absorption, the degree of both being characteristic for the medium. After leaving the object, the remaining photons can be visualized using either a fluorescent screen, a X-ray film or other photon detectors. The thus created image is the result of the attenuation and scatter of photons and is called a photon attenuation map. Photon interactions can be described using two relatively simple parameters: scatter and absorption. Both processes decrease the intensity of the radiation. At high voltages scatter is the prime interaction where at lower voltages absorption is the main interaction.

The attenuation of photons depends on the composition and thickness of the material under consideration. For a homogeneous material this can be described using equation 3.1⁶⁷.

eq 3.1
$$I_t = I_0 \cdot e^{-\mu \cdot d}$$

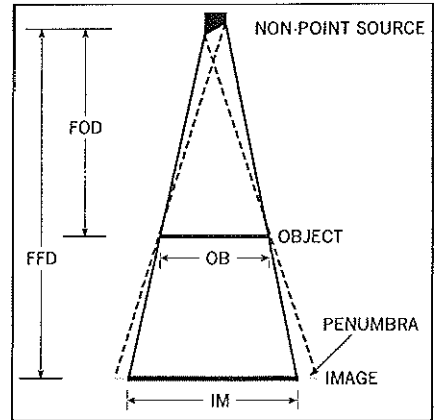
Where I_t equals the transmitted intensity (μSv), I_0 equals the incident intensity (μSv), μ equals the linear attenuation coefficient (m^{-1}), and d equals the thickness of the object (m).

Figure 3.1 - Penumbra (geometric unsharpness)

FOD = focus object distance
 FFD = focus film distance
 OB = object size
 IM = image size

Since an X-ray beam is a divergent beam each image is magnified to a certain extent (figure 3.1). The amount of magnification can be easily calculated using equation 3.2⁸⁹.

$$\text{eq 3.2} \quad IM = \frac{FFD \cdot OB}{FOD}$$



Where IM=image, FFD=focus film distance, OB=object size and FOD=focus object distance.

Magnification introduces some distortion and a relative unsharpness of the image. Distortion is inherent to the three-dimensional structure of objects, since the parts close to the focal point will be magnified more than those further away from it. The image unsharpness is caused by four principal sources:

1. Unsharpness due to the shape of the object. This is caused by the partial attenuation at the edges of an object. This unsharpness is inherent to imaging and can only be limited by increasing the focus object distance.
2. Motion artifacts, either movements of the patient or the imaging system. Due to the use of short exposure times motion artifacts are, in day to day conventional radiography, a minor problem.
3. Screen unsharpness, caused by the image receptor itself and dependent on the properties of the film/detectors.
4. Unsharpness or penumbra, caused by the size of the focal spot (figure 3.1). As a result of the angle of the anode, the penumbra is larger on the cathode side of an image.

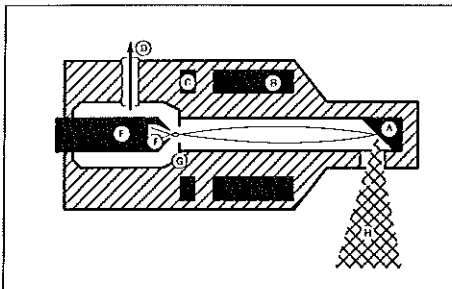


Figure 3.2 - Schematic diagram of a direct magnification (DIMA) X-ray tube

- A. Target
- B. Electromagnet
- C. Electromagnetic coil
- D. Vacuum pump
- E. Isolator
- F. Filament (cathode)
- G. Anode
- H. X-ray beam

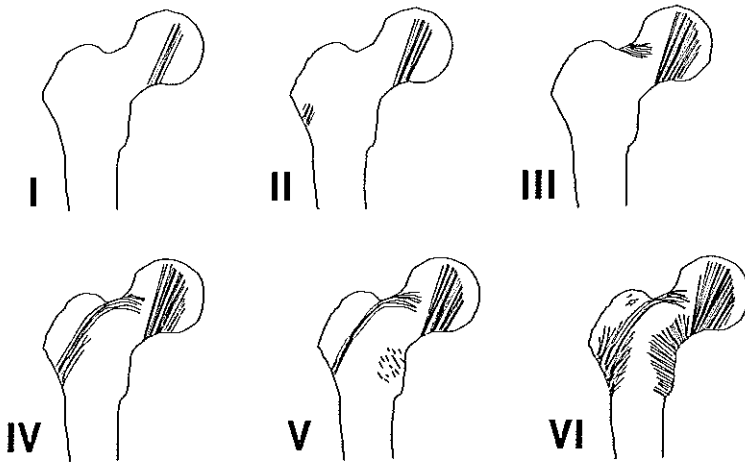


Figure 3.3 - Singh's index for osteoporosis ranging from grade 1 (severe osteoporosis) to grade 6 (normal)

In radiography penumbra is in general the main source of unsharpness. To alleviate this problem direct magnification (DIMA), was introduced¹⁰⁻¹². The principle of DIMA will be explained with the use of figure 3.2. The electrons emitted from the cathode are focussed by a pinhole opening in the anode (3.2.G). To ensure that all electrons traverse the electromagnetic field in a symmetric pathway, the ray is centred using an electromagnetic coil (3.2.C). Subsequently the X-rays transverse the electromagnetic field in which it is further focussed up to the smallest focal point (3.2.B). This results in a focal spot size of 0.03-0.2 mm², which is significantly smaller than the focal spot size used in conventional bucky radiography (0.3-1.3 mm²)^{10,12-14}. This in turn allows for magnifications of up to 9 times, although in day to day practice a magnification of four times appears adequate. Up to a magnification of four times, the exposure equals that of conventional radiography¹⁵.

As a result of the magnification, in theory a higher precision in measurements made using DIMA radiography could be expected. Research has shown that this technique could have benefits in several medical specialties: e.g. rheumatology, orthopaedics and oncology^{11,16-22}.

Because of its widespread availability and relative low costs of operation conventional radiography could be a useful tool in predicting osteoporotic hip fractures. Using conventional radiography, anterior-posterior (AP) projection, Singh et al. described the apparent trabecular morphology of the proximal femur^{23,24}. They designed a classification, known as the Singh index, ranging from 1 (severe osteoporosis) to 6 (normal) (figure 3.3). However, scoring the Singh index is a technique with a poor precision caused by inter-observer variability²⁵⁻²⁸.

More recently researchers have focussed on the geometry of the hip with regard to hip fracture risk²⁹⁻³⁶. Epidemiological studies show that the hip axis length (HAL) is an important predictor of hip fracture risk³⁰. The HAL is measured from the inner brim of the pelvis to the lateral aspect of the femur along the femoral axis. In this study, using cadaver femora, we measured the proximal femoral axis length (PFAL). The PFAL is measured along the axis of the femoral neck from the lateral aspect of the femur to outer brim of the caput femoris.

The aim of this chapter is to a) gather geometric data on our cadaver specimen, and b) to compare the precision of conventional versus direct magnification radiography.

3.2 Materials and methods

Femora

To compare conventional versus DIMA geometric measurements of the proximal femur 34 embalmed cadaver femora (mean age of 78.6 years, 54.3-98.7 years) were used. Of a second set of 42 femora (mean age 82.2 years, 67.3-96.8 years), only conventional radiographs were obtained. The bodies from which the femora originated, were embalmed by vascular perfusion between 48 to 60 hours after death. This was done using a medium containing: 50 g Phenol 99%, 20g MgSO₄, 20 g NaSO₄, 10 g NaCl, 60 ml formaldehyde 37%, 60 ml glycerine, H₂O ad 1000 ml³⁷. All femora were excarticulated in the hip and excised, about two hand-widths above the knee. After removal of surrounding soft tissue the femora were kept in a phenol/formaldehyde solution.

Radiography

To position the femora in a horizontal plane a special holder was constructed (figure 3.4). We placed a lead indicator (1.5×1.0 cm) at the level of the centre of the corpus femoris, to allow for the calculation of the magnification factor. All femora of the first set were imaged twice, once by conventional and once

by DIMA radiography.

Conventional radiography was performed with a Pandoros Optimatic X-ray tube and generator (Siemens, Germany), using 1.10 m focus-film distance (46 kV, 8 mAs)

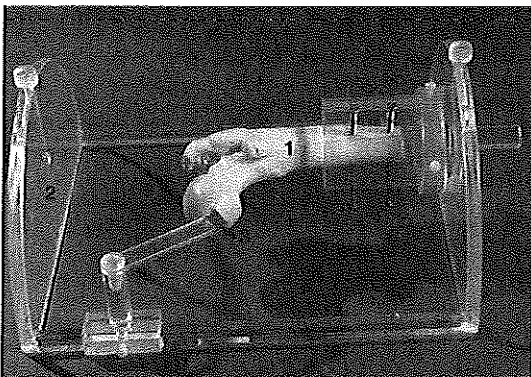
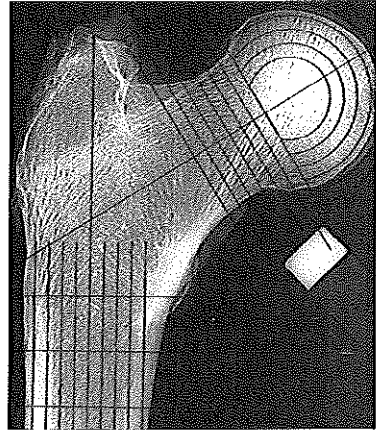


Figure 3.4 - Setup used for conventional and direct magnification radiography.

1. Phantom femur
2. Plexiglas holder
3. Lead strip

Figure 3.5 - Direct magnification radiograph with the template in place.

and Dupont Ultra-vision™ film/intensifier screens. DIMA radiography was performed using a Feinfocus DIMA tec-013 (Feinfocus Medizintechnik GmbH, Garbsen, Germany), 1.10 m focus-film distance (60 kV, automatic mAs (range 0.14-0.91 mAs) and exposure time (range 0.08-0.38 sec) selection). This was done in combination with Digital Luminescence Radiography (DLR). DLR was performed using a storage phosphor unit (Model FCR-7000; Fuji, Tokyo, Japan), cassette size 35×43 cm with a pixel size of 200 μ m (matrix size: 1.760×2.140). Two prints were obtained from each exposure (AC-I; Fuji, Tokyo, Japan): a normal DLR print and an edge-enhanced DLR print. The latter acquired using pre-installed unsharp-mask filtering software.



Measurements were made on conventional and edge-enhanced DIMA radiographs, using a positioning template and a ruler (division of scale: 0.5 mm) (figure 3.5). The following geometric dimensions were measured (figure 3.6) ^{30,34,38}:

1. Proximal femoral axis length (PFAL), adapted from the hip axis length (HAL) ^{29,30}
2. Head width, measured perpendicular to the neck axis through the centre of the femoral head (HW).
3. Neck width, measured perpendicular to the neck axis at the smallest width of the femoral neck (NW).

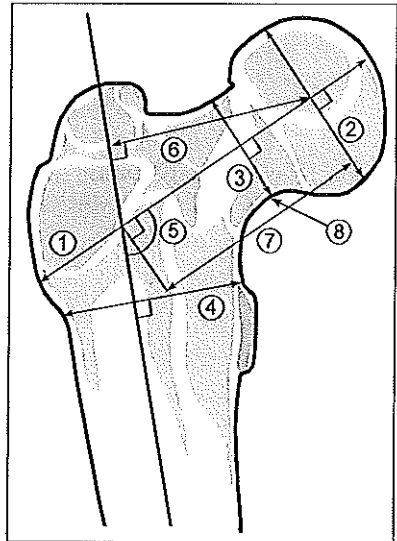


Figure 3.6 - Schematic diagram of the geometric measurements

1. Proximal femur axis length (PFAL)
2. Head width (HW)
3. Neck width (NW)
4. Shaft width (SW)
5. Neck shaft angle (NSA)
6. Offset
7. Internal femur axis length (IFAL)
8. Caudal cortical thickness

4. Shaft width, measured perpendicular to the axis of the corpus femoris above the trochanter minor (SW).
5. Neck-shaft angle (NSA).
6. Offset, distance from the center of the femoral head perpendicular to the axis of the femoral body.
7. Length of the internal femoral axis length, measured from the center of the femoral head to the line of intersection of the axis of the femoral neck and body (IFAL).
8. Caudal cortical thickness at the smallest width of the femoral neck (CCT). Division of this measurement with the NW yields the cortical index of the femoral neck ³⁹.

In addition to the above mentioned the Singh index was assessed (conventional versus non-edge-enhanced DIMA radiographs) ²³. We opted for the use of non-edge-enhanced DIMA radiographs as the representation of trabeculae is comparable to that in conventional radiography.

Statistical analysis

For the assessment of intra- and inter-observer variability two investigators measured six femora, from the first set, twice in a blinded fashion. Statistical analysis was done according to the equations recommended in the 'Draft Guidance for review of Bone densitometers' by the FDA ⁴⁰. An independent paired Student's t- test was performed to test for differences between the measurements obtained by conventional and DIMA. radiography.

3.3 Results

Of the first set all 34 radiographs were available for evaluation. Table 3.1 lists the intra- and inter-observer variability of the measurements made with both techniques, conventional vs. DIMA radiography. Table 3.2 presents the values of measurements (mean \pm SD) and their correlation, as assessed by one observer only. The Singh index and NSA differed significantly between both techniques ($p < 0.001$). The other measurements did not differ significantly and showed a good correlation, $0.719 < r < 0.956$. Of the second set all 42 radiographs were available for evaluation. The results for the whole study (76 femora) are presented in table 3.3.

Table 3.1 - Intra- and inter-observer variability (CV%) for geometry measurements (n=6).

Conventional radiology			
Measurement	Investigator 1	Investigator 2	Inter-observer
Singh	17.29	0	11.68
PFAL	2.77	0.65	2.02
HW	0.87	0.29	0.65
NW	1.01	0.59	0.82
SW	3.32	1.48	2.55
IFAL	1.78	1.15	1.49
NSA	1.43	0.73	1.13
Offset	2.15	1.02	1.69

Direct magnification radiology			
Measurement	Investigator 1	Investigator 2	Inter-observer
Singh	11.13	12.83	12.24
PFAL	1.74	0.23	1.24
HW	0.43	0.25	0.35
NW	3.03	0.84	2.21
SW	0.89	1.07	0.98
IFAL	3.86	1.71	3.04
NSA	1.59	1.88	1.74
Offset	5.46	2.26	4.33

Table 3.2 - Singh index and femoral geometry of our cadaver study after correction for magnification (n=34)

Measurement (units)	Mean (\pm SD)	
	Conventional	DIMA
Singh index (grade)	4.6 (\pm 1.0)	3.9 (\pm 1.1) ^a
PFAL (mm)	102.3 (\pm 11.0)	103.0 (\pm 7.5) ^b
HW (mm)	48.2 (\pm 3.4)	47.9 (\pm 3.5) ^b
NW (mm)	32.7 (\pm 2.8)	32.5 (\pm 2.7) ^b
SW (mm)	43.0 (\pm 3.4)	40.6 (\pm 3.5) ^b
IFAL (mm)	55.7 (\pm 4.9)	56.5 (\pm 3.0) ^b
NSA ($^{\circ}$)	122.9 (\pm 4.9)	125.4 (\pm 4.6) ^a
OFFSET (mm)	47.0 (\pm 5.0)	46.3 (\pm 5.5) ^b

PFAL = proximal femoral axis length, HW = head width
 NW = neck width, SW = shaft width, IFAL = internal femoral axis length, NSA = neck-shaft angle.

^a = Measurements between both methods differ significantly (p<0.001).

^b = Measurements between both methods do not differ significantly (p>0.05).

Table 3.3 - Singh index and femoral geometry of our cadaver study after correction for magnification measured on conventional radiographs (SD between brackets).

Measurement (Unit)	All femora (n=76)	Female femora (n=40)	Male femora (n=36)
Age (years)	80.7 (9.8)	83.0 (9.5)	78.1 (9.6) ^{NS}
PFAL (mm)	100.3 (±7.2)	100.4 (6.3)	107.3 (7.1)**
HW (mm)	48.0 (±3.4)	47.1 (2.8)	52.3 (2.0)**
NW (mm)	32.5 (±3.0)	32.0 (2.9)	35.4 (2.0)**
SW (mm)	43.3 (±3.9)	43.4 (4.0)	46.0 (3.7)'
FAL (mm)	55.8 (±4.7)	56.5 (4.5)	58.9 (5.2)'
NSA (°)	122.5 (±4.6)	122.3 (4.7)	122.6 (4.6) ^{NS}
Offset (mm)	47.2 (±5.2)	48.0 (4.9)	49.8 (5.6) ^{NS}
Singh index (grade)	4.7 (±1.0)	4.7 (0.9)	4.8 (1.1) ^{NS}
Femoral neck index	0.059 (0.03)	0.068 (0.03)	0.050 (0.02)'

' p<0.05, **p<0.001, ^{NS} No significant difference compared to women.

PFAL = proximal femoral axis length, HW = head width, NW = neck width, SW = shaft width, IFAL = internal femoral axis length, NSA = neck-shaft angle.

3.4 Discussion

As stated in the introduction one of the aims of this chapter was to assess the difference in precision of geometry measurements made on conventional radiographs compared to DIMA radiographs. The proximal femoral axis length can be equally well measured using both techniques. DIMA radiography seems to have no additional value for measuring this, from an epidemiological point of view, important geometrical parameter^{29,30,41-43}. Scoring the Singh index has a lower inter- and intra-observer variance on conventional radiographs compared to DIMA radiographs. The low intra-observer variability for the second observer may be attributed to the fact that this observer performed the measurements in a relative short time span. The higher precision on conventional radiographs could be expected as Singh et al. originally developed this classification on conventional radiographs²³. Magnification seems to lead to under classification, i.e. conventional 4.6 (SD 1.0) versus non-edge-enhanced DIMA 3.9 (SD 1.1), p<0.001.

The higher intra-observer variability of the NSA on DIMA radiographs might be explained by the fact that only the part of the femoral body above the trochanter minor can be seen on DIMA radiographs, interfering with accurate placement of our template along the axis of the femoral body. Comparison of our geometrical data with previous studies is difficult since they represent data collected in vivo, with unknown magnification factors^{29,30,44-46}.

3.5 References

1. Eisenberg RL 1992 Röntgen and the discovery of X-ray's. In: Radiology; an illustrated history. Mosby Year Book, St. Louis, pp 22-42.
2. Mould RF 1993 Discovery of X-rays: Wilhelm Conrad Röntgen. In: A century of X-rays and radioactivity in medicine: With emphasis on photographic records of the early years. Institute of Physics Publishing, London, pp 1-9.
3. van Wylick WAH 1966 Röntgen en Nederland; Röntgens betrekkingen tot Nederland en de opkomst der Röntgenologie hier te lande, 1 ed. J. Hoeijenbos N.V., Utrecht, pp -255.
4. Kal HB 1995 Röntgen; 100 jaar straling doorgelicht. Inmerc, Wormer, pp 88.
5. Currey III TS, Dowdey JE, Murry jr RC 1990 Computed tomography. In: Christensen's physics of diagnostic radiology, 4th ed. Lea & Febiger, Philadelphia / London, pp 289-322.
6. van Kuijk C 1991 Evaluation of postprocessing dual-energy quantitative computed tomography [dissertation] Department of Experimental Radiology. Erasmus University, Rotterdam, pp 115.
7. Webb S 1988 The physics of medical imaging. In: Mould RF (ed.) Medical science series. Adam Hilger, Bristol.
8. van Bodegom JW, Kuiper JW, van Rijn RR, van Kuijk C, Zwamborn AW, Grashuis JL 1998 Vertebral dimensions: Influence of X-ray technique and patient size on measurements. *Calcif Tissue Int* 62(3):214-8.
9. Wolbarst AB 1993 Screen-film radiography IV: Magnification and Resolution. In: Physics of Radiology. Prentice Hall International, London, pp 193-200.
10. Pruneau D, Faszold S, Sostarich D, Weinshilbaum K 1987 A practical approach to direct magnification radiography. *Radiol Technol* 59(2):121-7.
11. Schlossarek W, Wunderer S, Früwald F 1987 Direkte Röntgenvergrößerung und ihre Aussagekraft bei Strukturänderungen im Spongiosabereich. *Fortschr Kiefer Gesichtschir* 32:14-6.
12. Feinfocus 1995 Produktbeschreibung (DIMA Tec 013): Spezifikation der Hauptkomponenten. Feinfocus Medizintechnik GmbH, Garbsen.
13. Buchmann F, Kleine Schaars HWG, Koster WG 1990 X-ray tubes: The clinical requirements. *Medica Mundi* 35:38-48.
14. Gebureck P, Fredow G, Sperner W 1991 Anlagenkonzept eines Mikrofocusröntgensystems für die klinische Anwendung. *Radiologe* 31:407-12.
15. Krohnholz HL 1991 Direktradiographischen Vergrößerung und Strahlenexposition. *Radiologe* 31:413-7.
16. Link TM, Rummeny EJ, Lenzen H, Reuter I, Roos N, Peters PE 1994 Artificial bone erosions: Detection with direct radiography versus conventional high-resolution radiography. *Radiology* 192(3):861-4.
17. Poulsen Nautrup C, Berens von Rautenfeld D 1991 Direktradiographischen Vergrößerung in der experimentellen Medizin. *Radiologe* 31:430-4.
18. Reuther G, Krohnholz HL, Hüttenbrink KB 1991 Entwicklung und Perspektiven der medizinischen Vergrößerungsradiographie. *Radiologe* 31(9):403-6.
19. Reuther G, Krohnholz HL 1991 Direktradiographische Vergrößerung in Kombination mit digitaler Radiographie für die Skelettdiagnostik. *Radiologe* 31(9):424-9.
20. Winckler S, Richter KD 1991 Direktradiographischen Vergrößerung bei Knocheninfektionen. *Radiologe* 31(9):447-51.

21. Keßler T, Link TM, Overbeck J, Lange T, Klein W 1994 Verlaufskontrolle der Frakturheilung : Indikationen und klinische Relevanz der Direktradiographischen vergrößerung im Vergleich zur konventionellen Röntgenaufnahme. *Unfallchirurg* 97:619-24.
22. Wülker N, Siebert WE 1993 Bestandsaufnahme der direktvergrößernden Röntgentechnik in der Orthopädie. *Akt Radiol* 3:100-4.
23. Singh M, Nagrath AR, Maini PS 1970 Changes in trabecular pattern of the upper end of the femur as an index of osteoporosis. *J Bone Joint Surg* 52-A(3):457-67.
24. Singh M, Riggs L, Beabout JW, Jowsey J 1972 Femoral trabecular-pattern index for evaluation of spinal osteoporosis. *Ann Int Med* 77:63-7.
25. Helelä T, Telkkä A, Virtama P 1969 Bone pattern of the femoral neck as a measure of bone density and susceptibility to hip fractures. *Ann Clin Res* 1:85-7.
26. Kawashima T, Uthhoff HK 1991 Pattern of bone loss of the proximal femur: A radiologic, densitometric, and histomorphometric study. *J Orthop Res* 9:634-40.
27. Koot VCM, Kesselaer SMMJ, Clevers GJ, de Hooze P, Weits T, van der Werken C 1996 Evaluation of the Singh index for measuring osteoporosis. *J Bone Joint Surg* 78B(5):831-4.
28. Smyth PP, Adams JE, Whitehouse RW, Taylor CJ 1997 Application of computer texture analysis to the Singh index. *Br J Radiol* 79:242-7.
29. Glüer CC, Cummings SR, Pressman A, Li J, Glüer K, Faulkner KG, Grampp S, Genant HK 1994 Prediction of hip fractures from pelvic radiographs: The study of osteoporotic fractures. *J Bone Miner Res* 9(5):671-7.
30. Faulkner KG, Cummings SR, Black D, Palermo L, Glüer CC, Genant HK 1993 Simple measurement of femoral geometry predicts hip fracture: The study of osteoporotic fractures. *J Bone Miner Res* 8(10):1211-7.
31. Gómez Alonso C 1994 Bone mineral density and geometric measurements as predictors of risk for hip fracture. In: Ring EJF, Elvins DM, Bhalke AK (eds.) Fourth Bath conference on osteoporosis and bone mineral measurement. British Institute of Radiology, Bath, pp 24.
32. Karlsson KM, Sernbo I, Obrant KJ, Redlund-Johnell I, Johnell O 1996 Femoral neck geometry and radiographic signs of osteoporosis as predictors of hip fracture. *Bone* 18(4):327-30.
33. Nakamura T, Turner CH, Yoshikawa T, Slemenda CW, Peacock M, Burr DB, Mizuno Y, Orimo H, Ouchi Y, Johnston Jr CC 1994 Do variations in hip geometry explain differences in hip fracture risk between Japanese and white Americans. *J Bone Miner Res* 9(7):1071-6.
34. Rubin PJ, Leyvraz PF, Aubaniac JM, Argenson JN, Esteve P, de Roguin B 1992 The morphology of the proximal femur: A three-dimensional radiographic analysis. *J Bone Joint Surg* 74-B(1):28-32.
35. Sievänen H, Kannus P, Oja P, Vuori I 1994 Dual energy X-ray absorptiometry is also an accurate and precise method to measure the dimensions of human long bones. *Calcif Tissue Int* 54(2):101-5.
36. Yoshikawa T, Turner CH, Peacock M, Slemenda CW, Weaver CM, Teegarden D, Markwardt P, Burr DB 1994 Geometric studies of the femoral neck using dual-energy X-ray absorptiometry. *J Bone Miner Res* 9:1053-64.
37. Kleinrensink GJ, Stoockart R, Vleeming A, Snijders CJ, Mulder PGH, van Wingerden JP 1995 Peripheral nerve tension due to joint motion; a comparison between embalmed

- and unembalmed human bodies. *Clin Biomech* 10(5):235-9.
38. Boonen S, Koutri R, Dequeker J, Aerssens J, Lowet G, Nijs J, Verbeke G, Lesaffre E, Geusens P 1995 Measurement of femoral geometry in type I and type II osteoporosis: Differences in hip axis length consistent with heterogeneity in the pathogenesis of osteoporotic fractures. *J Bone Miner Res* 10(12):1908-12.
 39. Fredensborg N, Nilsson BE 1977 Cortical index of the femoral neck. *Acta Radiol Diagnos* 18:492-6.
 40. Arnaudo JS 1992 Draft guidance for review of bone densitometers 510(k). In: *Guide to clinical trials*. Raven, New York, pp 24-7.
 41. Slis HW, van Daele PLA, Kuiper JW, Burger H, Algra D, Hofman A, Birkenhäger JC, Pols HAP 1995 The use of simple geometric measurements on standard pelvic X-rays in the prediction of hip fractures. *Osteoporosis Int* 5(4):311.
 42. Reid IR, Chin K, Evans MC, Jones JG 1994 Relation between increase in length of hip axis in older women between 1950s and 1990s and increase in age specific rates of hip fractures. *BMJ* 309:508-9.
 43. Mikhail MB, Vaswani AN, Aloia JF 1996 Racial differences in femoral dimensions and their relation to hip fracture. *Osteoporosis Int* 6:22-4.
 44. Faulkner KG, Mac Clung M, Cummings SR 1994 Automated evaluation of hip axis length for predicting hip fracture. *J Bone Miner Res* 9(7):1065-70.
 45. Kuiper JW, Slis HW, van Daele PLA 1995 Comparison DXA scans and conventional radiography for evaluation of femoral geometry. *Osteoporosis Int* 5(4):312.
 46. Peacock M, Turner CH, Liu G, Manatunga AK, Timmerman L, Johnston jr CC 1995 Better discrimination of hip fracture using bone density, geometry and architecture. *Osteoporosis Int* 5:167-73.

Chapter 4

Dual-energy X-ray absorptiometry

Felson's Law: To steal ideas from one person is plagiarism;
to steal from many is research

4.1 Introduction

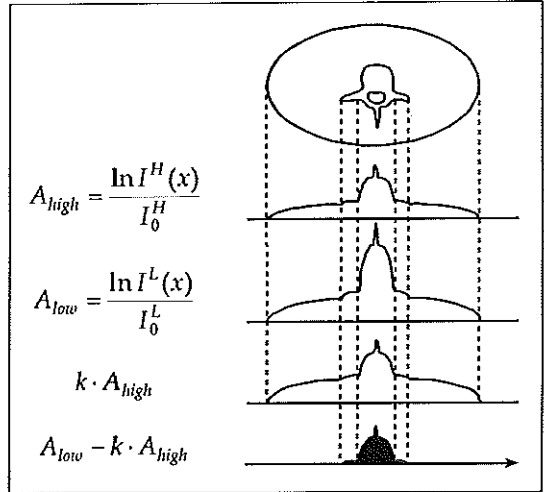
As explained in chapter 3, photon attenuation depends on the medium through which it passes. Although human tissue and bone are not homogenous, this principle can be used to measure bone density^{1,2}. Absorptiometry scanners scan along a scan line (x-coordinate) across the measured object (y-coordinate). Each pixel therefore has a x- and a y-coordinate, allowing for the calculation of a region of interest (ROI) and bone mineral content (BMC), expressed in grams (g). Dividing the BMC by the area under consideration yields the bone mineral density (BMD), expressed in grams per square centimetre (gcm^{-2}). Although the term BMD is not a proper mass density unit, it is accepted in medical literature and will therefore be used in this dissertation^{3,4}.

In 1963 Cameron and Sorensen introduced single-energy photon absorptiometry (SPA)⁵. This is a technique which uses a single energy source either ^{125}I (28 keV) or ^{241}Am (60 keV). In order to perform the measurement, the arm or heel of a subject was placed in an environment of known dimensions. Since water has about the same linear attenuation coefficient as soft tissue, usually a water bath was used⁶⁻¹⁴. In SPA it is assumed that the arm or heel consists only of muscles, soft tissue (both closely simulated with water) and bone. Therefore, BMC or BMD within the scanned path is proportional to the additional attenuation caused by bone. SPA is a technique with a good precision (2% error). It is however not useful in predicting BMD of the spine (standard error of estimate 15%) or hip (standard error of estimate 20%)¹⁵.

A second step was the addition of a second energy, obtained using ^{153}Gd (44 keV and 100 keV)¹⁶. This allowed measurement of tissue which cannot be surrounded by a constant soft tissue equivalent, e.g. spine, hip and total body¹⁷⁻²⁸. The rationale behind this technique is based on the fact that the

Figure 4.1 - Schematic illustration of the principle of DXA systems

attenuation, of any given medium, depends on photon energy. In dual-energy photon absorptiometry (DPA) photon attenuation profiles are measured at two levels. Multiplying the soft tissue attenuation with a constant, so that the difference between the two profiles becomes zero over soft tissue areas, has the same effect as a water bath (figure 4.1)²⁹. The mathematical background is explained in appendix 4-A. Although DPA was a significant improvement over SPA it still had a number of disadvantages. Scan times could be as long as 20-40 min, and the resolution was limited. The use of ¹⁵³Gd has a major drawback since this source is rather unstable and has to be replaced each year. DPA measures BMD very precise, with respective precision errors of less than 3%, 2% and 1% for the hip, spine and total body¹⁵. The longitudinal precision however, is less due to the unstable source²³.



In order to overcome these problems, dual-energy X-ray absorptiometry (DXA) was introduced³⁰⁻³³. Instead of using the unstable ¹⁵³Gd source, a stable x-ray source is used. Besides a reduction in operating cost, scan times, radiation dose and an improvement in reproducibility was obtained. Nowadays DXA is the main choice for bone densitometry in clinical practice³⁴⁻³⁷. The rationale behind DXA is the same as that behind DPA. To obtain two different energy levels in DXA two techniques can be used either energy switching or implementation of a filter²⁹.

In energy switching systems the X-ray potential is rapidly switched between two energies. In most commercial available systems (e.g. Hologic systems[®]) the two effective energy levels are 45 keV and 100 keV. The system is continuously calibrated. This is done by interposing calibration materials into the beam. The calibration materials mimic bone and soft tissue, and are mounted on a disc which rotates synchronous with the X-ray pulses. As X-ray beams are polychromatic, i.e. composed of many different energy levels, beam hardening can occur. Beam hardening is caused by the fact that photons with a low energy are more likely to be absorbed than photons with a high energy. Therefore the exiting beam contains relatively more high energy photons, i.e. the beam is said to be harder. To compensate for beam

hardening, DXA systems are equipped with filters, usually brass and aluminium, in order to narrow the spectrum of the beam²⁹. The exiting photons are measured using wide range, current-integrated detectors.

Filtered DXA systems (e.g. Lunar systems[®]) use a rare earth filter, usually cerium or samarium, these filters are better known as K-edge filters. K-edge filtering depends on the fact that, due to their specific atomic structure these rare earths selectively filter X-ray beams into two separate components. The effective energies of these two components are 40 keV and 70 keV. These systems use pulse counting detectors that process each incoming photon and decide whether it is a low or high energy photon. In these systems pile-up and cross-over can occur. Pile-up occurs when a photon hits the detector while this detector is still processing the previous photon (modern DXA systems can process 300.000 pulses per second thus decreasing the risk of pile-up). Cross-over occurs when the detector counts a high energy photon as a low energy photon. To compensate for this phenomena a fraction of the low energy photons is assigned to the high energy level.

It is important to bear in mind that DXA uses a two 'component model', i.e. it assumes that the object to be measured consists of two materials: soft tissue and bone. Due to the distribution of fat in both tissues, this assumption introduces an important error in DXA measurements, the so called fat error³⁸⁻⁴². A second drawback of DXA is the fact that it is a two dimensional technique, it is therefore impossible to discern trabecular from cortical bone⁴³.

In clinical practice the DXA measurements are compared to young, sex-matched, normal values and expressed as a T-score. This T-score is calculated as the difference between the patients BMD and the mean BMD of young normals over the standard deviation of this mean (equation 4.1)²⁹:

$$\text{eq 4.1} \quad T_{\text{score}} = \frac{BMD_{\text{patient}} - BMD_{\text{young-normal}}}{SD_{\text{young-normal}}}$$

This T-score is indicative for the fracture risk. The World Health Organisation has based the diagnostic categories of osteoporosis are based on the T-score³³. A T-score higher than -1 is normal. A T-score between -1 and -2.5 indicates osteopenia. These persons are at high risk of developing osteoporosis. A T-score lower than -2.5 is indicative for osteoporosis. These persons have a significantly increased risk for fractures³³.

As DXA is the most widely accepted and used technique for the diagnosis of osteoporosis data on all cadaver femora in this study were gathered using this technique.

4.2 Materials and methods

Femora

A total of seventy-six femora, median age 82.9 years (range 54.3-98.7 years), were used in this study. All femora were ex-articulated in the hip and excised, about two hand-widths above the knee. And after removal of surrounding soft tissue the femora were kept in a phenol/formaldehyde solution. In order to remove air bubbles trapped within the specimen, the femora were thoroughly degassed under water in a vacuum desiccator prior to investigation.

Dual-energy X-ray Absorptiometry

To simulate soft tissue the femora were placed in a water bath, filled with 20 cm of water, and supported by a holder. All DXA measurements were performed, by one investigator, using a Lunar DPX-L scanner (76 kVp with cerium filter, 0.75 mA, 1.68 mm collimator diameter, Lunar corp., Madison, USA). For analysis the standard DXA software (version 1.3) for the proximal femur was used. The BMC, area and BMD of the Neck, Ward's triangle and the trochanter major were assessed according to the guidelines stated in the manual (figure 4.2).

Statistical analysis

Statistics were performed using the Statistical Package for the Social Sciences (SPSS version 7.5.2, SPSS Inc., Chicago, USA). An independent Students t-test was performed to test for sex differences in the DXA measurements. Intra-observer variability was assessed according to the guidelines recommended in the 'Draft Guidance for review of Bone densitometers' by the Food and Drugs Administration (FDA) ⁴⁴. All cadaver femora were scanned twice after replacement.

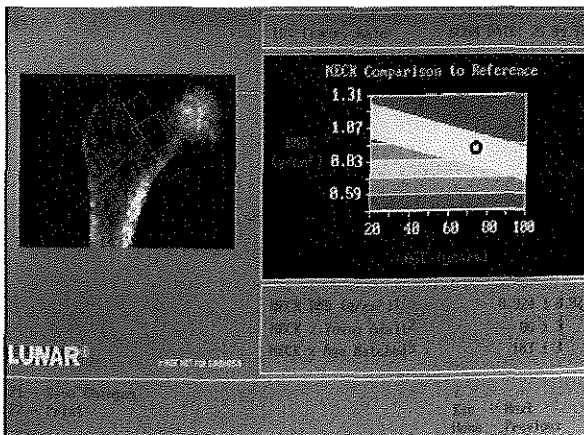


Figure 4.2 - DXA scan of a cadaver femur.

The left side of the screen shows the DXA scan, with the regions of interest. The right side a femoral neck BMD versus age graph (the BMD of the specimen is denoted with an asterisk)

4.3 Results

All seventy-six femora were eligible for evaluation. Table 4.1 shows the statistical measurements for all, male and female femora. The intra-observer variation for the various DXA measurements are shown in table 4.2.

Table 4.1 - DXA measurements for all, female, and male femora (SD between brackets)

	all (n=76)	female (n=40)	male (n=36)
Neck BMC (g)	3.73 (1.45)	3.23 (1.02)	4.29 (1.64)**
Neck area (cm ²)	5.02 (0.72)	4.78 (0.61)	5.29 (0.76)*
Neck BMD (gcm ⁻²)	0.72 (0.20)	0.66 (0.16)	0.79 (0.22)*
Ward BMC (g)	1.69 (0.96)	1.36 (0.11)	2.06 (1.07)**
Ward area (cm ²)	2.81 (0.81)	2.51 (0.72)	3.13 (0.79)**
Ward BMD (gcm ⁻²)	0.56 (0.21)	0.50 (0.19)	0.62 (0.23)*
Trochanteric BMC (g)	9.96 (5.61)	8.21 (4.39)	11.94 (6.08)*
Trochanteric area (cm ²)	12.45 (4.94)	11.61 (4.40)	13.51 (0.86) ^{NS}
Trochanteric BMD (gcm ⁻²)	0.74 (0.20)	0.68 (0.15)	0.82 (0.23)*
T-score	-1.24 (1.43)	-1.37 (1.33)	-1.10 (1.54) ^{NS}

* p<0.05, **p<0.001, ^{NS} No significant difference compared to women.

Table 4.2 - Coefficient of variation and standard deviation for the DXA measurements.

	CV (%)	SD
Neck BMC (g)	3.45	0.136
Neck area (cm ²)	3.7	0.196
Neck BMD (gcm ⁻²)	1.63	0.012
Ward BMC (g)	10.63	0.202
Ward area (cm ²)	8.01	0.254
Ward BMD (gcm ⁻²)	6.45	0.036
Trochanteric BMC (g)	9.11	0.971
Trochanteric area (cm ²)	7.17	0.055
Trochanteric BMD (gcm ⁻²)	0.95	0.007

4.4 Discussion

The precision of our measurements varies; the BMD of the neck and trochanter show a good precision, comparable to data published previously⁴³. The BMD measurement of Ward's area has a low precision (6.45%), this may be attributed to the fact that positioning of this region of interest influences measurements to a great extent.

In the Rotterdam study, a prospective single center cohort study comprising all inhabitants of Ommoord (a Rotterdam suburb) aged 55 years or older on

January 1st 1990, femoral BMD values were assessed using the Lunar DPX-L⁴⁵⁻⁵⁰. The trochanteric BMD values assessed in our study were comparable with the data obtained in a corresponding age group of the Rotterdam study (table 4.3)⁴⁶. The BMD for femoral neck and Ward's area were significantly lower. However it must be stated that the Rotterdam study is an in-vivo study and that our study was performed in a water bath simulating soft tissue⁴².

Table 4.3 - Comparison of BMD assessed in our study with BMD found in the Rotterdam study, for a corresponding age group (between brackets SD)⁴⁶

Region of interest	female		male	
	Our study	Rotterdam study	Our study	Rotterdam study
Neck BMD (gcm ²)	0.66 (0.16)	0.76 (0.11)	0.79 (0.22)	0.87 (0.14)
Ward's BMD (gcm ²)	0.50 (0.19)	0.61 (0.13)	0.62 (0.23)	0.70 (0.16)
Trochanteric BMD (gcm ²)	0.68 (0.15)	0.70 (0.15)	0.82 (0.23)	0.84 (0.14)

Appendix 4 A
Mathematical considerations concerning DXA ²⁹

According to Beer's law the attenuation of an X-ray beam in a homogeneous material, depends on the composition of the material and the thickness of the material (equation A.1).

$$\text{eq A.1} \quad I_t = I_0 \cdot e^{-\mu d}$$

Using two energy levels two equations can be obtained and two variables can be calculated (equations A.2.1 & A.2.2).

$$\text{eq A.2.1} \quad I_t^L(x) = I_0^L \cdot e^{-\mu_s^L \sigma_s(x) - \mu_b^L \sigma_b(x)} \quad \text{eq A.2.2} \quad I_t^H(x) = I_0^H \cdot e^{-\mu_s^H \sigma_s(x) - \mu_b^H \sigma_b(x)}$$

Considering the areal densities of bone and soft tissue to be the unknown quantities, we can solve the two equations for the two unknowns (equations A.3.1 and A.3.2).

$$\text{eq A.3.1} \quad \sigma_b(x) = \frac{\left(\frac{\mu_s^L}{\mu_s^H}\right) \cdot \ln\left[\frac{I_t^H(x)}{I_0^H}\right] - \ln\left[\frac{I_t^L(x)}{I_0^L}\right]}{\mu_b^L - \mu_b^H \cdot \left(\frac{\mu_s^L}{\mu_s^H}\right)}$$

$$\text{eq A.3.2} \quad \sigma_s(x) = \frac{\ln\left[\frac{I_t^L(x)}{I_0^L}\right] - \left(\frac{\mu_b^L}{\mu_b^H}\right) \cdot \ln\left[\frac{I_t^H(x)}{I_0^H}\right]}{\mu_s^H \cdot \left(\frac{\mu_b^L}{\mu_b^H}\right) - \mu_s^L}$$

If we assume, for practical purposes, that lean tissue and fat are equally distributed throughout the soft tissue, we can measure the attenuation coefficients of soft tissue at two energy levels to calculate the areal density of bone. We can then use a 'R-factor' (equation A.4).

$$\text{eq A.4} \quad R_s = \frac{\mu_s^L}{\mu_s^H}$$

We can substitute this 'R-factor' into equation A.3.1 (equation A.5).

$$\text{eq A.5} \quad \sigma_b(x) = \frac{R_s \cdot \ln\left[\frac{I_t^H(x)}{I_0^H}\right] - \ln\left[\frac{I_t^L(x)}{I_0^L}\right]}{\mu_b^L - \mu_b^H \cdot R_s}$$

If a measurement is made at a given point x at which no bone is present then $\sigma_b=0$ and $I_{(x)}=I_{s(x)}$. Equation A.5 can be solved for R_s (equation A.6)

$$\text{eq A.6} \quad R_s = \frac{\ln\left[\frac{I_s^L}{I_0^L}\right]}{\ln\left[\frac{I_s^H}{I_0^H}\right]}$$

Using the following procedure R_s can be estimated and the BMD can be computed:

1. Estimating R_s by an 'educated guess', using an estimate of R_s from the first scan line.
2. Calculating bone at each point using equation A.5.
3. Separating measurements into bone and non-bone points by applying a threshold.
4. Calculate R_s using equation A.6 for each non-bone point.
5. Repeat steps 2 to 4 until R_s becomes stable
6. Smooth bone edges to eliminate noise generation.
7. Display bone and non-bone for operator approval.
8. Determine ROIs.
9. Calculate BMC by adding BMC values for each bone point within the ROI.
10. Determine the area by counting the bone points within the ROI
11. Calculate BMD as BMC/area.

Parameters

I_t =transmitted intensity (μSv)

I_0 =incident intensity (μSv)

μ =mass attenuation coefficient (cm^2g^{-1})

ρ = density (gcm^{-3})

d = thickness (cm)

σ =areal density (gcm^{-2})

H and L denote the energy level

4.5 References

1. Huddleston AA 1988 *Quantitative methods in bone densitometry*, 1 ed. Kluwer Academic publishers, Boston, pp 217.
2. van Berkum FNR, Pols HAP, Birkenhäger JC 1988 Niet invasieve meting van de botmassa en osteoporose. *Ned Tijdschr Geneesk* 132(49):2233-7.
3. Cohen ER, Giacomo P 1987 Symbols, units, nomenclature and fundamental constants in physics. International union of pure and applied physics, SUNAMCO commission.
4. Nederlands Meetinstituut 1996 Grootheden en meeteenheden. In: Druyvesteyn WF, Heijn J, Hoogenboom AM, Lingeman EWA, Stecher-Rasmussen F (eds.) *Gids '96. Nederlandse Natuurkundige Vereniging*, Amsterdam, pp 93-9.
5. Cameron JR, Sorensen J 1963 Measurement of bone mineral in vivo: An improved method. *Science* 143:230.
6. Bradley JG, Huang HK, Ledley RS 1978 Evaluation of calcium concentration in bones from CT scans. *Radiology* 128:103-7.
7. Gärdsell P, Johnell O, Nilsson BE 1990 The predictive value of forearm bone mineral content measurement in men. *Bone* 11:229-32.
8. Hassanger C, Borg J, Christiansen C 1989 Measurement of the subcutaneous fat in the distal forearm by single photon absorptiometry. *Metabolism* 38(2):159-65.
9. Health and public policy committee American college of physicians 1984 Radiologic methods to evaluate bone mineral content. *Ann Int Med* 100:908-11.
10. Mazess RB, Barden HS 1988 Measurement of bone by dual-photon absorptiometry (DPA) and dual-energy X-ray absorptiometry (DEXA). *Ann Chir Gynaecol* 77:197-203.
11. Oyster N, Smith FW 1988 A postmortem correlation of four techniques of assessment of osteoporosis with force of bone compression. *Calcif Tissue Int* 43:77-82.
12. Raymakers JA 1992 Meting van de botmassa. In: Duursma SA, Raymakers JA (eds.) *Veroudering van gonaden en bot*. Stichting Postuniversitair Onderwijs, Utrecht, pp 47-56.
13. van Kuijk C, Genant HK, Schütte HE 1992 Botdensitometrie en osteoporose. *Ned Tijdschr Geneesk* 136(25):1193-7.
14. Zamenhof RGA 1989 Techniques for bone mineral measurement. In: Tavares JM, Ferrucci JT (eds.) *Radiology, Diagnosis - Imaging - Intervention*, Revised edition 1989 ed. J.B. Lippincott comp., Philadelphia.
15. Mazess RB, Barden H, Vetter J, Ettinger M 1989 Advances in noninvasive bone measurement. *Ann Biomed Eng* 17:177-81.
16. Mazess R, Collick B, Trempe J, Barden H, Hanson J 1989 Performance evaluation of a dual-energy X-ray bone densitometer. *Calcif Tissue Int* 44:228-32.
17. Balseiro J, Fahey FH, Ziessman HA, Le TV 1988 Comparison of bone mineral density in both hips. *Radiology* 167:151-3.
18. Borders J, Kerr E, Sartoris DJ, Stein JA, Ramos E, Moscona AA, Resnick DA 1989 Quantitative dual-energy radiographic absorptiometry of the lumbar spine: In vivo comparison with dual-photon absorptiometry. *Radiology* 170:129-31.
19. Brailion P, Duboeuf F, Meary MF, Barret P, Demas PD, Meunier PJ 1989 Mesure du contenu minéral osseux par radiographie digitale quantitative: Premiers résultats au niveau vertébral lombaire. *Presse Med* 18(21):1062-5.
20. Cullum ID, Ryder JP, Ell PJ 1989 X-ray dual-photon absorptiometry: A new method for the measurement of bone density. *Br J Radiol* 62:587-92.
21. Eriksson S, Isberg B, Lindgren U 1988 Vertebral bone mineral measurement using dual

- photon absorptiometry and computed tomography. *Acta Radiol* 29:89-94.
22. Erman J, Ott SM 1993 Accuracy of dual-photon absorptiometry in excised femurs. *J Nucl Med* 29:1853-5.
 23. Gitter CC, Steiger P, Genant HK 1988 Validity of dual-photon absorptiometry. *Radiology* 166:574-5.
 24. Goodsitt MM, Murano R, Richardson ML 1989 A DPA technique for simultaneously measuring bone, soft tissue, and fat content. *Invest Radiol* 24(10):762-7.
 25. Krolner B, Nielsen SP 1980 Measurement of bone mineral content (BMC) of the lumbar spine. I: Theory and application of a new two dimensional dual-photon attenuation method. *Scan J Clin Lab Invest* 40:653-63.
 26. Krolner B, Nielsen SP, Lund B, Lund B, Sorensen OH, Uhrenholdt A 1980 Measurement of bone mineral content (BMC) of the lumbar spine. II: Correlation between forearm BMC and lumbar spine BMC. *Scan J Clin Lab Invest* 40:665-70.
 27. Reginster JY, Geusens P, Nijs J, Denis D, Franchimont P, Dequeker J 1989 In vivo long-term precision of spinal bone mass measurement by dual photon absorptiometry (letter). *Bone Miner* 6:225-9.
 28. Uebelhart D, Duboeuf F, Meunier PJ, Delmas PD 1990 Lateral dual-photon absorptiometry: A new technique to measure the bone mineral density at the lumbar spine. *J Bone Miner Res* 5(5):525-31.
 29. Wahner HW, Fogelmann I 1994 The evaluation of osteoporosis: Dual energy X-ray absorptiometry in clinical practice. In: Fogelmann I (ed.) *Metabolic bone disease*. University Press, Cambridge, pp 296.
 30. Blake GM, McKeeney DB, Chaya SC, Ryan PJ 1992 Dual-energy X-ray absorptiometry: The effect of beam hardening on bone density measurement. *Med Phys* 19(2):459-65.
 31. Peppler WW, Mazess RB 1981 Total body bone mineral and lean body mass by dual-photon absorptiometry. I: Theory and measurement procedure. *Calcif Tissue Int* 22:353-9.
 32. van Kuijk C, Hagiwara S, Genant HK 1994 Radiologic assessment of osteoporosis. *J Musculoskeletal Med* April:25-32.
 33. WHO study group 1994 Assessment of fracture risk and its application to screening for postmenopausal osteoporosis. WHO Technical reports series, Geneva.
 34. Pearson J, Dequeker J, Reeve J, D. F, Henley M, Bright J, Lunt M, Adams J, Diaz Curiel M, Geusens P, Jaeger P, Kröger H 1995 Dual X-ray absorptiometry of the proximal femur: Normal European values standardized with the European spine phantom. *J Bone Miner Res* 10(2):315-24.
 35. Ravn P, Hetland ML, Overgaard K, Christiansen C 1994 Premenopausal and postmenopausal changes in bone mineral density of the proximal femur measured by dual-energy X-ray absorptiometry. *J Bone Miner Res* 9(12):1975-80.
 36. Rizzolli R, Slosman D, Bonjour JP 1995 The role of dual energy X-ray absorptiometry of lumbar spine and proximal femur in the diagnosis and follow-up of osteoporosis. *Am J Med* 98(suppl 2A):33-6.
 37. Netelenbos JC, Lips P 1996 Botdichtheidsmeting en de preventie van fracturen: Wie komen hiervoor in aanmerking? *Ned Tijdschr Geneesk* 140(20):1061-4.
 38. Formica C, Loro ML, Gilsanz V, Seeman E 1995 Inhomogeneity in body fat distribution may result in inaccuracy in the measurement of vertebral bone mass. *J Bone Miner Res* 10(10):1504-1511.
 39. Hangartner TN, Johnston CC 1990 Influence of fat on bone measurement with dual-

- energy absorptiometry. *Bone Miner* 9:71-81.
40. Kuiper JW, van Kuijk C, Grashuis JL, Ederveen AGH, Schütte HE 1996 Accuracy and the influence of marrow fat on quantitative CT and dual-energy X-ray absorptiometry measurements of the femoral neck in vitro. *Osteoporosis Int* 6:23-30.
 41. Tothill P, Avenell A 1994 Errors in dual-energy X-ray absorptiometry of the lumbar spine owing to fat distribution and soft tissue thickness during weight change. *Br J Radiol* 67:71-5.
 42. Tothill P, Hannan WJ, Cowen S, Freeman CP 1997 Anomalies in the measurement of changes in total-body bone mineral by dual-energy X-ray absorptiometry during weight change. *J Bone Miner Res* 12(11):1908-21.
 43. Genant HK, Engelke K, Fuerst T, Glüer CC, Grampp S, Harris ST, Jergas M, Lang T, Majumdar S, Mathur A, Takada M 1996 Noninvasive assessment of bone mineral and structure: State of the art [review]. *J Bone Miner Res* 11(6):707-30.
 44. Arnaudo JS 1992 Draft guidance for review of bone densitometers 510(k). In: *Guide to clinical trials*. Raven, New York, pp 24-7.
 45. Burger H, van Daele PLA, van den Ouweland FA, Grobbee DE, Hofman A, van Kuijk C, Schütte HE, Birkenhäger JC, Pols HAP 1994 The association between age and bone mineral density in men and women aged 55 years and over: The Rotterdam study. *Bone Miner* 25:1-13.
 46. Burger H 1995 Epidemiological studies on bone mineral density and fractures [dissertation] *Epidemiology*. Erasmus University, Rotterdam, pp 111.
 47. Burger H, van Daele PL, Odding E, Valkenburg HA, Hofman A, Grobbee DE, Schütte HE, Birkenhäger JC, Pols HA 1996 Association of radiographically evident osteoarthritis with higher bone mineral density and increased bone loss with age. The Rotterdam study. *Arthritis Rheum* 39(1):81-6.
 48. de Laet CE, van Hout BA, Burger H, Hofman A, Pols HA 1997 Bone density and risk of hip fracture in men and women: Cross sectional analysis. *BMJ* 315(7102):221-5.
 49. Stolk RP, van Daele PL, Pols HA, Burger H, Hofman H, Birkenhäger JC, Lamberts SW, Grobbee DE 1996 Hyperinsulinemia and bone mineral density in an elderly population: The Rotterdam study. *Bone* 18(6):545-9.
 50. van Daele PLA 1996 Prediction of osteoporotic fractures; the Rotterdam study [dissertation] *Epidemiology*. Erasmus University, Rotterdam, pp 123.

Chapter 5

Volumetric quantitative computed tomography

The most exciting phrase to hear in science, the one that heralds new discoveries, is not 'Eureka!' but 'That's funny...'

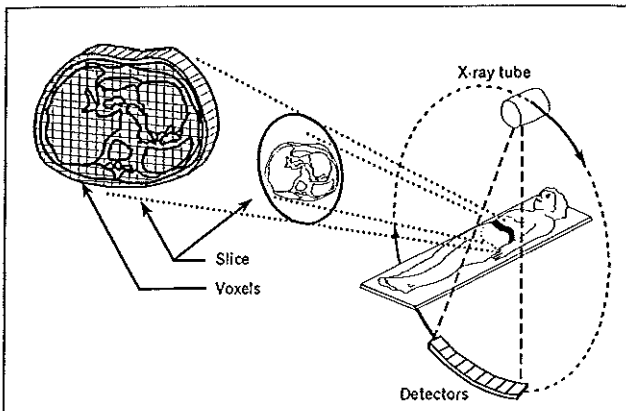
Isaac Asimov

5.1 Introduction

Computed tomography (CT) is based on the mathematical principle that the internal structure of an object can be reconstructed from multiple projections of this object^{1,2}. Along the scan lines, from the X-ray source to the detectors, the photon attenuation of a thin slice of tissue can be measured. Using these measurements, a photon attenuation map can be reconstructed. Although CT scans are usually regarded as two-dimensional representations of an object, the actual reconstructed picture elements or 'pixels' represent three-dimensional volumes or 'voxels' (figure 5.1)³.

In CT, the linear attenuation coefficients of each voxel can be reconstructed. The CT attenuation is expressed in Hounsfield units (HU), named after Sir Godfrey Newbold Hounsfield (1919-) Nobel prize winner and one of the pioneers in the field of CT (equation 5.1)^{4,6}.

$$\text{eq 5.1} \quad HU = 1000 \cdot \frac{\mu_{\text{object}} - \mu_{\text{water}}}{\mu_{\text{water}}}$$



Where HU= Hounsfield unit, μ = linear attenuation coefficient of material under consideration, μ_w = linear attenuation coefficient of water. By definition the HU for water is 0 and for air it is -1000, all other tissues are related to these two substances. Tissues which

Figure 5.1 - Principle of CT scanning

attenuate the photon beam less than water have a negative HU and tissues which attenuate the photon beam more than water have a positive HU^{7,8}. Partial volume effects in CT must be taken into account when quantitative measurements are performed on CT data. Partial volume effects occur when a voxel is composed of two or more different tissues. Under those circumstances the resulting linear attenuation coefficient will be proportional to the equivalent of the linear attenuation coefficients of the composing tissues. In a study performed by Horrocks and Speller a significant difference was found between phantom data obtained by sequential and spiral CT, as a result of increased partial volume effects⁹. The authors stated in their discussion that 'quantitative CT analysis in clinical work would be affected'.

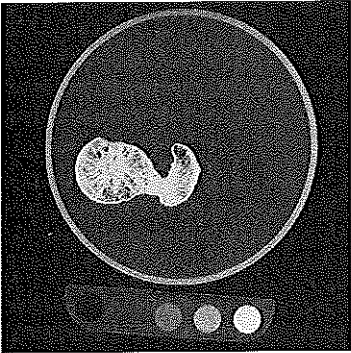
The use of CT to measure bone mass, later known as quantitative computed tomography (QCT), was originally proposed in 1977 by H.K. Genant and D. Boyd¹⁰. Within an object a region of interest (ROI) is selected. The average CT number of this ROI can then be compared with the CT number of a phantom with a known concentration of hydroxyapatite¹¹. The measured BMD is expressed as equivalent hydroxyapatite per cubic centimetre (Hap cm⁻³). This value is independent of the size of the object and therefore is a proper mass density¹². The main improvement of QCT over DXA is the ability of QCT to separate cortical and trabecular bone¹³⁻¹⁷. The precision of this technique is reported to be 2-4%. The examination time is 10-15 min. during which the patient receives an estimated effective dose equivalent of 50-100 μ Sv¹⁶.

To date, QCT has clinically only been used for BMD measurements of the lumbar spine and radius. These measurements are performed using single-slice QCT techniques. The implementation in femoral BMD has been hindered by the intricate geometry of the proximal femur, making reproducible slice placement very difficult¹⁸. The use of volumetric QCT has been proposed by several investigators to alleviate this problem^{19,20}. However, there are no systems available for the measurement of femoral BMD, in a clinical setting. Recently Lang et al. (Osteoporosis and Arthritis Research Group, University of California, San Francisco, USA) presented an experimental semi-automated image analysis procedure, to determine regional BMD and geometry measurements from volumetric QCT scans of the proximal^{21,22}. This image processing technique, using volumetric data, analyses the proximal femur geometry to extract femoral neck and trochanteric volumes of interest for densitometric and geometric analysis. The volumetric data may be obtained either by contiguous-slice or spiral CT techniques. Because of reduced scan time, which improves patient comfort and decreases the risk of patient motion, the spiral technique is highly attractive.

The aim of this chapter is: a) to provide densitometric data on our cadaver femora, and b) to determine whether spiral versus sequential scanning influences femoral QCT BMD measurements. As DXA is currently the most

Figure 5.2 - CT slice through the proximal femur, placed within a water bath. The reference phantom is visible underneath the water bath.

widely used technique in a clinical setting for measuring areal BMD, a linear regression analysis was performed between DXA (as presented in chapter 4) and QCT.



5.2 Materials and methods

Femora

A total of seventy-six femora, median age 82.9 years (range 54.3-98.7 years), were used in this study. All femora were ex-articulated in the hip and excised, about two hand-widths above the knee. After removal of surrounding soft tissue the femora were kept in a phenol/formaldehyde solution. Prior to investigation, they were thoroughly degassed under water in a vacuum desiccator. During scanning the femora were placed in a cylindrical container containing water, thus simulating soft tissue while at the same moment keeping the specimen air free.

Quantitative computed tomography

The femora were imaged first with thirty-six sequential slices and subsequently with the same number of spiral slices (slice thickness 3 mm, 3 mmsec⁻¹ table speed) covering the identical anatomical region. Measurements were performed on a GE prospeed S-fast (General Electric, Milwaukee, WI, USA) with a single-energy technique at 120 kV and 400 mAs. During scanning the femora were placed in a cylindrical container containing water, on the one hand simulating soft tissue, on the other hand to keep the specimen free from encapsulated air. Calibration of the CT image was achieved by simultaneous scanning of a calibration phantom (Image Analysis Inc., Columbia, KY, USA) containing various inserts of solid hydroxyapatite-equivalent material (200, 100, 50, 0 mgcm⁻³ Hap) (figure 5.2).

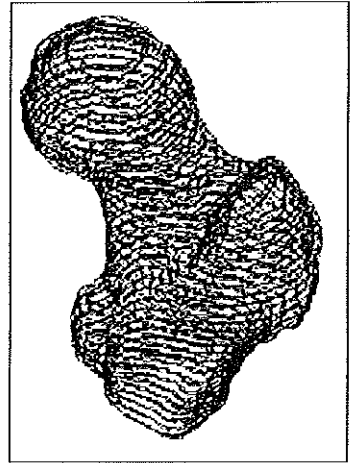
The data were stored on optical disk (OD, Pioneer DEC-702) after which it was transferred to advantage windows format and subsequently stored on digital audio tape (DAT, Maxell HS-4/60s, 4 mm). This was necessary since nearly all CT systems in Europa are equipped with ODs and in the USA, where image analysis took place, they are usually equipped with DAT readers only. The advantage windows format was needed by the image analysis software.

Image analysis ²¹

Image analysis was conducted at the Osteoporosis and Arthritis Research Group, UCSF, using in-house developed routines for AVS (Advanced Visual Systems Inc., Waltham, MA, USA) running on a Sun Sparc station 20 (Sun

Figure 5.3 - Binary model of the proximal femur generated from contours (courtesy of T.F. Lang, OARG, UCSF)

Microsystems Inc. Mountain view, CA, USA). Volumetric QCT data was mapped using an interactive threshold driven contour tracking algorithm at a threshold of 76 HU. The external contours of each of the 36 slices were used to generate a three dimensional binary model of the proximal femur (figure 5.3). The data were calibrated, converting HU to BMD (mgcm^{-3} Hap), using the calibration phantom. For calibration we used the first and last slice of each data set, thus ensuring a representative calibration for all 36 scans of each femur.



After mapping and calibration, the CT and binary data were interactively reformatted along the direction of the femoral neck axis. Operator interaction is needed to define the femoral neck axis on the coronal and the sagittal reformatted data set. The binary data were used in an automated process, that determines fixed volumes of interest (VOIs) for the determination of BMD and BMC. This algorithm operates by determining the cross-sectional femoral area along the femoral neck axis. This results in a map of cross-sectional area versus femoral neck position, showing two maxima corresponding to two landmarks: the mid-plane of the femoral head and the intertrochanteric plane (figure 5.4). Using this data it is possible to define the femoral neck VOI. The medial limit was set at 75% and the lateral limit at 25% of the distance between the intertrochanteric and femoral head maxima. A trochanteric VOI was defined by the lateral limit of the neck region and the lateral maximum of the cross-sectional area curve. The neck VOI and trochanteric VOI can be combined to yield the proximal femoral VOI (figure 5.5). The VOIs used in volumetric QCT do not coincide with the area in DXA for the assessment of femoral neck and trochanteric BMD.

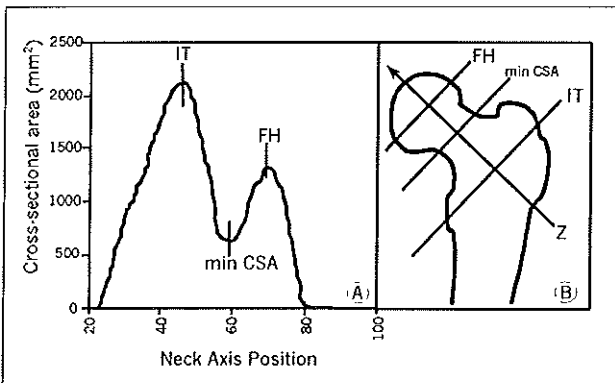


Figure 5.4

A. Plot of the proximal femur cross-sectional area versus the position along the femoral axis. FH indicates the femoral head maximum, MinCSA the minimal cross-sectional area, and IT indicates the intertrochanteric maximal cross-sectional area.
 B. Graphical representation of the Z-axis of the proximal femur.

(courtesy of T.F. Lang, OARG, UCSF)

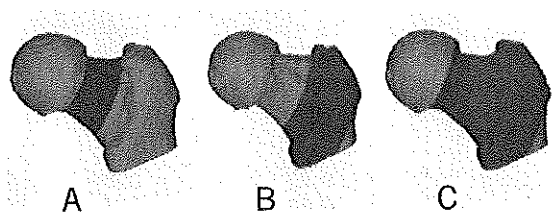


Figure 5.5 - Isosurface reconstruction of a QCT image of the proximal femur

Grey areas represent: A. the femoral neck - B. trochanteric - C. total proximal femur volumes of interest

(courtesy of T.F. Lang, OARG, UCSF)

Trabecular VOIs can be extracted from the integral VOIs by a 4 mm erosion of the external contours, residual cortical bone was removed by applying a 350 mgcm^{-3} Hap global threshold. The threshold eliminated the femoral calcar and any cortical bone left in the ROI. Subtraction of trabecular VOIs from integral VOIs yielded cortical VOIs, these VOIs were thresholded at 100 mgcm^{-3} Hap to remove all trabecular bone and partial volumes.

Simultaneously we assessed geometrical parameters, first the femoral neck axis length (FNAL_{QCT}), defined as the length of the line between the medial limit of the femoral head and the base of the trochanter. Secondly, the minimum cross-sectional area (minCSA), ie. the smallest area along the femoral neck axis. Finally the moments of inertia (x, y) of the minimum cross-sectional area were calculated (see chapter 6).

Statistical analysis

Intra observer variance was tested according to the guidelines stated by the FDA ²³. A Student's t-test was performed to test for differences between BMD values obtained by sequential and spiral techniques. To test the correlation between QCT and DXA a linear regression analysis was performed. The tests were performed using SPSS (version 7.5.2, SPSS inc., Chicago, USA).

5.3 Results

Table 5.1 shows the intra observer variance for the measurements. Table 5.2 shows the sequential QCT data for the 70 data sets that could be analysed. Due to technical problems, in transferring data from OD to DAT, in six cases the sequential QCT data could not be evaluated. For seven cases the spiral data could not be analysed. Significant differences between male and female femora were found for total trabecular, neck trabecular, trochanteric trabecular BMD ($p < 0.05$), minimal cross-sectional area and minimum moment of inertia along the x and y axis ($p < 0.001$). We found no significant differences between measurements obtained with sequential and spiral techniques, as demonstrated in table 5.3. The correlations between sequential QCT and DXA measurements were all highly significant ($p < 0.001$, table 5.4).

Table 5.1. - Intra observer variance (CV%) assessed using sequential data (n=10 and repetition=2)

Measurement	CV%
Integral BMD (gcm ⁻³)	1.01
Trabecular BMD (gcm ⁻³)	0.72
Cortical BMD (gcm ⁻³)	0.92
Neck integral BMD (gcm ⁻³)	3.89
Neck trabecular BMD (gcm ⁻³)	1.5
Neck cortical BMD (gcm ⁻³)	1.42
Trochanteric integral BMD (gcm ⁻³)	0.46
Trochanteric trabecular BMD (gcm ⁻³)	0.91
Trochanteric cortical BMD (gcm ⁻³)	1.82
Femur neck axis length (mm)	3.7

Table 5.2 Means, standard deviation and differences between female and male sequential QCT measurements

Measurement	All femora (n=70)		Female femora (n=36)		Male femora (n=34)		p value
	Mean	SD	Mean	SD	Mean	SD	
Integral BMD ¹	213.74	63.5	204.23	60.9	223.81	65.5	0.199
Cortical BMD	396.02	58.1	390.46	54.7	401.91	61.8	0.414
Trabecular BMD	111.59	36.9	102.13	30.9	121.61	40.3	0.026
Neck integral BMD	207.71	60.4	199.95	58.9	215.92	61.7	0.272
Neck cortical BMD	354.77	52.2	350.24	52.3	359.6	52.4	0.459
Neck trabecular BMD	118.56	39.4	108.31	33.7	129.42	42.5	0.024
Trochanteric integral BMD	225.34	68.3	215.21	64.5	236.06	71.5	0.204
Trochanteric cortical BMD	432.6	69.8 4	25.34	63.1	440.29	76.1	0.374
Trochanteric trabecular BMD	105.54	37.7	96.4	30.9	115.21	40.1	0.031
Femoral neck axis length (mm)	50.48	4.8	49.89	4.7	51.11	5	0.292
Min CSA (mm ²)	1048.58	160.3	945.25	114.9	1157.99	86.5	0.001
Minimum CSMI-X (mgmm ²)	26105.85	11895.6	19952.2	47265.4	32621.45	12443.4	<0.001
Minimum CSMI-Y (mgmm ²)	19849.48	10220.1	15096	6051	24882.62	11349.6	<0.001

* significant difference between male and female femora.

¹ All BMD measurements in mgcm⁻³, Min CSA = minimum cross-sectional area, CSMI = Cross-sectional moment of inertia.

5.4 Discussion

Quantitative computed tomography is considered the best technique for determining BMD^{24,25}. The strength of this technique is its capability of measuring true volumetric BMD, in grams per cubic centimetre, as well as separately assessing trabecular and cortical bone. The disadvantage of QCT is the relatively high effective dose equivalent and the high costs of scanning compared to DXA. The clinical use of QCT has so far been limited to measurements of the spine and radius²⁴.

Table 5.3 - Means, standard deviation and differences between spiral and sequential QCT measurements (n=69)

Measurement	Spiral/Sequential				p-value
	Mean	SD	Mean	SD	
Integral BMD ¹	210.95	64.5	214.6	63.5	0.734
Trabecular BMD	114.2	37.1	112.09	36.9	0.739
Cortical BMD	385.9	54.6	396.65	58.3	0.265
Neck integral BMD	202.96	60.9	208.5	60.4	0.591
Neck trabecular BMD	123.33	39.9	119.2	39.3	0.537
Neck cortical BMD	341.91	49.9	355.24	52.4	0.128
Trochanteric integral BMD	222.75	66.9	226.3	68.4	0.758
Trochanteric trabecular BMD	107.84	37	106.01	36.7	0.772
Trochanteric cortical BMD	420.19	66.2	433.3	70	0.26
Femoral neck axis length	50.17	4.6	50.5	4.9	0.676
Min CSA (mm ²)	1064.35	169.3	1049.76	161.2	0.605
Minimum CSMI-X (mgmm ²)	26146.94	11994	26163.94	11973	0.993
Minimum CSMI-Y (mgmm ²)	32592.85	86925	32311.15	85547	0.985

¹ All BMD measurements in mgcm⁻³, Min CSA = minimum cross-sectional area, CSMI = Cross-sectional moment of inertia.

Implementation in the hip has been hindered by the intricate geometry of the hip compared to the spine ¹⁸. However, using new software available today, implementation of hip BMD measurements is possible in a clinical setting. The technique, described in this chapter, has a high in-vitro precision, coefficient of variance (CV) ranging from 0.49 to 3.89% (table 1). These results correspond well with those found in-vivo by Lang et al. ²¹. These CVs are also comparable to those found in our in-vitro DXA study (as presented in chapter 4).

Our results show that both techniques, spiral and sequential, are equivalent in the measurement of hip BMD. Although none of the differences between spiral and sequential reached significance, a trend towards a lower level of significance of all cortical measurements was seen. This result might indicate that as cortical bone has a smaller volume and a higher density, it is more sensitive to partial volume effects. Furthermore, our data show a highly significant correlations between DXA and QCT measurements (all correlations p<0.001) (table 5.4).

Using spiral scan protocols instead of sequential scan protocols allows for shorter scan times, promoting higher patient comfort and lower operating costs (as more patients can be measured in a given time span). As trabecular bone, which can be assessed separately, has a higher metabolic activity compared to cortical bone, QCT would be a more sensitive method to

Table 5.4 - Pearson's correlation between QCT and DXA measurements (for all correlations p<0.001)

QCT	DXA			
	Neck BMD ²	Trochanteric BMD	Ward BMD	T-score
Integral BMD ¹	0.823	0.829	0.82	0.835
Cortical BMD	0.736	0.764	0.726	0.752
Trabecular BMD	0.867	0.858	0.856	0.848
Neck integral BMD	0.868	0.791	0.835	0.87
Neck cortical BMD	0.79	0.754	0.759	0.817
Neck trabecular BMD	0.87	0.778	0.851	0.835
Trochanteric integral BMD	0.78	0.818	0.793	0.798
Trochanteric cortical BMD	0.696	0.744	0.692	0.711
Trochanteric trabecular BMD	0.838	0.858	0.835	0.824

¹ All QCT BMD measurements in mgcm⁻³, ² All DXA BMD measurements in gcm⁻²

monitor changes over time. Generally QCT studies have shown a higher sensitivity in the diagnosis of spinal osteoporosis and in monitoring therapeutic effects ^{26,27}. This makes QCT a potentially strong technique to be used in follow-up intervention studies.

5.5 References

1. Currey III TS, Dowdey JE, Murry jr RC 1990 Computed tomography. In: Christensen's physics of diagnostic radiology, 4th ed. Lea & Febiger, Philadelphia / London, pp 289-322.
2. Hounsfield GN 1973 Computerized transverse axial scanning (tomography). Br J Radiol 46:1016.
3. McCullough EC 1977 Factors affecting the use of quantitative information from a CT scanner. Radiology 124:99-107.
4. Eisenberg RL 1992 Computed Tomography. In: Radiology; an illustrated history. Mosby Year Book, St. Louis, pp 467-71.
5. Hounsfield GN 1980 Computed medical imaging; Nobel lecture, December 8, 1979. J Comput Assist Tomogr 4(5):665-74.
6. Mould RF 1993 Diagnostic radiology: VI. In: A century of X-rays and radioactivity in medicine: With emphasis on photographic records of the early years. Institute of Physics Publishing, London, pp 92-5.
7. Brooks RA, Mitchell LG, O' Connor CM, di Chiro G 1981 On the relationship between computed tomography numbers and specific gravity. Phys Med Biol 26(1):141-7.
8. Hawkes DJ, Jackson DF 1980 An accurate parametrisation of the X-ray attenuation coefficient. Phys Med Biol 25(6):1167-71.
9. Horrocks JA, Speller RD 1994 Helical computed tomography: Where's the cut? Br J Radiol 67(793):107-11.
10. Genant HK, Boyd D 1977 Quantitative bone mineral analysis using dual-energy computed tomography. Invest Radiol 12(6):545-51.
11. Kalender WA, Suess C 1987 A new calibration phantom for quantitative computed tomography. Med Phys 14(5):863-6.
12. Cohen ER, Giacomo P 1987 Symbols, units, nomenclature and fundamental constants in physics. International union of pure and applied physics, SUNAMCO commission.
13. Tothill P 1989 Methods of mineral measurement (review article). Phys Med Biol 34(5):543-72.
14. van Kuijk C 1991 Evaluation of postprocessing dual-energy quantitative computed tomography [dissertation] Department of Experimental Radiology. Erasmus University, Rotterdam, pp 115.
15. van Kuijk C, Genant HK, Schütte HE 1992 Botdensitometrie en osteoporose. Ned Tijdschr Geneesk 136(25):1193-7.
16. van Kuijk C, Hagiwara S, Genant HK 1994 Radiologic assessment of osteoporosis. J Musculoskeletal Med April:25-32.
17. Zamenhof RGA 1989 Techniques for bone mineral measurement. In: Tavares JM, Ferrucci JT (eds.) Radiology, Diagnosis - Imaging - Intervention, Revised edition 1989 ed. J.B. Lippincott comp., Philadelphia.
18. Kuiper JW, van Kuijk C, Grashuis JL 1997 Distribution of trabecular and cortical bone related to geometry; a quantitative computed study of the femoral neck. Invest Radiol 32(2):83-9.
19. Bhasin S, Sartoris DJ, Fellingham L, Zlatkin MB, Andre M, Resnick D 1988 Three-dimensional quantitative CT of the proximal femur: Relationship to vertebral bone density in postmenopausal women. Radiology 167:145-9.
20. Sartoris DJ, Andre M, Resnick C, Resnick D 1986 Trabecular bone density in the proximal femur: Quantitative CT assessment. Radiology 160:707-12.

21. Lang TF, Keyak JH, Heitz MW, Augat P, Lu Y, Mathur A, Genant HK 1997 Volumetric quantitative computed tomography of the proximal femur: Precision and relation to bone strength. *Bone* 21(1):101-8.
22. Lang T, Heitz M, Keyak J, Genant HK 1996 A 3D anatomic coordinate system for hip QCT. *Osteoporosis Int* 6(suppl 1):203.
23. Arnaudo JS 1992 Draft guidance for review of bone densitometers 510(k). In: *Guide to clinical trials*. Raven, New York, pp 24-7.
24. Genant HK, Engelke K, Fuerst T, Glüer CC, Grampp S, Harris ST, Jergas M, Lang T, Majumdar S, Mathur A, Takada M 1996 Noninvasive assessment of bone mineral and structure: State of the art [review]. *J Bone Miner Res* 11(6):707-30.
25. Fujii Y, Chikawa T, Nakamura T, Goto B, Fujita T 1996 Comparison of trabecular bone density at vertebral and radial sites using quantitative computed tomography. *Osteoporosis Int* 6(6):486-90.
26. Berning B, van Kuijk C, Kuiper JW, Coelingh Bennink HJT, Kicovic PM, Fauser BCJM 1996 Effect of two doses of Tibolone on trabecular and cortical bone loss in early postmenopausal women: A two-year randomized, placebo-controlled study. *Bone* 19(4):395-9.
27. Grampp S, Genant HK, Mathur A, Lang P, Jergas M, Takada M, Glüer CC, Chavez M 1997 Comparison of noninvasive bone mineral measurements in assessing age related loss, fracture discrimination, and diagnostic classification. *J Bone Miner Res* 12(5):697-711.

Chapter 6

Biomechanics of the hip

Nature, and nature's laws lay hid in the night.
God said: 'let there be Newton! And all was light

Alexander Pope

6.1 Introduction

In this chapter we will discuss the biomechanics of the hip. In three paragraphs the following items will be presented:

1. Paragraph 6.2 gives an overview of the basic (bio)mechanical terms related to this study.
2. The biomechanics of the hip of a person in one-legged stance are discussed in paragraph 6.3.
3. The final paragraph (6.4) describes a theoretical model of a fall directed sideways. Using this model a rough estimate of the peak force during a fall can be calculated.

6.2 Basic biomechanical terms

Hatze defined biomechanics as 'the study of the structure and function of biological systems by means of the methods of mechanics'¹. It observes and describes motions and forces (intrinsic and external) of biological systems, such as the human body. As a science biomechanics dates back to Galileo Galilei (1564-1642), who was the first to publish a book on this subject 'Discorsi, e dimostrazioni matematiche, intorno a due nuove scienze attenenti alla mecanica, e i movimenti locali' (dialogues and mathematical demonstrations concerning two new sciences pertaining to mechanics and locomotion; 1638, Elsevier, The Netherlands)².

Biomechanics is based on the standard laws of physics. Here, we will restrict ourselves to the description of the basics of mechanics as relevant to this dissertation^{3,9}. For the interested reader, there are several excellent text books on (bio)mechanics and its applications in medicine^{10,11}.

6.2.1 Newton's laws

The name of Sir Isaac Newton (1643-1727) is inherently associated with the field of mechanics, as it was he who postulated the three main laws of mechanics in his book 'Philosophiae Naturalis Principia Mathematica' (1687)¹². His importance is underlined by the fact that the unit of force, newton, is named after this famous scientist.

When we push or pull a body, we exert on it a force F . Forces can also be exerted by inanimate objects, e.g. a spring. Force is a physical vectorial quantity that requires a specification of a magnitude as well as a direction in space. The line of action is a line of infinite length, on which the vector force is a segment. The point where the tail of the vector intersects with the object is called the point of application. This vector quantity is graphically represented as an arrow. Forces may be added and resolved using vector calculus. Force is expressed in newton (N), where one newton equals the force which gives a standard mass of one kg an acceleration of one ms^{-2} . When a body is in equilibrium (not necessarily a state of rest) the resultant of all forces acting on it is zero. Thus if two forces act on a body and a state of equilibrium is present, they must have the same line of action, but in opposite direction. When there are three or more forces acting on a body, and a state of equilibrium is present, they must be concurrent. This is Newton's first law of motion.

The rate of change of the velocity of a body, i.e. its acceleration (a), is equal to the resultant of all external forces exerted on the body divided by the mass (m) of the body, and is in the same direction as the resulting force. This is Newton's second law of motion.

It is very important to keep in mind that whenever a body exerts a force on an other body, the second always exerts a force which is equal in absolute magnitude, opposite in direction, and along the same line of action. This is Newton's third law of motion.

Each force gives rise to a moment (M), the moment or lever arm of a body is the perpendicular distance from an arbitrarily chosen origin to the action line of a force acting on this body. The moment of the resultant of two forces equals the sum of the moments of these two forces (Varignon's theorem). For a body to be in equilibrium, the resulting moment of all external forces, about any axis, has to be zero.

6.2.2 Pendulum

If a body, attached to a cord or shaft of length R , attached in point O , moves in a two-dimensional vertical plane, its motion is not uniform. The forces acting on such a body are the gravitational force (F_g) and the tension in the

cord/shaft (T). These forces can be resolved into two components. The component normal to the circle of motion, gives us a normal force, better known as the centripetal force (equation 6.1).

$$\text{eq 6.1} \quad F_n = T - F_g \cdot \cos \alpha$$

Where α is the angle of deflection from the normal. The second component is the tangential component, gives us a tangential force (F_t) (equation 6.2).

$$\text{eq 6.2} \quad F_c = F_g \cdot \sin \alpha$$

This force changes the magnitude of the velocity. The tangential acceleration can be deduced from Newton's second law (equation 6.3).

$$\begin{aligned} a_t &= \frac{F_t}{m} \\ &\Downarrow \\ \text{eq 6.3} \quad a_t &= \frac{(m \cdot g \cdot \sin \alpha)}{m} \\ &\Downarrow \\ a_t &= g \cdot \sin \alpha \end{aligned}$$

At the lowest point of the circular motion the angle (α) equals zero, therefore the tangential acceleration will be zero. Since the tangential acceleration is not constant but proportional to the sine of the angle α , we cannot use these equations to calculate the speed at any given moment. This has to be done using energy considerations.

6.2.3 Energy

Each moving body has a certain amount of kinetic energy (E_k). By definition this is one-half the product of the mass of a body times the square of the magnitude of its velocity (equation 6.4).

$$\text{eq 6.4} \quad E_k = \frac{1}{2} \cdot m \cdot v^2$$

In the gravitational field each body has potential energy (E_p), this is the product of the weight of the body (mg) and the height (h) of its centre of gravity, above a reference level (equation 6.5).

$$\text{eq 6.5} \quad E_p = m \cdot g \cdot h$$

Using the kinetic and potential energy the work (W) to bring an object from state 1 to 2, can be calculated (equation 6.6).

$$\begin{aligned} W &= (E_{k2} - E_{k1}) + (E_{p2} - E_{p1}) \\ \text{eq 6.6} \quad &\Downarrow \\ W &= \left(\frac{1}{2} \cdot m \cdot v_2^2 - \frac{1}{2} \cdot m \cdot v_1^2\right) + (m \cdot g \cdot h_2 - m \cdot g \cdot h_1) \end{aligned}$$

Work is done, when a force is exerted on a body while this body moves in such a way that the force has a component along the line of motion. Work is said to be positive, if this component is in the same direction as the displacement and negative when it is in an opposite direction. If the only force which acts on a body is gravity, work is zero. Using equation 6.6 the speed of a body in a circular vertical motion can be calculated.

6.2.4 Impulse

Forces which act in a short duration of time, e.g. collisions or explosions, are said to be impulsive forces. The impulse (p) is the integral of a force in time (equation 6.7).

$$\begin{aligned} p &= \int_{t_2}^{t_1} F \cdot dt \\ &\Downarrow \\ \text{eq 6.7} \quad p &= \int_{t_2}^{t_1} m \cdot a \cdot dt \\ &\Downarrow \\ p &= m \cdot v_2 - m \cdot v_1 \end{aligned}$$

6.2.5 Moment of inertia (see appendix 6-B)

If a body is forced to rotate about an axis, its tendency to resist angular acceleration depends on the body's mass moment of inertia (I) (equation 6.8).

$$\text{eq 6.8} \quad I = m \cdot r^2$$

Consider a rod length (l) and mass (m) which is rotated around its centre of gravity. The moment of inertia in this case is given by equation 6.9.

$$\text{eq 6.9} \quad I = \frac{1}{12} \cdot m \cdot l^2$$

If the rotation of the same rod would be around the end of the rod its moment of inertia would be (equation 6.10).

$$\text{eq 6.10} \quad I = \frac{1}{3} \cdot m \cdot l^2$$

If we consider a thin slice of material, with radius r , then the moment of inertia is given by the following equation (equation 6.11 and 6.12).

$$\text{eq 6.11} \quad I_x = \frac{1}{4} \cdot m \cdot r^2$$

$$\text{eq 6.12} \quad I_y = \frac{1}{4} \cdot m \cdot r^2$$

6.2.6 Load

If a load is applied to an object, deformation will occur. Load and deformation can be plotted against each other resulting in a load-deformation diagram (figure 6.1). For small deformations Hooke's law applies: the deformation is proportional to the applied load (elastic region). If the load exerted on the object is increased further the deformation becomes permanent and the material yields (plastic region). The yield point separates the elastic from the plastic region. Further increase of load will result in fracture.

The area under the load-deformation curve is a measure of the energy needed to cause a fracture, this is called the energy absorption or toughness. The load at the yield point is also known as the yield strength. The maximal load a material can sustain is called the ultimate strength. The breaking strength is the load at which a material actually fractures. It's worth nothing that the ultimate strength and the breaking strength do not necessarily coincide.

6.3 Biomechanics of the hip during one-legged stance

The construction of the proximal part of the femur is a compromise to its pure function as a weight bearing instrument. This is caused by the need of mobility of the hip joint and its relation to other joints such as the knee and the pelvic girdle¹³. During normal stance each hip will be loaded with approximately one third of the body weight (each leg weighing approximately one sixth of the total body weight, therefore each hip will be loaded with half of the remaining body weight, two thirds of the total body weight)⁴.

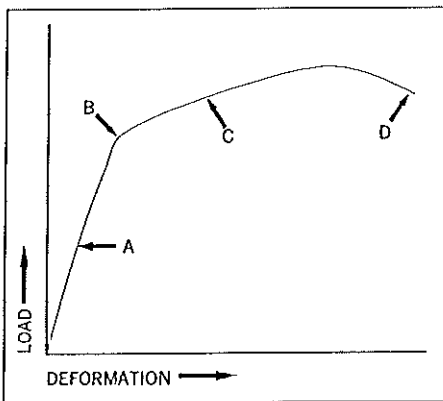


Figure 6.1 - Load deformation curve

- A. elastic area
- B. yield point
- C. plastic area
- D. fracture point

During one legged stance the load increases to approximately 2.5 times body weight (as explained later), during walking 2.8 times and while running it increases to 4-5 times body weight. The maximum load which a normal hip can sustain in vitro is approximately 12-15 times body weight^{13,14}.

Before describing the forces which act on the hip, we will take a closer look at the geometry and structure of the proximal femur. The proximal femur acts like a cantilever beam, loading of the femoral head will therefore cause flexion in the femoral shaft. Due to this process compression forces will occur on the medial side of the femur and tensile forces on the lateral side^{15,16}. The proximal femur has an internal weight bearing system to cope with forces acting upon it. This internal system consists of compressive and tensile trabeculae and the femoral calcar^{15,17,18}. This internal weight bearing system gives the femur its intrinsic strength. The function of the trabecular system can mechanically be compared with a honeycomb structure, withstanding high loads with a minimal amount of matter.

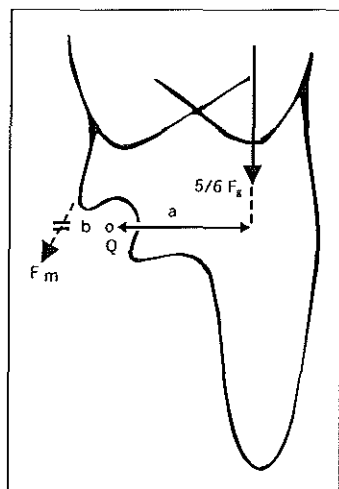
Under normal circumstances the hip will be loaded with a force along the femoral axis, e.g. in standing position or during walking. In this physiologically normal situation the femur can withstand the highest load. To keep the hip stable apart from the gravitational force muscular forces are also active.

We will now take a closer look at these forces, starting with the proximal femur of a body in one-legged stance in a static equilibrium⁴. Looking at the moments of forces, there are three forces in which we are interested:

1. The gravitational force (F_g): this force has a vertical direction and equals the body weight. As mentioned before, one leg weighs about one sixth of the body weight. Therefore the hip of the carrying leg will be loaded with $5/6 F_g$.
2. Muscular force (F_m): this force is produced by the abductor muscles, its direction can be deduced using radiographs, based on the origin and

Figure 6.2 - Schematic representation of the forces acting on the body during one legged stance

F_m = muscular force
 F_g = gravitational force
 Q = centre of the femoral head
 a = lever arm of the gravitational force
 b = lever arm of the muscular force

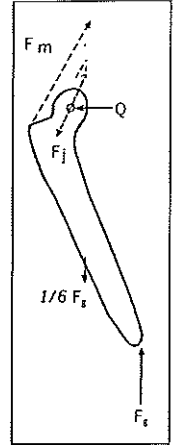


(courtesy of C.J. Snijders, department of biomedical physics and technology, Erasmus University)

Figure 6.3 - Schematic representation of the forces acting on the proximal femur during one legged stance

- F_m = muscular force
- F_g = gravitational force
- F_j = joint reaction force
- Q = centre of the femoral head

(courtesy of C.J. Snijders, department of biomedical physics and technology, Erasmus University)



- insertion of these muscles (normally 30° angulation with the vertical). The size of this force is unknown.
3. Joint reaction force (F_j); the size of this force is unknown as is its direction. We only know that its line of action goes through the centre of the femoral head.

We start by looking at the upper part of the body, which is sustained by the standing leg (figure 6.2). Three forces act upon this part of the body: $5/6 F_g$, F_j and F_m . If the body is in a state of equilibrium the following moments act with respect to the joint axis (equation 6.13).

$$\frac{5}{6} \cdot F_g \cdot a - F_m \cdot b = 0$$

⇓

$$F_m = \frac{5}{6} \cdot F_g \cdot \frac{a}{b}$$

where a and b can be found using radiographs, substitution yields (equation 6.14).

$$\text{eq 6.14} \quad F_m = 2 \cdot F_g$$

From radiographs we know that the angle of F_m with the vertical is 30° hence (equations 6.15 & 6.16):

$$F_{mx} = F_m \cdot \sin 30^\circ$$

⇓

$$\text{eq 6.15} \quad F_{mx} = F_m \cdot 0.5$$

⇓

$$F_{mx} = F_g$$

$$F_{my} = F_m \cdot \cos 30^\circ$$

⇓

$$\text{eq 6.16} \quad F_{my} = F_m \cdot 0.866$$

⇓

$$F_{my} = F_g \cdot 1.7$$

The third force can be obtained from the forces acting upon the body itself (figure 6.3). Since we still look at the body in a state of equilibrium all moments of forces in the horizontal and vertical must be zero (equations 6.17 & 6.18).

$$F_{mx} - F_{jx} = 0$$

$$\Downarrow$$

$$\text{eq 6.17} \quad F_{jx} = F_{mx}$$

$$\Downarrow$$

$$F_{jx} = F_g$$

$$F_{my} - F_{jy} - \frac{1}{6} \cdot F_g + F_g = 0$$

$$\Downarrow$$

$$\text{eq 6.18} \quad F_{jy} = 1.7 \cdot F_g + \frac{5}{6} \cdot F_g$$

$$\Downarrow$$

$$F_{jy} = 2.5 \cdot F_g$$

The size and angle of the joint reaction force, using F_{my} and F_{mx} , can now be calculated based on the assumptions stated before (equation 6.19 & 6.20).

$$F_j^2 = F_{jx}^2 + F_{jy}^2$$

$$\Downarrow$$

$$\text{eq 6.19} \quad F_j^2 = F_g^2 + (2.5 \cdot F_g)^2$$

$$\Downarrow$$

$$F_j = 2.7 \cdot F_g$$

$$\tan \alpha = \frac{F_{jy}}{F_{jx}}$$

$$\Downarrow$$

$$\tan \alpha = 0.5$$

$$\Downarrow$$

$$\alpha = 69^\circ$$

6.4 Biomechanics of the hip during a fall

In her PhD. study at the Massachusetts Institute of Technology (Cambridge, USA) A. v/d Kroonenberg described a basic dynamic model for sideways falls from standing heights. We will discuss this model in brief¹⁹. In a fall the body can be considered as an undamped single-degree-of-freedom mass-spring system with an effective mass (m_{eff}) moving in the vertical direction with velocity v prior to impact (figure 6.4). In this representation m_{eff} is the effective mass which contributes to the impact. The soft tissue overlying the major trochanter is represented as a linear spring with spring constant 'c'. In this model the peak impact force is equal to the maximum force of the spring (equation 6.21).

$$\text{eq 6.21} \quad F_{\text{peak}} = v \cdot \sqrt{c \cdot m_{\text{eff}}}$$

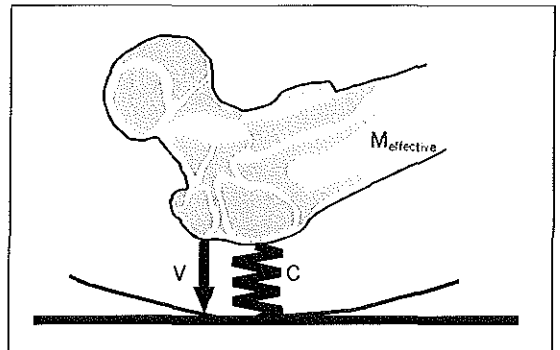
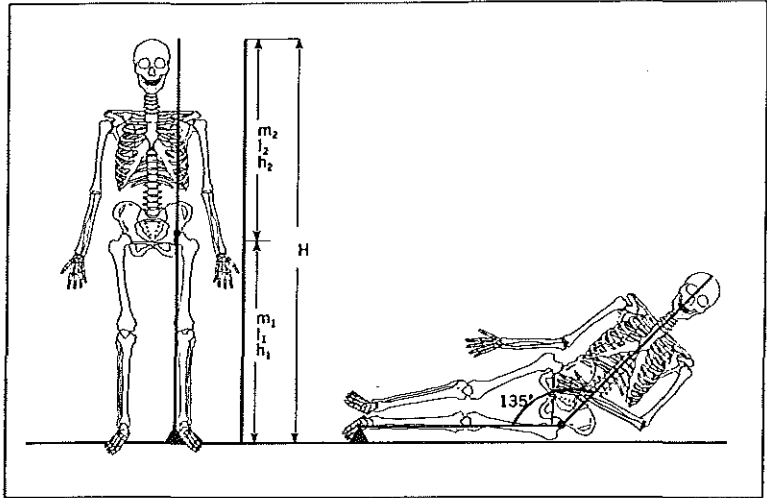


Figure 6.4 - Representation of the trochanteric region as an undamped single-degree-of-freedom mass-spring system

$M_{\text{effective}}$ = effective mass of the body
 v = velocity of the body
 C = spring constant

Figure 6.5 - Two-link model of the human body

H = height of the total body, m_1 = mass of the lower link ($1/3 m$), I_1 = moment of inertia of the lower link, h_1 = height of the lower link ($1/2 H$), m_2 = mass of upper link ($2/3 m$), I_2 = moment of inertia of the upper link, and h_2 = height of the upper link ($1/2 H$).



The body itself can be represented as a two-link model, consisting of two slender bars: a leg and a trunk component, these components are equal in length but not in mass (figure 6.5). The leg is connected to the floor via a hinge and the leg and trunk components are also interconnected by a hinge (representing the hip). In this model we assume that the trunk component has a 45° angle, towards the vertical, at the moment of impact. In-vivo volunteer studies have shown the fall angle to range from -8° to 61°²⁰. Furthermore, we also assume that no energy is stored in muscles, that all hinges are frictionless, and that the rotational energy of the body can be neglected. The energy just before impact consists of the potential and kinetic energy of both the trunk and the legs (equation 6.22).

$$\text{eq 6.22} \quad m_1 \cdot g \cdot h_1^{cg} + m_2 \cdot g \cdot h_2^{cg} = \frac{1}{2} \cdot I_1 \cdot \omega_1^2 + \frac{1}{2} \cdot I_2 \cdot \omega_2^2 + \frac{1}{2} \cdot m_2 \cdot v_2^2 + \frac{1}{2} \cdot m_2 \cdot g \cdot h_2 \cdot \cos\alpha$$

With: $v_2 = v$; $\omega_1 = 2v/h$; $h^{cg}_1 = 1/4h$; $h^{cg}_2 = 3/4h$; $m_1 = 1/3m$ and $m_2 = 2/3m$.

In equation 6.18 I_1 is the moment of inertia of link one with respect to the hinge and I_2 is the moment of inertia with respect to its center of gravity. We now can calculate I_1 and I_2 (equations 6.23 & 6.24, see appendix B).

$$\text{eq 6.23} \quad I_1 = \frac{1}{3} \cdot m_1 \cdot h_1^2 \qquad \text{eq 6.24} \quad I_2 = \frac{1}{12} \cdot m_2 \cdot h_2^2$$

Van den Kroonenberg calculated that the angular velocity of the leg is 1.38 times the angular velocity of the trunk¹⁹. If we substitute $1/1.38\omega_1$ for ω_2 . We can rewrite equation 6.22 to (equation 6.25).

$$\text{eq 6.25} \quad v = 2.72 \cdot \sqrt{h}$$

The effective mass in case of a fall depends on the angle of each link with respect to the vertical. In this model the leg has an angle of 90° with respect to the vertical, in which case the effective mass is $1/4$ times the mass of this link. The trunk has, at the moment of impact, an angle of 45° , in which case the effective mass is $2/5$ times the mass of this link¹⁹. The resultant effective mass can be calculated using (equation 6.26).

$$\begin{aligned}
 m_{eff} &= \frac{1}{4} \cdot m_1 + \frac{2}{5} \cdot m_2 \\
 &\Downarrow \\
 \text{eq 6.26} \quad m_{eff} &= \frac{1}{12} \cdot m + \frac{1}{15} \cdot m \\
 &\Downarrow \\
 m_{eff} &= \frac{7}{20} \cdot m
 \end{aligned}$$

Robinovitch and McMahon calculated that c has an average value of 71 kNm^{-1} ²¹. Substitution of this value for c , the effective mass and the velocity in equation 6.21 yields (equation 6.27).

$$\begin{aligned}
 F_{peak} &= 2.72 \cdot \sqrt{h \cdot 71 \cdot \frac{7}{20} \cdot m} \\
 &\Downarrow \\
 \text{eq 6.27} \quad F_{peak} &= 2.72 \cdot \sqrt{24.85 \cdot h \cdot m} \\
 &\Downarrow \\
 F_{peak} &= 13.6 \cdot \sqrt{h \cdot m}
 \end{aligned}$$

With this equation it is possible to approximate the peak force for an individual during a fall.

Appendix 6 A: Quantities and Units

Quantity	Equation	Symbol	Unit
Angle		α	rad
Angular velocity	$d\alpha/dt$	ω	rads ⁻¹
Force	$m \times a$	F	N = kgms ⁻²
Gravitational potential energy	$m \times g \times h$	E_p	J=Nm
Impulse	$m \times v$	p	kgms ⁻¹ = Ns
Kinetic energy	$\frac{1}{2} \times m \times v^2$	E_k	J=Nm
Load/weight	$m \times g$	G	N
Moment	$F \times a$	M	Nm
Mass moment of inertia	$m \times r^2$	I	kgm ²
Spring constant	$F/\Delta l$	C	Nm ⁻¹
Work	$F \times s \times \cos\alpha$	W	J=Nm

Appendix 6 B: Moment of inertia

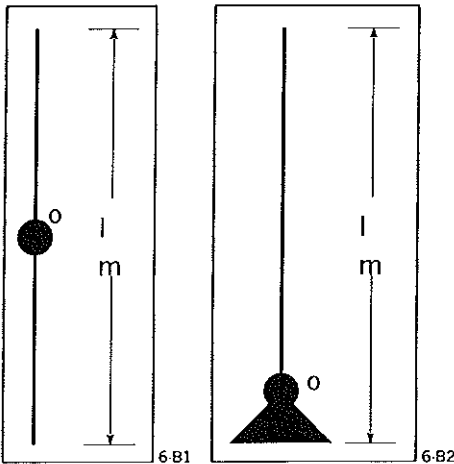
Consider a rod length (l) and mass (m) which is rotated around its center of gravity (figure B.1). The moment of inertia is given by equation B.1:

$$\text{eq B.1} \quad I = m \cdot l^2$$

The mass per length equals m/l , the proportional mass change equals (equation B.2):

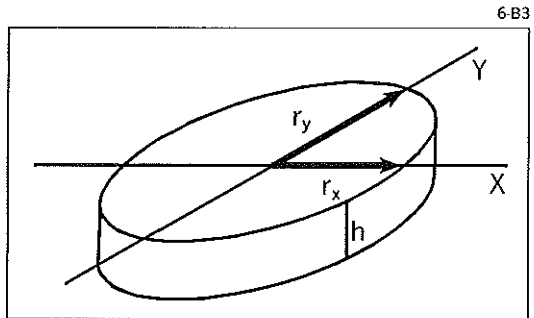
$$\text{eq B.2} \quad dm = \frac{m}{l} \cdot dr$$

Substituting equation B.2 in equation b.1 yields (equation B.3):



Figures 6-B1, 6-B2, and 6-B3

l = length
 m = mass
 h = thickness



$$\begin{aligned}
 I &= \int_{-\frac{1}{2}l}^{\frac{1}{2}l} r^2 \cdot dm \\
 &\Downarrow \\
 I &= \int_{-\frac{1}{2}l}^{\frac{1}{2}l} r^2 \cdot \rho \cdot A \cdot dr \\
 &\Downarrow \\
 \text{eq B.3} \quad I &= \rho \cdot A \cdot \int_{-\frac{1}{2}l}^{\frac{1}{2}l} r^2 \cdot dr \\
 &\Downarrow \\
 I &= \rho \cdot A \cdot \left[\frac{1}{3} \cdot \left(\frac{1}{2} \cdot l \right)^3 - \frac{1}{3} \cdot \left(-\frac{1}{2} \cdot l \right)^3 \right] \\
 &\Downarrow \\
 I &= \frac{1}{12} \cdot \rho \cdot A \cdot l \cdot l^2 \\
 &\Downarrow \\
 I &= \frac{1}{12} \cdot m \cdot l^2
 \end{aligned}$$

Where ρ equals the density (kgm^{-3}) and A the area (m). If the rotation of the same rod would be around the end of the rod (figure B.2). Then the integral in equation B.3 would range from 0 to l (equation B.4).

$$\begin{aligned}
 I &= \int_0^l r^2 \cdot dm \\
 &\Downarrow \\
 I &= \int_0^l r^2 \cdot \rho \cdot A \cdot dr \\
 &\Downarrow \\
 \text{eq B.4} \quad I &= \rho \cdot A \cdot \int_0^l r^2 \cdot dr \\
 &\Downarrow \\
 I &= \rho \cdot A \cdot \left[\frac{1}{3} \cdot l^3 \right] \\
 &\Downarrow \\
 I &= \frac{1}{3} \cdot \rho \cdot A \cdot l \cdot l^2 \\
 &\Downarrow \\
 I &= \frac{1}{3} \cdot m \cdot l^2
 \end{aligned}$$

If we consider a slice of material with a known radius (r), thickness (h) and mass (m), which is rotated along an axis through the centre and perpendicular to the slice (figure B.3). Then the moment of inertia is given by equation B.5.

$$I = \int_0^r \rho \cdot r^2 \cdot (2 \cdot \pi \cdot h \cdot r) dr$$

$$\Downarrow$$

eq B.5

$$I = 2 \cdot \pi \cdot \rho \cdot h \int_0^r r^3 \cdot dr$$

$$\Downarrow$$

$$I = \frac{1}{2} \cdot \pi \cdot \rho \cdot h \cdot r^4$$

As $\pi r^2 h$ equals the volume and the mass of the slice is equivalent to $\pi r^2 h$ times ρ , we can rewrite equation B.5 to equation B.6.

eq B.6

$$I = \frac{1}{2} \cdot m \cdot r^2$$

If we consider a slice which is rotated along an axis which coincides with the midline, then the following applies (equation B.7 & B.8)

eq B.7

$$I_x = I_y$$

eq B.8

$$I_z = I_x + I_y = 2 \cdot I_x$$

Therefore the moment of inertia is given by equation B.9.

eq B.9

$$I_x = \frac{1}{2} I_z$$

$$\Downarrow$$

$$I_x = \frac{1}{4} \cdot m \cdot r^2$$

6.5 References

1. Hatze H 1974 The meaning of the term 'biomechanics'. *J Biomech* 7:189-90.
2. Ascenzi A 1993 Biomechanics and Galileo Galilei. *J Biomech* 26(2):95-100.
3. Glockenberg A 1988 The biomechanics of traumatically applied loads. *Clin Podiatr Med Surg* 5(3):561-9.
4. Nordin M, Frankel VH 1995 Biomechanica van de heup. In: Snijders CJ, Nordin M, Frankel VH (eds.) *Biomechanica van het spier-skeletstelsel*. Lemma b.v., Utrecht, pp 183-210.
5. Pugh J, Frankel VH 1985 Biomechanics of hip fracture. In: Ryan Jr. JD, Perveiler FM (eds.) *Fractures of the hip*. Year Book Medical Publishers, Inc., New York, pp 23-37.
6. Sears FW, Zemansky MW 1964 *University physics*, third ed. Addison-Wesley publishing company, inc., London, pp 1028.
7. Soave RL, Lupo PJ, Positano RG, Barone SA 1988 Applied biomechanics of bone: Functional and clinical perspectives (review). *Clin Podiatr Med Surg* 5(3):449-58.
8. Snijders CJ 1995 Mechanicabeginselen. In: Snijders CJ, Nordin M, Frankel VH (eds.) *Biomechanica van het spier-skeletstelsel*. Lemma b.v., Utrecht, pp 13-58.
9. Turner CH, Burr DB 1993 Basic biomechanical measurements of bone: A tutorial. *Bone* 14:595-608.
10. Ohanian HC 1994 *Principles of physics*. W.W. Norton & Company, New York, pp 916.
11. Snijders CJ, Nordin M, Frankel VH 1995 *Biomechanica van het spier-skeletstelsel*. Lemma, Utrecht, pp 603.
12. Westfall RS 1996 Isaac Newton; Newton's life. Isaac Newton Institute for Mathematical Sciences <http://www.newton.cam.ac.uk/newtlife.html>.
13. Rydell N 1973 Biomechanics of the hip-joint. *Clin Orthop Rel Res* 92:6-15.
14. Fielding JW, Cochran GV, Zickel RE 1974 Biomechanical characteristics and surgical management of subtrochanteric fractures (review). *Orthop Clin N Am* 5(3):629-50.
15. Garden RS 1961 The structure and function of the proximal end of the femur. *J Bone Joint Surg* 43-B(3):576-89.
16. Gruebel-Lee DM 1983 Biomechanical considerations. In: *Disorders of the hip*. J.B. Lippincott Comp., pp 30-48.
17. Cooper C, Barker DJP, Hall AJ 1986 Evaluation of the Singh index and femoral calcar width as epidemiological methods for measuring bone mass in the femoral neck. *Clin Radiol* 37:123-5.
18. Stiles RG, Laverina CJ, Resnick D, Convery FR 1990 The calcar femorale: An anatomic, radiologic, and surgical correlative study. *Invest Radiol* 25:1311-5.
19. van den Kroonenberg A 1995 Dynamic models of human falls for prediction of hip fracture risk [dissertation] Department of mechanical engineering. Massachusetts Institute of Technology, Boston.
20. van den Kroonenberg AJ, Hayes WC, McMahon TA 1996 Hip impact velocities and body configurations for voluntary falls from standing height. *J Biomechanics* 29(6):807-11.
21. Robinovitch SN, Hayes WC, McMahon TA 1991 Prediction of femoral impact forces in falls on the hip. *J Biomech Eng* 113:366-74.

Chapter 7

Generating hip fractures in vitro

The difference between men and boys is the price of their toys

J.M. Heffner

7.1 Introduction

Measuring the strength of the proximal femur is a complex process, which requires adequate knowledge of both biomechanics and anatomy. There are two major methods to investigate bone strength. The first method uses small pieces of bone, with standardized dimensions, which are then loaded and measured¹⁻³. It provides us with valuable data e.g. the elastic modulus for bone. The second method uses whole, or large parts, of human cadaveric bone. We will look further into this method, as we will be applying this in this study.

In literature three techniques of measuring the strength of the proximal femur were found. We will discuss each technique and describe its advantages and disadvantages.

The first technique focuses solely on fractures of the femoral neck^{4,6}. A plastic block is moulded around the proximal femur, thereby leaving the neck and the head of the proximal femur free (figure 7.1). The theory behind this experiment is the fact that only fractures of the neck are investigated. A

major problem is the fact that one might expect forces at the brim of the plastic mould, thus creating artificial forces during loading. A second problem is the fact that the majority of fractures described in these experiments are clinically not relevant, as most of these fractures run perpendicular to the femoral neck axis.

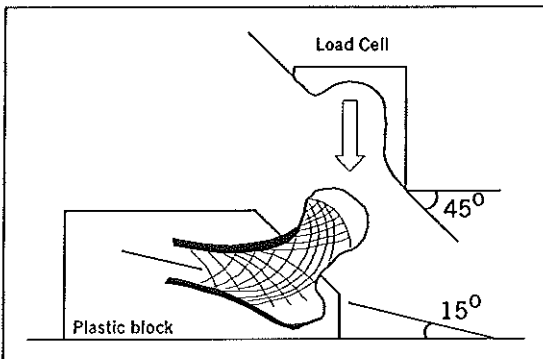


Figure 7.1 - Schematic representation of the technique used by Dalén et al.⁵

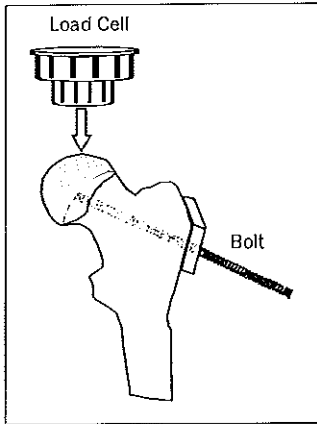


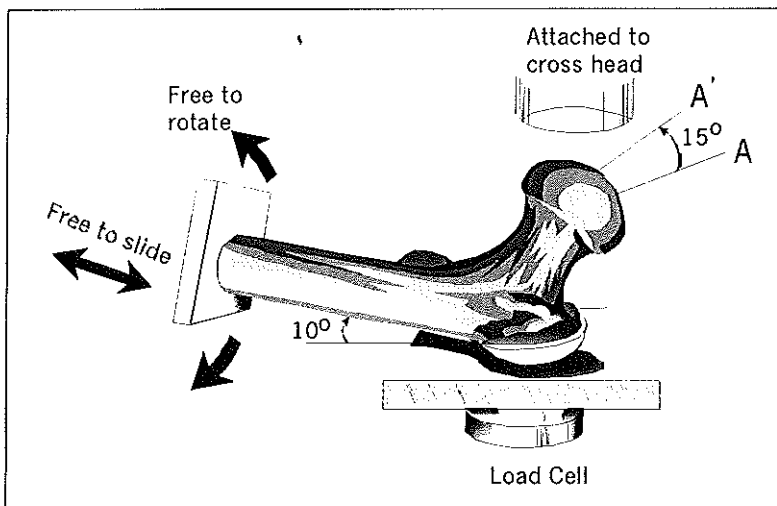
Figure 7.2 - Schematic representation of the technique applied by Hirsch et al.¹⁵

The second technique involves loading the femur in a way that it resembles one legged stance⁷⁻¹⁴. Although this technique offers reproducible results, it neither resembles the real life situation nor does it provide fractures as seen clinically, since the plane of fracture is essentially parallel to the load vector. An adaptation to this technique was used by Hirsch et al.¹⁵. Before loading the femur they applied a force along the axis of the femoral neck in order to simulate muscular compression forces. This force was produced using a bolt which fitted over the head of the femur and the trochanter major (figure 7.2). Although this technique resulted in fractures as seen clinically, loading a femur in one legged stance does not resemble the natural aetiology of hip fractures.

Although this technique resulted in fractures as seen clinically, loading a femur in one legged stance does not resemble the natural aetiology of hip fractures.

The third technique is used in most recent studies¹⁶⁻²⁰. Here the proximal femur is loaded in such a way that it resembles the moment of impact during a fall, i.e. the femur is placed with its trochanter major on the ground with the angle of the femoral shaft at 10° with respect to the horizontal and the femoral neck rotated 15° internally (figure 7.3). With this technique it is possible to generate fractures as seen in clinical practice. This technique will be discussed in full in chapter nine. A limitation of all the techniques above is the relative low loading rate (2 mms^{-1}) compared to the loading rate estimated for a fall from standing height (2.75 ms^{-1})^{21,22}.

Figure 7.3 - Schematic representation of the technique used in several studies¹⁶⁻²⁰



7.2 Theory

The subject of this chapter is the design of a device capable of producing fractures of the proximal femur which not only resemble those seen clinically in osteoporosis related hip fractures, but also emulates their aetiology. Although the measurement of bone density and geometry are recognized as a useful tool in predicting hip fracture risk, little is known about the direct relation between bone mineral density (BMD) or geometry and the strength of the proximal femur²³. The purpose of our new design is to investigate this relation.

In order to do so a few assumptions must be made. These assumptions are based on data obtained from literature.

1. For a fall to result in a hip fracture it must be directed sideways²⁴. This becomes clear when we recall the chain of events during a fall. If one falls face forward the arms will be stretched in a reflex in order to absorb the shock; this may result in a distal radius 'Colles' fracture. If on the other hand one falls backwards the buttocks will absorb most of the energy, most of the fall results in just a bruise. However, if one falls sideways the impact will be directed on the major trochanter. Since the trochanter major is covered with a shallow layer of soft tissue, most of the energy will be absorbed by the proximal femur resulting in direct loading of the femoral neck.
2. A fracture of the proximal femur is not only caused by external forces, but there also exists an important muscular component¹⁵. The muscles will pull the proximal femur into the acetabulum, in combination with the load of the body weight this will result in an axial compression of the femoral neck. From an anatomical point of view, these muscles can be divided into two groups. The first group acts above the axis of the neck and consists of the hip abductors and those lateral rotators that insert in the upper part of the trochanter major. The second group acts below the axis of the femoral neck and consists of the adductor muscles and the iliopsoas muscles. Exact axial pressures during a fall are unknown, we therefore assume to be in the range of those occurring during one-legged stance. Kotzar and al. obtained data using telemeterized hip joint prostheses. His data showed axial forces to be in the range of 2.5 times body weight²⁵.
3. In a study performed at the department of mechanical engineering of the Massachusetts Institute of Technology (Cambridge, USA), hip impact velocities were measured using young healthy volunteers²². Average values for hip impact velocities were 3.17 ms^{-1} ^{22,26}. Therefore, the loading rate must be higher than those used up to now.

7.3 Design of the device

The device consists of two main components:

- A. the steel frame and drop hammer (figure 7.4)
- B. the femur clamping device (figure 7.5)

In order to gain the required impact velocity, the drop angle (α) ranges from 90° to 50° , this is illustrated using equations 7.1 to 7.3 and figure 7.6. In order to calculate the velocity it is necessary to know the height from which the mass is being released, this can be assessed using equation 7.1.

$$\text{eq 7.1} \quad h = r \cdot (1 - \cos \alpha)$$

The velocity at the moment of impact can be calculated using equation 7.2. (see chapter 6).

$$\text{eq 7.2} \quad m \cdot g \cdot h = \frac{1}{2} \cdot m \cdot v^2$$

$$\Downarrow$$

$$v = \sqrt{2 \cdot g \cdot h}$$

Substitution of equation 7.1 in equation 7.2 yields equation 7.3, in this equation all parameters are known and therefore the velocity at the moment of impact can be calculated.

$$\text{eq 7.3} \quad v = \sqrt{2 \cdot g \cdot r \cdot (1 - \cos \alpha)}$$

In table 7.1 theoretic velocities for five different drop angles are given. Adjustments of the fall angle can be made by using several lengths of kevlar

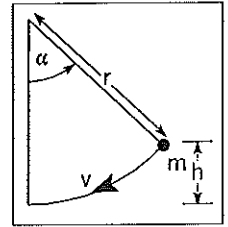


Figure 7.6 - Diagram showing the parameters involved during a fall.

- h. height
- r. length of the rod of the drop hammer
- α . starting angle
- m. mass of the drop hammer
- v. velocity

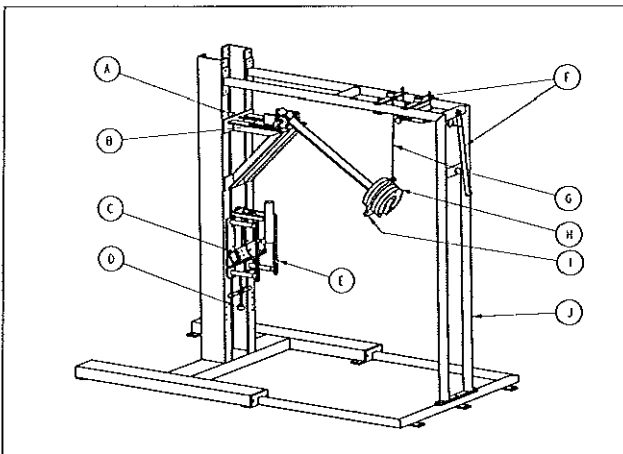


Figure 7.4 - Drawing of the device developed for this study

- A. horizontal adjustment
- B. pivot of the drop hammer
- C. femur clamping device
- D. vertical adjustment
- E. vertical safety bar to protect the dynamometers
- F. release mechanism
- G. Kevlar cord
- H. detachable masses
- I. drop hammer head
- J. steel frame.

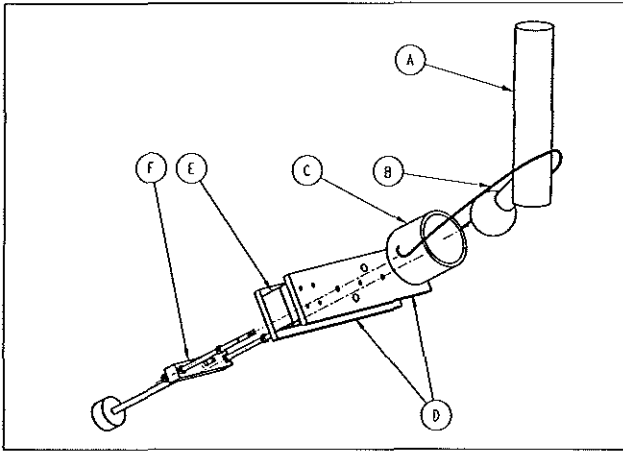


Figure 7.5 - Detailed drawing of the femur clamping device

- A. proximal femur
- B. Kevlar rope
- C. poly-oxy-methylene conus
- D. bridge
- E. dynamometers
- F. tightening screws

cord, which does not show any appreciable creep. The angle can be measured using a potentiometer fixed on the pivot of the drop hammer. The load on the hammer is variable, with a maximum load of 70 kg. The highest value of impact velocity and load will result in a kinetic energy of the hammer, at the moment of impact, of 521 J.

Strength calculations on our device, require values for the deceleration of the mass of the hammer. These are very difficult to predict. Especially at the higher values of impact velocity and load, where fractures surely will occur, it is impossible to estimate the amount of energy that will be absorbed by the fracturing femur, nor the length of the deceleration distance of the hammer. However, the pivot of the drop hammer is designed to resist forces up to 105 kN.

In the case of a realistic fall to the side the femur can be hit at different angles. The range of these angles is estimated at 30°. In the device the line of impact force is always horizontal. To be able to study the influence of the different angles the clamping device is designed to accept femora at all angles over a range of 30°.

The femora are placed in a poly-oxy-methylene conus simulating the acetabulum (figure 7.5). The femora are kept in place by a kevlar rope (ø6 mm) that can be tightened by screws, thus simulating muscular (compression) forces in a hip joint. Under the clamping device two dynamometers are mounted to measure either the compression force of the rope or the impact force when the femur is hit by the hammer. The dynamometers are custom made, shear force type meters, based on strain gauge techniques. The signals of the strain gauges are amplified using a strain gauge conditioner and amplifier system (type

(°)	v (ms ⁻¹)
50	2.31
60	2.73
70	3.13
80	3.51
90	3.86

Table 7.1 Angles and the corresponding velocity at the moment of impact

2100[®], Micromasurement) and processed using a personal computer (486-DX2) equipped with an analogue/digital converter (DAS 1802TS[®], Keithly Instruments Inc., Cleveland, Ohio, USA). The data acquisition and processing were performed using in-house developed software (MKR, multi channel registration, CDAI, University Hospital 'Dijkzigt' Rotterdam, the Netherlands). The sample frequency was set at 30.000 per second, to obtain sufficient data in the very short collision time.

To simulate overlying soft-tissue, an eighteen millimetre thick cork and rubber multilayer (rubber 80° shore and cork 70° shore, type PK, GMT, Bühl, Germany) was mounted on the head of the drop hammer.

The drop hammer and clamping device are mounted together to a heavy steel frame. Adjustments can be made to realign the clamping device and drop hammer. The hammer is released using a double secured, two-handed operated mechanism. This release mechanism is designed to ensure the safety of the operators.

Kinematic energy values (Joules) of the drop hammer at the moment of collision are calculated from equation 7.4:

$$\text{eq 7.4} \quad E(\alpha) = m \cdot g \cdot l \cdot (1 - \cos \alpha)$$

where α ranges from 90° (horizontal) to 45°, mass (m) ranges from 6.3 to 31.3 kg (mass hammer rod and head 6.3 kg, which can be increased by weights of 5 kg each) and the length of the hammer rod (L) equals 0.76 m

From the point of energy calculations the instrument can be seen as a chain of springs and dampers in which certainly energy will be absorbed. The instrument was tested using a steel ball (diameter 60 mm) placed within the poly-oxy-methylene conus. By measuring the maximum angle to which the hammer returned after collision with the steel ball, it was possible, using equation 7.5, to calculate energy absorption of the complete system.

$$\begin{aligned} E_{system} &= E_1 - E_2 \\ &\Downarrow \\ E_{system} &= m \cdot g \cdot h_1 - m \cdot g \cdot h_2 \\ &\Downarrow \\ \text{eq 7.5} \quad E_{system} &= m \cdot g \cdot (h_1 - h_2) \\ &\Downarrow \\ E_{system} &= m \cdot g \cdot l \cdot [(1 - \cos \alpha_1) - (1 - \cos \alpha_2)] \end{aligned}$$

Where E_{system} = energy absorbed by system, E_1 = potential energy before release, E_2 = potential energy after collision, m = mass of drop hammer and arm, L = length of the hammer rod (0,76 m), and g = 9.8 ms⁻¹.

Table 7.2 shows the amount of energy absorbed by the system, at different starting angles and with different masses. The amount of energy absorbed by the femur can be assessed using equation 7.6:

$$\text{eq 7.6} \quad E_{femur} = E_1 - E_2 - E_{system}$$

Where E_{femur} = Energy absorbed by femur, E_1 = potential energy before release, E_2 = Potential energy after collision, and E_{system} = Energy absorbed by the system.

7.4 Discussion

The essential point of our design is that it mimics the aetiology of the sequences leading to a hip fracture^{22,24,27}. By changing the angle and the weight of the drop hammer, several impact energies can be attained. The clamping device realistically simulates the acetabulum and the muscles surrounding the femur. Furthermore, by using the cork rubber multilayer soft tissue overlying the trochanter is simulated.

However, our design has two inherent drawbacks. The main drawback relies to the fact that it is not possible to place the femur in endo-rotation. In a recent article Pinilla et al. showed that rotation from 0° to 30°, yielded a significant decrease in femoral strength of 24%²⁸. The second drawback is that the pre-load is limited to approximately 600 N, where in-vivo these loads are in the range of 1700 to 2200 N²⁵.

The use of this new technique, which can give us information on energy dissipation, loads, and impact moments, could in combination with radiological and densitometric techniques provide us with an insight in the relation between bone mineral density, geometry and strength of the proximal femur. As such this device could open new perspectives for research into the biomechanics of hip fractures.

Table 7.2 - Amount of energy absorbed by the device at different loading angles and weights

Angle (°)	Mass (kg)	Potential energy (J)	Energy absorbed by the system (J)	Energy absorbed by the system (%)
45	6.3	13.74	3.76	27.4
45	11.3	24.65	5.64	22.8
45	16.3	35.56	7.21	20.3
45	21.3	46.47	9.23	20.1
60	11.3	42.08	10.55	25.1
60	16.3	60.70	14.31	23.6
60	21.3	79.32	17.93	22.6

7.5 References

1. Moyle DD, Bowden RW 1984 Fracture of human femoral bone. *J Biomech* 17(3):203-13.
2. Oyster N, Smith FW 1988 A postmortem correlation of four techniques of assessment of osteoporosis with force of bone compression. *Calcif Tissue Int* 43:77-82.
3. Reilly DT, Burstein AH, Frankel VH 1974 The elastic modulus for bone. *J Biomechanics* 7:271-5.
4. Klyver H, Scavenius M, Iversen BF 1995 Formation of impacted fractures of the femoral neck: An experimental study. *Clin Biomech* 10(5):268-70.
5. Dalén N, Hellström LG, Jacobson B 1976 Bone mineral content and mechanical strength of the femoral neck. *Acta Orthop Scand* 47:503-8.
6. Werner C, Iversen BF, Therkildsen MH 1988 Contribution of trabecular component to mechanical strength and bone mineral content of the femoral neck. An experimental study on cadaver bones. *Scand J Clin Lab Invest* 48:457-60.
7. Allhö A, Husby T, Hoiseth A 1988 Bone mineral content and mechanical strength: An ex vivo study on human femora at autopsy. *Clin Orthop Rel Res* 227:292-7.
8. Beck TJ, Ruff CB, Warden KE, Scott WW, Rao GU 1990 Predicting femoral neck strength from bone mineral data: A structural approach. *Invest Radiol* 25(1):6-18.
9. Phillips JR, Williams JF, Melick RA 1975 Prediction of the strength of the neck of the femur from its radiological appearance. *Biomed Eng* :367-72.
10. Sartoris DJ, Sommer FG, Kosek J, Gies AA, Carter D 1985 Dual energy projection radiography in the evaluation of femoral neck strength, density and mineralization. *Invest Radiol* 20:476-85.
11. Spears GN, Owen JT 1949 The etiology of trochanteric fractures of the femur. *J Bone Joint Surg* 31-A(3):548-52.
12. Vose GP, Beery-Mack P 1963 Roentgenologic assessment of femoral neck density as related to fracturing. *Am J Roentgenol* 89:1296-1301.
13. Wenzl H, Blomer R 1974 Proceedings: Die praktische bedeutung des Federverhaltens des menschlichen Femurs. *Z Orthop Ihre Grenzgeb* 112(4):710-3.
14. Yoshikawa T, Turner CH, Peacock M, Slemenda CW, Weaver CM, Teegarden D, Markwardt P, Burr DB 1994 Geometric studies of the femoral neck using dual-energy X-ray absorptiometry. *J Bone Miner Res* 9:1053-64.
15. Hirsch C, Frankel VH 1960 Analysis of forces producing fractures of the proximal end of the femur. *J Bone Joint Surg* 42-B(3):633-40.
16. Bouxsein ML, Courtney AC, Hayes WC 1995 Ultrasound and densitometry of the calcaneus correlate with the failure loads of cadaveric femurs. *Calcif Tissue Int* 56:99-103.
17. Cheng XC, Lowet G, Boonen S, Nicholson PHF, Brys P, Nijs J, Dequeker J 1997 Assessment of strength of the proximal femur in vitro: Relationship to femoral bone mineral density and femoral geometry. *Bone* 20(3):213-8.
18. Courtney AC, Wachtel EF, Myers ER, Hayes WC 1995 Age-related reduction in the strength of the femur tested in a fall-loading configuration. *J Bone Joint Surg* 77-A(3):387-95.
19. Lotz JC, Hayes WC 1990 The use of quantitative computed tomography to estimate risk of fracture of the hip from fall. *J Bone Joint Surg* 72-A(5):689-700.
20. Nicholson PHF, Lowet G, Cheng XG, Boonen S, van der Perre G, Dequeker J 1997

Assesment of the strength of the proximal femur in vitro: Relationship with ultrasonic measurement of the calcaneus. *Bone* 20(3):219-24.

21. Robinovitch SN, Hayes WC, McMahon TA 1991 Prediction of femoral impact forces in falls on the hip. *J Biomech Eng* 113:366-74.
22. van den Kroonenberg A 1995 Dynamic models of human falls for prediction of hip fracture risk [dissertation] Department of mechanical engineering. Massachusetts Institute of Technology, Boston.
23. Recker RR 1989 Low bone mass may not be the only cause of skeletal fragility in osteoporosis. *Proc Soc Exp Biol Med* 191(3):272-4.
24. Cummings SR, Nevitt MC 1989 A hypothesis: The cause of hip fractures. *J Geront* 44(4):M107-11.
25. Kotzar GM, Davy DT, Goldberg VM, Heiple KG, Berilla J, Heiple K, Jr., Brown RH, Burstein AH 1991 Telemeterized in vivo hip joint force data: A report on two patients after total hip surgery. *J Orthop Res* 9(5):621-33.
26. Askegaard V, Lauritzen JB 1996 Load in unprotected falls on the hip. *Osteoporosis Int* 6(suppl 1):158.
27. van den Kroonenberg AJ, Hayes WC, McMahon TA 1996 Hip impact velocities and body configurations for voluntary falls from standing height. *J Biomechanics* 29(6):807-11.
28. Pinilla TP, Boardman KC, Boussein ML, Myers ER, Hayes WC 1996 Impact direction from fall influences the failure load of the proximal femur as much as age-related bone loss. *Calcif Tissue Int* 58:231-5.

Chapter 8

Dynamic loading of the proximal femur

Doubt is the father of invention

Galileo Galilei

8.1 Introduction

In chapter seven we described a new design for in-vitro dynamic loading of the femur ^{1,2}. With this device we can obtain a dynamic simulation of a fall to the side, the leading cause of osteoporotic hip fractures, using loading speeds which meet the in-vivo rates reported by van den Kroonenberg et al. ^{3,4}. Our model also incorporates the muscular component over the femoral neck, which seems to play a role in hip fractures, an advantage over the semi-static techniques used in reported studies ⁵⁻¹⁰. In short, this semi-static technique consists of loading the femur in a fashion representing the moment of impact, ie. with an angle of 10° with respect to the horizontal and in 15° endo-rotation, and with loading speeds ranging from 2 to 14 mms⁻¹ (see chapter nine).

The aim of this chapter is to: a) verify whether this loading device can produce realistic fractures, as seen in clinical practice, and b) to compare radiological and densitometric parameters, as presented in chapters three to five, to fracture resistance.

8.2 Materials and methods

Femora

Thirty-seven femora, median age 82.9 (range 54.3-98.7 years), were drawn in a paired a-select fashion from the total pool of seventy-six available human cadaver femora. The femora were obtained from the department of anatomy, Erasmus University Rotterdam, the Netherlands. Medical records of the donors were not available. After removal of surrounding soft tissue the femora were kept in a medium containing Phenol and Formaldehyde (Phenol 99%, Acros Organics, New Jersey, USA. Formaldehyde 37%, Boom, Meppel, the Netherlands) ¹¹.

Radiography

All femora were radiographed using a Pandoros Optimatic X-ray tube and generator (Siemens, Germany), 1.10 m focus-film distance (46 kV, 8 mAs) and Dupont Ultra-vision™ film/intensifier screens. The radiographs were used to exclude pre-existing abnormalities such as: fractures, osteoarthritic changes or metastatic disease. Furthermore, they were used to measure the geometry. The following dimensions were assessed; proximal femur axis length (PFAL), head width (HW), neck width (NW), shaft width (SW), neck-shaft angle (NSA), offset, and the internal femoral axis length (IFAL) (a full description of these measurements can be found in chapter 3)¹²⁻¹⁴. In addition the Singh and femoral neck index were scored^{15,16}. After mechanical testing, radiography was repeated to score all fractures according to the classification system introduced by the Arbeitsgemeinschaft für Osteosynthesefragen (AO)¹⁷.

DXA

All DXA measurements were performed with a Lunar DPX-L scanner (see chapter 4). Standard DXA software (version 1.3) for the proximal femur was used. Bone Mineral Density (BMD) of the neck, Ward's area and of the trochanter major was assessed according to the guidelines stated in the manual.

QCT

Measurements were performed on a GE Prospeed S-fast (General Electric, Milwaukee, WI, USA) with a sequential single-energy technique at 120 kV and 400 mAs. Calibration of the CT image was achieved by a simultaneous scanning of a calibration phantom (Image Analysis Inc., Columbia, KY, USA) containing various inserts of solid calcium Hydroxy-apatite equivalent material (200, 100, 50, 0 mgcm⁻³ Hap). Image analysis took place at the Osteoporosis and Arthritis Research Group, University of California, San Francisco, USA, using in-house developed software. This technique was described in full in chapter 5 of this dissertation. In summary, this technique converts volumetric data from Hounsfield units to BMD (mgcm⁻³ hydroxy-apatite). After mapping the external contours a 3D binary model of the proximal femur was obtained. Thereafter, the binary and CT data were interactively reformatted along the axis of the femoral neck. The binary data were also used in an automated process that determines fixed volumes of interest (VOIs) for the measurement of BMD. In total three such VOIs were assessed; a femoral neck VOI, a trochanteric VOI, and a total VOI, consisting of neck and trochanteric VOI. For each VOI trabecular, cortical and integral BMD was assessed.

Two geometrical parameters were assessed. First the femoral neck axis length (FNAL), defined as the length of the line between the medial limit of the femoral head and the base of the trochanter. Secondly, the minimum cross-sectional area (minCSA) was assessed. Using this the minimum cross-sectional moments of inertia along the x- and y- axis were computed

(minCSI-x and minCSI-y). For one specimen the QCT data could not be assessed due to an error in the data file.

Mechanical testing

The device described in chapter seven was used for all tests. Pilot tests had shown that it is critically important to fine tune the loading conditions. For this study a mass of 21.3 kg and a drop angle of 60° was used. With these parameters a potential energy of 79.3 J is available. As shown in chapter seven, the test device absorbs 17.9 J with these settings.

Statistical analysis

Statistical analysis was performed using the Statistical Package for the Social Sciences (SPSS version 7.5.2, SPSS inc., Chicago, USA). An independent Student's t-test was performed to test for sex differences and for differences between fractured and non-fractured femora. Logistic regression was used to test for the strongest predictor of femoral fracture resistance.

8.3 Results

Table 8.1 shows the results for radiographic classification after biomechanical testing. We found 13.5% (n=5) cervical, 43.2% (n=16) trochanteric, and 5.5% (n=2) subtrochanteric fractures, and 37.8% (n=14) showed no fractures (figure 8.1). Tables 8.2 to 8.4 show the results for conventional radiography, DXA

Figure 8.1 - Two radiographs of fractures after mechanical testing



Table 8.1 - Classification of fractures, according to the AO classification system ¹⁷.

Fracture classification	Number of fractures	Percentage (of all femora)
31A11	1	2.7
31A12	1	2.7
31A23	6	16.2
31A31	1	2.7
31A32	1	2.7
31B12	2	5.4
31D	11	24.2

Table 8.2 - Conventional Radiology parameters of the femora used in this study (SD between brackets)

	All femora (n=37)	Female femora (n=20)	Male femora (n=17)	p value
Age (years)	80.6 (9.5)	83.1 (9.4)	77.6 (9.0)	0.08
PFAL (mm)	103.4 (7.1)	100.0 (5.7)	107.4 (6.5)	0.001*
IFAL (mm)	58.1 (3.8)	57.4 (3.6)	58.9 (3.9)	0.22
Head width (mm)	49.4 (3.5)	47.0 (2.7)	52.2 (1.7)	<0.001*
Neck width (mm)	33.2 (3.1)	31.6 (3.1)	35.1 (1.8)	<0.001*
Shaft width (mm)	44.4 (4.2)	43.0 (4.5)	46.0 (3.2)	0.027*
Neck shaft angle (°)	122.1 (4.6)	121.3 (4.6)	123.1 (4.4)	0.247
Offset (mm)	49.6 (4.5)	49.3 (4.7)	49.9 (4.4)	0.686
Femoral neck index	0.057 (0.024)	0.063 (0.024)	0.048 (0.02)	0.054
Singh grade	4.9 (1.0)	5.0 (0.7)	4.8 (1.2)	0.593

* significant difference between male and female femora.

PFAL = Proximal femur axis length, IFAL = Internal femur axis length

Table 8.3 - DXA parameters of the femora used in this study (SD between brackets)

	All femora (n=37)	Female femora (n=20)	Male femora (n=17)	p value
Neck BMD (gcm ²)	0.730 (0.222)	0.669 (0.174)	0.803 (0.254)	0.067
Trochanteric BMD (gcm ²)	0.760 (0.211)	0.683 (0.178)	0.851 (0.224)	0.013*
Ward's BMD (gcm ²)	0.566 (0.223)	0.509 (0.0426)	0.632 (0.245)	0.096
T score	-1.2 (1.5)	-1.3 (1.4)	-1.1 (1.7)	0.7

* significant difference between male and female femora.

and QCT parameters for all femora and for female and male femora separately. We found significant differences between male and female femora for the following parameters: PFAL, HW, NW, SW, trochanteric BMD as measured with DXA, integral trabecular BMD, trochanteric trabecular BMD, min CSA, and min CSMI in both the X and Y plane (p<0.05). All the other parameters showed no significant difference between male and female femora. Tables 8.5 to 8.7 show the results of the independent Student's t-test between fractured and non-fractured femora. Except for the femoral neck index, NSA, offset, and Singh index all geometrical and BMD parameters

Table 8.4 - QCT parameters of the femora used in this study (SD between brackets)

	All femora (n=37)	Female femora (n=20)	Male femora (n=17)	p value
Total integral BMD ¹	215.37 (68.05)	199.86 (61.65)	232.7 (72.45)	0.151
Total cortical BMD	397.32 (62.82)	388.36 (57.91)	407.34 (68.26)	0.373
Total trabecular BMD	113.54 (39.41)	101.3 (31.07)	127.22 (43.99)	0.047*
Neck integral BMD	210.1 (65.68)	198.44 (61.72)	223.13 (69.34)	0.266
Neck cortical BMD	355.44 (54.49)	348.89 (55.03)	362.77 (54.59)	0.453
Neck trabecular BMD	120.49 (43.44)	107.56 (36.28)	134.94 (47.20)	0.058
Troch. integral BMD	226.16 (72.56)	209.19 (64.45)	245.14 (78.23)	0.14
Troch. cortical BMD	430.99 (74.57)	419.04 (66.70)	444.34 (82.45)	0.316
Troch. trabecular BMD	108.25 (38.65)	96.38 (30.29)	121.52 (43.38)	0.050*
Femoral neck axis length	50.4 (4.52)	49.2 (4.44)	51.73 (4.36)	0.094
Minimum CSA (mm ²)	1018.8 (152.38)	918.53 (125.51)	1130.87 (88.26)	0.001*
Min. CSMI-X (mgmm ²)	24702.8 (12376.7)	18833.5 (6837.50)	31262.46 (13994.04)	0.002*
Min. CSMI-Y (mgmm ²)	18559.3 (8899.6)	14359.1 (6179.12)	23253.71 (9270.30)	0.002*

min CSMI: minimum cross-sectional moment of inertia, * significant difference between female and male femora (p<0.05).

Table 8.5 - Differences in geometry between fractured and non-fractured femora (SD between brackets)

	Fractured femora (n=23)	Non-fractured femora (n=14)	p value
Proximal femur axis length (mm)	100.3 (4.5)	108.4 (7.7)	<0.001*
Internal femur axis length (mm)	57.0 (2.7)	59.8 (4.7)	0.026*
Head width (mm)	48.3 (2.8)	51.3 (3.7)	0.007*
Neck width (mm)	32.3 (3.3)	34.7 (2.3)	0.023*
Shaft width (mm)	43.2 (4.1)	46.4 (3.6)	0.024*
Neck shaft angle (°)	121.3 (4.9)	123.4 (3.6)	0.172
Offset (mm)	49.0 (4.6)	50.6 (4.3)	0.301
Femoral neck index	0.061 (0.03)	0.047 (0.02)	0.085
Singh grade	4.8 (1.0)	5.1 (1.0)	0.469

* significant difference between fractured and non-fractured femora.

showed significant differences between fractured and non-fractured femora. The calculated sensitivity of all parameters was high (>78%), however, the specificity appeared to be lower and was generally in the order between 50% and 79% (an overview of sensitivity and specificity is given in appendix 8-A). Total trabecular BMD, trochanteric trabecular BMD, min CSMI-Y and PFAL had the strongest sensitivity, respectively 90.9%, 90.9%, 95.5%, 91.3%, and specificity, respectively 78.6%, 78.6%, 78.6%, and 64.3%. Adding more parameters to the logistic regression did not improve sensitivity or specificity. In a stepwise logistic regression total trabecular BMD always remained as the only significant parameter. Total trabecular BMD, trochanteric trabecular BMD, min CSMI-Y and PFAL are shown in graphs 8.1 to 8.4, all box-plots show a considerable overlap between fractured and non-fractured cases.

Table 8.6 - Differences in DXA parameters between fractured and non-fractured femora (SD between brackets)

	Fractured femora (n=23)	Non-fractured femora (n=14)	p value
Neck BMD (gcm ²)	0.641 (0.176)	0.877 (0.220)	0.001*
Trochanteric BMD (gcm ²)	0.670 (0.171)	0.908 (0.188)	<0.001*
Ward's BMD (gcm ²)	0.479 (0.182)	0.708 (0.216)	0.001*
T score	-1.7 (1.4)	-0.3 (1.3)	0.005*

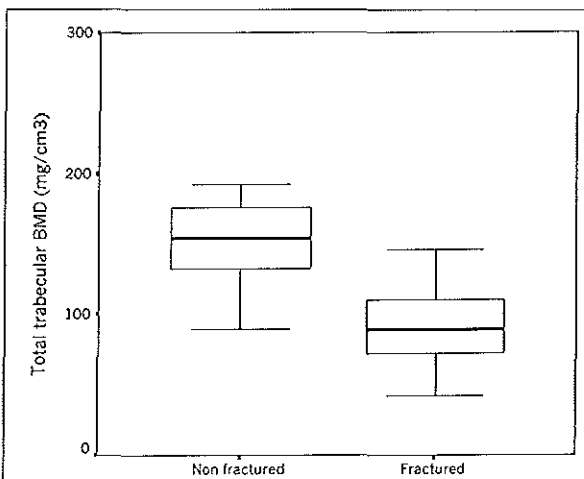
* significant difference between fractured and non-fractured femora.

Table 8.7 - Differences in QCT parameters between fractured and non-fractured femora (SD between brackets)

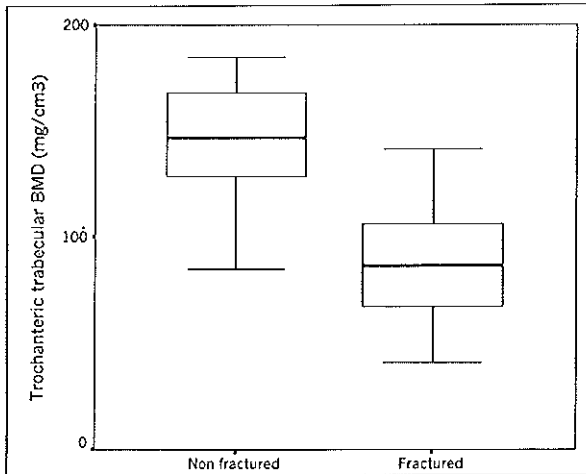
	Fractured femora (n=23)	Non-fractured femora (n=14)	p value
Total integral BMD ¹	185.32 (58.73)	262.59 (54.47)	<0.001*
Total cortical BMD	373.97 (62.67)	434.02 (43.69)	0.004*
Total trabecular BMD	92.71 (27.45)	146.26 (32.84)	<0.001*
Neck integral BMD	182.19 (55.60)	253.95 (56.88)	0.001*
Neck cortical BMD	332.49 (49.74)	391.52 (41.30)	0.001*
Neck trabecular BMD	100.04 (33.53)	152.63 (38.02)	<0.001*
Troch. integral BMD	194.14 (63.40)	276.50 (56.74)	<0.001*
Troch. cortical BMD	402.54 (74.10)	475.70 (50.77)	0.003*
Troch. trabecular BMD	87.85 (26.46)	140.31 (32.87)	<0.001*
FNAL (mm)	48.97 (3.45)	52.64 (5.19)	0.015*
Minimum CSA (mm ²)	971.91 (146.65)	1092.49 (134.93)	0.018*
Min CSMI X (mgmm ²)	18878.71 (6117.86)	33854.80 (14293.64)	<0.001*
Min CSMI-Y (mgmm ²)	14371.93 (7232.49)	25139.48 (7241.44)	<0.001*

¹ all BMD measurements in gcm³, min CSMI: minimum cross-sectional moment of inertia

* significant difference between fractured and non-fractured femora.

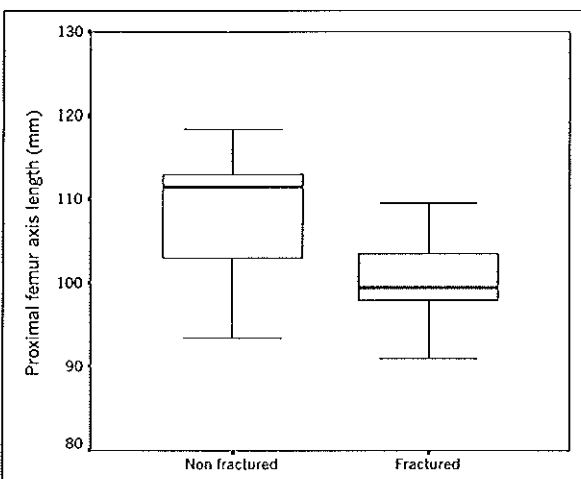
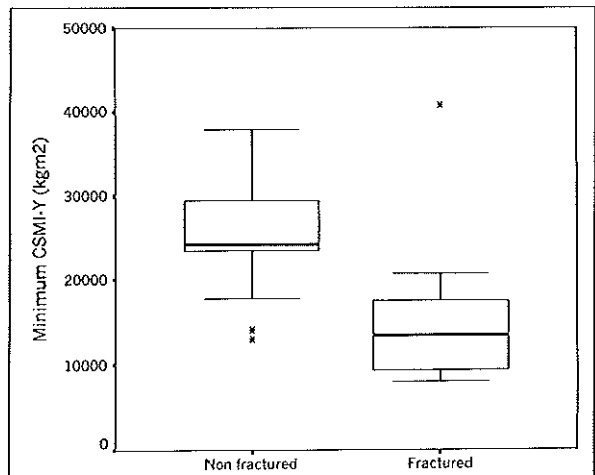


Graph 8.1 - Box-plot for fracture versus total trabecular BMD as assessed using QCT

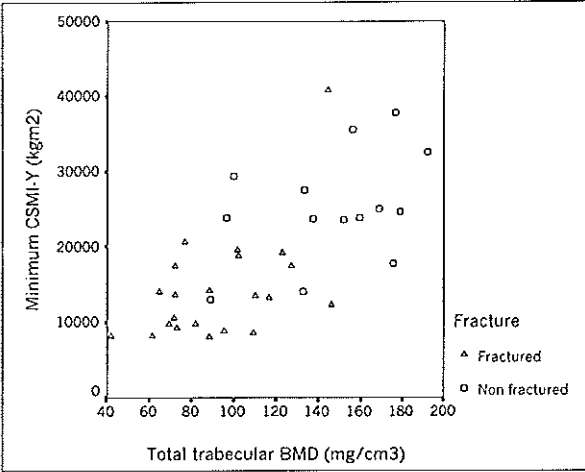


Graph 8.2 - Box-plot for fracture versus trochanteric trabecular BMD as assessed using QCT

Graph 8.3 - Box-plot for fracture versus minimum cross-sectional moment of inertia along the y-axis as assessed using QCT

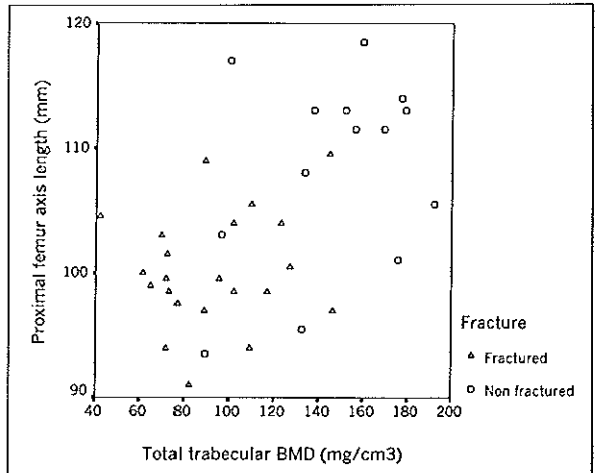


Graph 8.4 - Box-plot for fracture versus proximal femur axis length as assessed on conventional radiographs



Graph 8.5 - Scatter-plot for total trabecular BMD (QCT) versus minimum cross-sectional moment of inertia along the y-axis (QCT)

Graph 8.6 - Scatter-plot for total trabecular BMD (QCT) versus proximal femur axis length (conventional radiographs)



8.4 Discussion

As stated in the introduction one of the aims of this study was to test whether the loading device is capable of producing fractures as seen in a clinical setting. Our results show that it is possible to generate such fractures. The distribution between cervical and trochanteric fractures, is similar to clinical practice taking into account the high average age (82.9 years) of our donors. Although in most societies cervical and trochanteric fractures occur with equal frequency, the average age of a patient with a trochanteric fracture is approximately five years higher.

Based on severity of outcome, the two groups showed significant differences in geometrical and BMD parameters (tables 8.6 to 8.8). The group with

fractures had a significantly shorter PFAL, IFAL, and FNAL than the unfractured specimen. Epidemiological studies have shown that a longer hip axis length (HAL), from which our parameters were derived, had a positive correlation with hip fracture risk^{13,18-22}. This finding could not be demonstrated by our and other in-vitro studies^{6,23}. This suggests that the acetabular component of the HAL plays a role in the correlation with hip fracture risk^{6,24}. In an epidemiological study by Glüer et al. acetabular bone width was assessed and showed an odds ratio of 1.6 for each standard deviation increase in bone width.

The radiological parameters reflecting bone size, ie. HW, NW, and SW, showed significant differences between the fractured and non-fractured femora. This is in agreement with reported studies²⁵. The Singh index, a radiographic tool for the classification of osteoporosis, showed no significant difference between both groups. The same negative result was found in an in-vivo study by Koot et al²⁶. All BMD parameters of the fractured groups were significantly lower than that of the unfractured group. These findings were also reported when a semi-static technique was performed^{6,7,10,27}.

Combination of different parameters did not enhance the sensitivity or specificity with regard to fracture prediction. However, taking into account our relatively small sample size, larger studies are required to further investigate the findings. The box-plots of the four strongest individual parameters show the characteristic overlap that is also seen in clinical practice. It can be speculated that other factors than bone mineral density or geometrical parameters play a role in fracture resistance. Bone architecture and inherent bone quality are suggested as additional parameters predicting bone strength. Scatter-plots of the total trabecular BMD against min CSMI-Y or PFAL show only a moderate correlation. Most of the fractured femora have a relatively low BMD as well as a relatively low min CSMI-Y or PFAL (graphs 8.5 and 8.6) The question remains if a better discrimination can be achieved by a combination of parameters. Again this has to be tested on larger sample sizes.

An interesting finding is that we found no significant differences in energy absorption between the two classification groups. Furthermore, no significant correlations were found between energy absorption and any radiological or densitometric parameter. This observation contradicts the results published by Courtney et al. who showed a significant decrease in energy absorption for lower BMD values⁷.

Our study shows that size dependent geometrical parameters and BMD play an important role in the strength of the proximal femur. In conclusion, the strong point of our study is that we used a new approach, emulating a real life fall situation, and that it is to our knowledge the first study to combine geometry, DXA and volumetric QCT with respect to their ability to predict fracture resistance.

Appendix 8 A

Calculated sensitivity and specificity for radiographic and densitometric parameters

Parameter	Sens %	Spec %	Parameter	Sens %	Spec %
PFAL (mm)	91.3	64.3	Total integral BMD ¹	81.8	64.3
IFAL (mm)	87	50	Total cortical BMD	81.3	57.1
Head width (mm)	87	78.6	Total trabecular BMD	90.9	78.6
Neck width (mm)	82.6	50	Neck integral BMD	81.8	57.1
Shaft width (mm)	82.6	42.9	Neck cortical BMD	81.8	57.1
NSA (°)	82.6	28.6	Neck trabecular BMD	81.8	64.3
Offset (mm)	91.3	7.1	Troch. integral BMD	86.4	71.4
Femoral neck index	87	14.3	Troch. cortical BMD	81.8	57.1
Singh grade	100	0	Troch. trabecular BMD	90.9	78.6
Neck BMD (gcm ⁻²)	78.3	64.3	FNAL (mm)	81.8	50
Troch. BMD (gcm ⁻²)	78.3	64.3	Minimum CSA (mm ²)	86.4	57.1
Ward's BMD (gcm ⁻²)	87	57.1	Minimal CSMI X plane ²	86.4	71.4
T score	87	61.5	Minimal CSMI Y plane	95.5	78.6

¹All QCT BMD values in mgcm⁻³, ² mgmm²

8.5 References

1. van Rijn RR, Niesing R, Mulder BN, Grashuis JL 1996 Generating in vitro fractures of the hip; a novel technique. 10th conference of the European Society of Biomechanics, Leuven, Belgium, pp 381.
2. van Rijn RR, Niesing R, Mulder BN, Grashuis JL 1996 Realistic hip fractures in vitro; a different approach. *Osteoporosis Int* 6(suppl 1):145.
3. van den Kroonenberg A 1995 Dynamic models of human falls for prediction of hip fracture risk [dissertation] Department of mechanical engineering, Massachusetts Institute of Technology, Boston.
4. van den Kroonenberg AJ, Hayes WC, McMahon TA 1996 Hip impact velocities and body configurations for voluntary falls from standing height. *J Biomechanics* 29(6):807-11.
5. Bouxsein ML, Courtney AC, Hayes WC 1995 Ultrasound and densitometry of the calcaneus correlate with the failure loads of cadaveric femurs. *Calcif Tissue Int* 56:99-103.
6. Cheng XC, Lowet G, Boonen S, Nicholson PHF, Brys P, Nijs J, Dequeker J 1997 Assessment of strength of the proximal femur in vitro: Relationship to femoral bone mineral density and femoral geometry. *Bone* 20(3):213-8.
7. Courtney AC, Wachtel EF, Myers ER, Hayes WC 1995 Age-related reduction in the strength of the femur tested in a fall-loading configuration. *J Bone Joint Surg* 77-A(3):387-95.
8. Hirsch C, Frankel VH 1960 Analysis of forces producing fractures of the proximal end of the femur. *J Bone Joint Surg* 42-B(3):633-40.
9. Lotz JC, Hayes WC 1990 The use of quantitative computed tomography to estimate risk of fracture of the hip from fall. *J Bone Joint Surg* 72-A(5):689-700.
10. Pinilla TP, Boardman KC, Bouxsein ML, Myers ER, Hayes WC 1996 Impact direction from fall influences the failure load of the proximal femur as much as age-related bone loss. *Calcif Tissue Int* 58:231-5.
11. Kleinrensink GJ, Stoeckart R, Vleeming A, Snijders CJ, Mulder PGH, van Wingerden JP 1995 Peripheral nerve tension due to joint motion; a comparison between embalmed and unembalmed human bodies. *Clin Biomech* 10(5):235-9.
12. Boonen S, Koutri R, Dequeker J, Aerssens J, Lowet G, Nijs J, Verbeke G, Lesaffre E, Geusens P 1995 Measurement of femoral geometry in type I and type II osteoporosis: Differences in hip axis length consistent with heterogeneity in the pathogenesis of osteoporotic fractures. *J Bone Miner Res* 10(12):1908-12.
13. Faulkner KG, Cummings SR, Black D, Palermo L, Glüer CC, Genant HK 1993 Simple measurement of femoral geometry predicts hip fracture: The study of osteoporotic fractures. *J Bone Miner Res* 8(10):1211-7.
14. Rubin PJ, Leyvraz PE, Aubaniac JM, Argenson JN, Esteve P, de Roguin B 1992 The morphology of the proximal femur: A three-dimensional radiographic analysis. *J Bone Joint Surg* 74-B(1):28-32.
15. Fredensborg N, Nilsson BE 1977 Cortical index of the femoral neck. *Acta Radiol Diagnos* 18:492-6.
16. Singh M, Nagrath AR, Maini PS 1970 Changes in trabecular pattern of the upper end of the femur as an index of osteoporosis. *J Bone Joint Surg* 52-A(3):457-67.
17. Müller ME, Nazarian S, Koch P, Schatzker J 1990 The comprehensive classification of fractures of long bones. Springer-Verlag, Berlin Heidelberg, pp 116-27.

18. Faulkner KG, Mac Clung M, Cummings SR 1994 Automated evaluation of hip axis length for predicting hip fracture. *J Bone Miner Res* 9(7):1065-70.
19. Gómez Alonso C 1994 Bone mineral density and geometric measurements as predictors of risk for hip fracture. In: Ring EJF, Elvins DM, Bhalle AK (eds.) Fourth Bath conference on osteoporosis and bone mineral measurement. British Institute of Radiology, Bath, pp 24.
20. Granpp S 1992 Korrelation von Knochenmasse, Knochengeometrie und Bruchfestigkeit am Schenkelhals [dissertation] Klinik für Radiologie, Nuklearmedizin und Physikalische Therapie. Freien Universität, Berlin, pp 94.
21. Peacock M, Turner CH, Liu G, Manatunga AK, Timmerman L, Johnston jr CC 1995 Better discrimination of hip fracture using bone density, geometry and architecture. *Osteoporosis Int* 5:167-73.
22. Slis HW, van Daele PLA, Kuiper JW, Burger H, Algra D, Hofman A, Birkenhäger JC, Pols HAP 1995 The use of simple geometric measurements on standard pelvic X-rays in the prediction of hip fractures. *Osteoporosis Int* 5(4):311.
23. Bouxsein ML, Boardman KC, Pinilla TP, Myers EM 1995 Ability of bone properties at the femur, forearm, and calcaneus to predict the structural capacity of the proximal femur during a sideways fall. *J Bone Miner Res* 10(suppl 1):178.
24. Karlsson KM, Sernbo I, Obrant KJ, Redlund-Johnell I, Johnell O 1996 Femoral neck geometry and radiographic signs of osteoporosis as predictors of hip fracture. *Bone* 18(4):327-30.
25. Cordey J, Schneider M, Belendez C, Ziegler WJ, Rahn BA, Perren SM 1992 Effect of bone size, not density, on the stiffness of the proximal part of normal and osteoporotic human femora. *J Bone Miner Res* 7(suppl 2):S437-44.
26. Koot VCM, Kesselaer SMMJ, Clevers GJ, de Hooge P, Weits T, van der Werken C 1996 Evaluation of the Singh index for measuring osteoporosis. *J Bone Joint Surg* 78B(5):831-4.
27. Boden SD, Labropulos P, Saunders R 1990 Hip fracture in young patients: Is this early osteoporosis? *Calcif Tissue Int* 46:65-72.

Chapter 9

Semi-static loading of the proximal femur

An expert is a man who has made all the mistakes
which can be made in a very narrow field

N. Bohr

9.1 Introduction

In clinical studies bone geometry and bone mineral density (BMD) have proven to show a positive correlation with fracture risk¹⁻⁵. In addition several in-vitro studies have been reported on the correlation between radiographic and densitometric parameters and failure loads of cadaveric femora⁶⁻¹¹. One in-vitro study also assessed the energy absorption and stiffness of the femur in correlation with radiographic and densitometric parameters⁸. Mostly all recent in-vitro studies have been performed using one and the same semi-static loading technique, in contrast to the dynamic technique employed by us and described in chapters seven and eight. In short the semi-static loading technique consists of loading the femur in a configuration designed to simulate a fall to the side, ie. in an angle of 10° with respect to the horizontal and in 15° endo-rotation, and with the force applied over the greater trochanter^{8,9}. This technique generally yields fractures which resemble those seen in a clinical setting.

So far no studies have been published that discuss the prediction of fracture risk combined with conventional radiography, DXA, and volumetric QCT. The aim of this chapter is to compare these three techniques with respect to their ability to predict femoral strength. Secondly, in contrast to all previously published studies our study used embalmed cadaver specimen. The use of fresh cadaver material, at least in the Netherlands, is limited due to a relative shortage and associated bio-hazards of working with fresh cadaver material. It would therefore be beneficiary if embalmed material could serve as well in biomechanical studies. The additional question we therefore address is whether embalming alters biomechanical properties in such a way that it influences the outcome of biomechanical studies.

9.2 Materials and methods

Femora

We used 39 cadaver femora median age 82.9 years (54.3-98.7 years). Medical records of the donors were not available. The bodies, from which the femora originated, were embalmed by vascular perfusion between 48 to 60 hours after death. All femora were exarticulated in the hip and, after removal of the surrounding soft tissue, kept in a solution containing Phenol and Formaldehyde (Phenol 99%, Acros Organics, New Jersey, USA. Formaldehyde 37%, Boom, Meppel, the Netherlands). Medical records of these donors were not available.

Radiography

All femora were radiographed using a Pandoros Optimatic X-ray tube and generator (Siemens, Germany, 1.10 m focus-film distance, 46 kV, 8 mAs, and Dupont Ultra-vision™ film/intensifier screens). The radiographs were used to exclude pre-existing abnormalities such as: fractures, osteoarthritic changes or metastatic disease. Furthermore, they were used to measure the geometry, the following dimensions were assessed; proximal femur axis length (PFAL), head width (HW), neck width (NW), shaft width (SW), neck-shaft angle (NSA), offset, and the internal femoral axis length (IFAL) (a full description of these measurements is presented in chapter 3)¹²⁻¹⁴. In addition the Singh and femoral neck index were scored^{15,16}. After mechanical testing, radiography was repeated to score all fractures according to the system introduced by the 'Arbeitsgemeinschaft für Osteosynthesefragen (AO)'¹⁷.

DXA

Dual-energy X-ray absorptiometry measurements were performed with a Lunar DPX-L scanner (see chapter 4). For analysis the standard DXA software (version 1.3) for the proximal femur was used. The bone mineral density (BMD) of the neck, Ward's area and the trochanter major were assessed according to the guidelines stated in the manual.

QCT

Measurements were performed on a GE prospeed S-fast (General Electric, Milwaukee, WI, USA) with a sequential single-energy technique at 120 kV and 400 mAs. Calibration of the CT image was achieved by a simultaneous scanning of a calibration phantom (Image Analysis Inc., Columbia, KY, USA) containing various inserts of solid calcium Hydroxy-apatite equivalent material (200, 100, 50, 0 mgcm⁻³ Hap). Image analysis was performed at the osteoporosis and arthritis research group, UCSF, USA, using in house developed software as previously described in chapter 5. In summary, this technique converts volumetric data from Hounsfield units to BMD (mgcm⁻³ hydroxy-apatite). After mapping the external contours a 3D binary model of the proximal femur was obtained. Thereafter, the binary and CT data were interactively reformatted along the femoral neck axis. The binary data were also used in an automated process that determines fixed volumes of interest

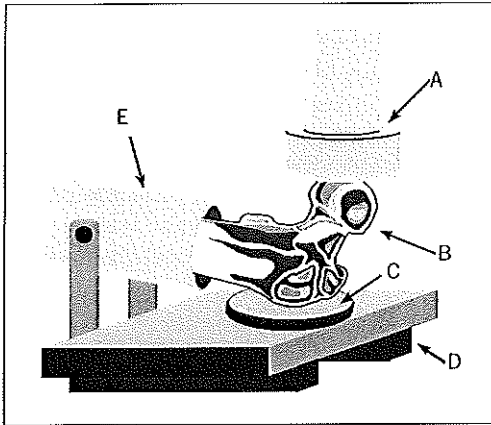


Figure 9.1 - Schematic representation of the holder for the femora

- A. load cell,
- B. femur,
- C. polyurethane cushion,
- D. ball bearings, making the setup free to slide
- E. holder for the femur, free to rotate along the axis

(VOIs) for the measurement of BMD. In total three such VOIs were assessed; a femoral neck VOI, a trochanteric VOI, and a total VOI, consisting of neck and trochanteric VOI. For each VOI

trabecular, cortical and integral BMD was assessed.

Two geometrical parameters were assessed. First the femoral neck axis length (FNAL), defined as the length of the line between the medial limit of the femoral head and the base of the trochanter. Secondly, the minimum cross-sectional area (minCSA) was assessed. Additionally the minimum cross-sectional moments of inertia along the x- and y- axis (minCSI-x and minCSI-y) were assessed. For four specimen the QCT data could not be assessed due to errors in the data file.

Mechanical testing

The femora were placed in a holder especially designed for mechanical testing (figure 9.1). The holder positions the femora in an angle of 10° with respect to the horizontal and in 15° endo-rotation. The femur was free to rotate in the vertical plane and, by placing the whole unit on ball-bearings, the system was also allowed free horizontal translation. To prevent the femur from rotating along its length axis the femoral body was fixed within the holder by means of six sharp pointed steel bolts which were driven, approximately 0.5 cm., into the femoral cortex.

Mechanical testing was performed using a Zwick universal testing system (model 1418, Zwick GmbH, Willich Mönchheide, Germany), at the Faculty of Mechanical Engineering and Marine

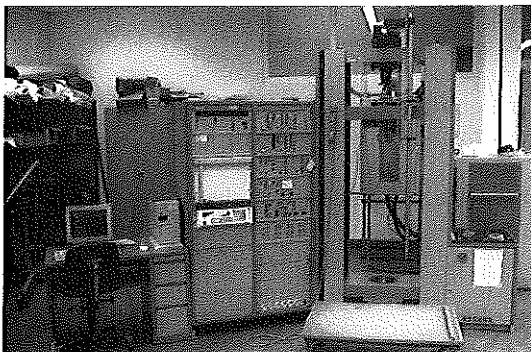


Figure 9.2 - Photo of the Zwick, model 1418, situated at the Faculty of Mechanical Engineering and Marine Technology of the Delft University of Technology, the Netherlands.

Technology, Delft University of Technology, the Netherlands (figure 9.2). The rate of displacement was two millimetres per second. Load and displacement were recorded via a digital-to-analogue converter and in-house developed data acquisition software (Delft University of Technology).

To prevent local crushing of the cortices of either the trochanter major or the femoral head, a polyurethane slab (thickness 5 mm, 90° shore) was placed between the femur and the testing system. The displacement and energy absorption of the polyurethane cushions was measured separately replacing the femur by a steel ball-bearing (diameter 60 mm). All femoral measurement data were corrected for this side-effect.

Data analysis

Statistical analysis was performed using the Statistical Package for the Social Sciences (SPSS version 7.5.2, Chicago, USA). An independent Student's t-test was performed to test for sex differences. Correlations were computed using a partial correlation tests, controlling for sex of the donor. Forward stepwise multiple regression was performed to determine which of the parameters contributed independently to the prediction of mechanical parameters.

9.3 Results

The thirty-nine femora showed no signs of pre-existent fractures, osteoarthritic changes or metastatic disease. In four specimen the mechanical testing failed, in these four cases the data acquisition software crashed and all data was lost, thereby leaving 35 femora for analysis. After mechanical testing we found 48.6% (n=17) femoral neck, 45.7% (n=16) trochanteric and 5.7% (n=2) subtrochanteric fractures (fig 9.3). All fractures were scored using the AO system (table 9.1).

To correct for the presence of the polyurethane cushion a test with a steel ball was performed. The load displacement curve showed a linear relation between displacement and load, up to 3637 Newton and 6.84 mm. Using this data a correction for displacement was performed on all data of the test (equation 9.1)

$$\text{eq 9.1} \quad \text{Displacement}_{\text{bone}} = \text{Displacement}_{\text{bone \& polyurethane}} - \text{Load}_{\text{measured}} * (6.84/3637)$$

Using the corrected data the yield point (N), maximum load (N), slope (kNm⁻¹), and energy absorption at the yield point (J) could be calculated.

Tables 9.2 to 9.4 give a summary of the radiological and densitometric parameters. Significant differences between male and female femora were found for HW, minimum CSA, and minimum CSMI along both the x- and y-axis.

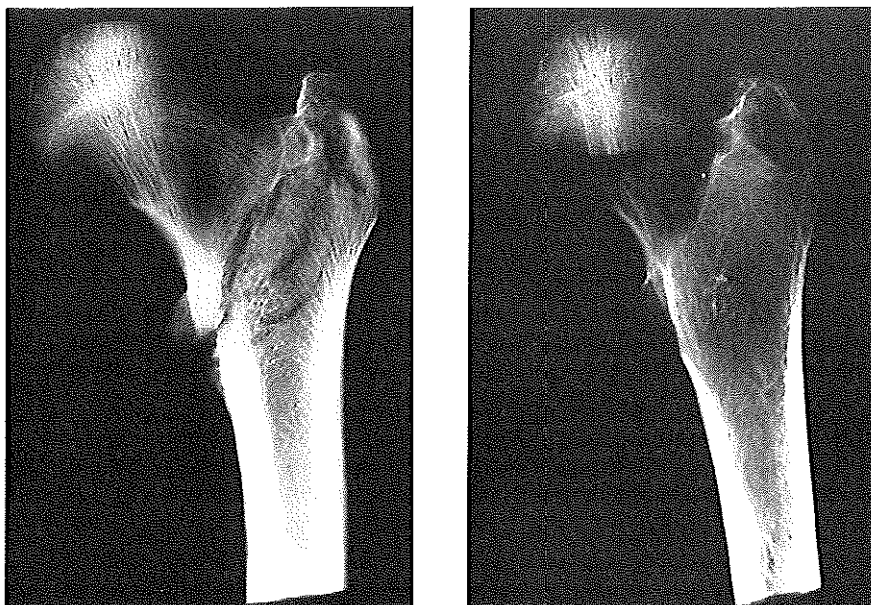


Figure 9.3 - Radiographs of fractures after semi-static testing

Table 9.1 - Classification of fractures, according to the AO classification, obtained by mechanical testing (n=35)¹⁷

Fracture classification	Number	Percentage
31A11	7	19.9
31A21	1	2.9
31A22	1	2.9
31A23	1	2.9
31A31	1	2.9
31B12	1	2.9
31B13	3	8.6
31B21	7	19.9
31B22	1	2.9
31B23	3	8.6
31D1 9	2	5.6

In table 9.5 the mean values for the biomechanical tests are shown. Only the maximum load showed a significant difference between male and female femora ($p=0.02$).

As shown in table 9.6 for geometry only three parameters showed significant correlations stiffness vs offset and IFAL, maximum load vs PFAL, HW, offset, IFAL and the Singh grade, and energy absorption at the yield point vs PFAL, HW, offset, IFAL, and the Singh grade. The strongest correlation was

Table 9.2 - Means for age and geometrical parameters (SD between brackets)

	All (n=35)	Female (n=20)	Male (n=15)	p value
Age (years)	82.0 (10.4)	83.0 (9.9)	80.7 (10.4)	0.522
PFAL (mm)	102.97 (7.9)	100.81 (7.0)	105.87 (8.4)	0.060
HW (mm)	49.17 (3.7)	47.08 (3.0)	51.97 (2.4)	<0.001 *
NW (mm)	33.63 (3.1)	32.30 (3.7)	35.5 (2.4)	0.001 *
SW (mm)	44.64 (3.9)	43.70 (3.6)	45.87 (4.2)	0.114
NSA (°)	122.83 (4.8)	123.25 (4.7)	122.30 (5.2)	0.559
Offset (mm)	47.69 (5.8)	46.65 (4.8)	49.07 (6.9)	0.231
IFAL (mm)	56.76 (5.9)	55.65 (5.2)	58.23 (6.6)	0.202
Singh (grade)	4.46 (0.9)	4.40 (0.9)	4.5 (0.9)	0.677
Neck index	0.064 (0.036)	0.073 (0.043)	0.053 (0.022)	0.112

* significant difference compared to women.

PFAL: proximal femur axis length, HW: Head Width, NW: Neck Width, SW: Shaft Width, NSA: Neck Shaft Angle, IFAL: Internal femur axis length.

Table 9.3 - Means for the DXA variables studied (SD between brackets)

	All (n=35)	Female (n=20)	Male (n=15)	p value
Neck BMD ¹	0.685 (0.181)	0.634 (0.153)	0.752 (0.199)	0.054
Ward's BMD	0.511 (0.196)	0.465 (0.104)	0.574 (0.200)	0.103
Trochanteric BMD	0.694 (0.92)	0.647 (0.147)	0.757 (0.230)	0.096
T-score	-1.48 (1.4)	-1.62 (1.3)	1.3 (1.5)	0.501

¹all BMD measurements in gcm⁻²

Table 9.4 - Means for the QCT parameters studied (between brackets)

	All (n=35)	Female (n=20)	Male (n=15)	p value
Total integral BMD ¹	206.20 (58.1)	209.12 (61.4)	202.6 (55.8)	0.764
Total cortical BMD	390.22 (53.0)	392.82 (52.5)	387.07 (55.3)	0.769
Total trabecular BMD	105.60 (33.2)	103.06 (31.7)	108.68 (35.8)	0.647
Neck integral BMD	199.76 (54.5)	201.64 (57.4)	197.47 (52.8)	0.836
Neck cortical BMD	349.18 (49.6)	351.76 (50.7)	346.06 (50.0)	0.756
Neck trabecular BMD	112.53 (33.9)	109.14 (31.7)	116.65 (37.2)	0.549
Troc integral BMD	218.02 (63.0)	221.94 (31.7)	213.26 (61.4)	0.709
Troc cortical BMD	428.83 (64.3)	432.38 (60.0)	424.53 (71.2)	0.741
Troc trabecular BMD	98.78 (33.6)	96.42 (32.6)	101.65 (35.8)	0.647
FNAL (mm)	50.05 (5.0)	50.65 (4.9)	49.31 (5.2)	0.464
Min CSA (mm ²)	1072.20 (169.4)	975.11 (162.6)	1190.08 (80.0)	<0.001 *
Min CSMI-X (mgmm ²)	26271.44 (10990.0)	21202.56 (7728.2)	32426.50 (11437.5)	0.003 *
Min CSMI-Y (mgmm ²)	20482.99 (11562.7)	15919.55 (5981.2)	26024.3 (14289.8)	0.013 *

* significant difference compared to women.

¹ BMD measurements in gcm⁻³, FNAL: Femoral Neck Axis Length, Min CSA: minimum cross-sectional area.

Table 9.5 - Results for mechanical testing (SD between brackets)

	All (n=35)	Female (n=20)	Male (n=15)	p value
Stiffness (kNm ⁻¹)	269.62 (79.8)	244.68 (77.4)	300.80 (74.2)	0.068
Maximum load (kN)	2729.5 (1380.4)	2266.9 (1125.0)	3346.3 (1482.3)	0.020 *
Energy yield (mJ)	10921.5 (1380.4)	9367.9 (8172.2)	12889.3 (7500.7)	0.205

* significant difference compared to women.

Table 9.6 - Linear regression correlations between geometrical parameters and mechanical parameters (r²)

	Stiffness (kNm ⁻¹)	Maximum load (kN)	Energy Yield (mJ)
PFAL (mm)	0.08	0.20 **	0.13 *
HW (mm)	0.07	0.27 **	0.17 *
NW (mm)	0.00	0.10	0.06
SW (mm)	0.02	0.04	0.02
NSA (°)	0.17 *	0.03	0.06
Offset (mm)	0.22 *	0.18 *	0.19 **
IFAL (mm)	0.17 *	0.23 **	0.21 **
Singh (grade)	0.11 *	0.18 *	0.12 *
Neck index	0.02	0.02	0.00

* p<0.05, **p<0.01

PFAL: Proximal Femur Axis Length, HW: Head Width, NW: Neck Width, SW: Shaft Width, NSA: Neck Shaft Angle, IFAL: Internal Femur Axis Length.

Table 9.7 - Linear regression correlations between DXA parameters and mechanical parameters (r²)

	Stiffness (kNm ⁻¹)	Maximum load (kN)	Energy Yield (mJ)
Neck BMD (gcm ⁻²)	0.46 ***	0.61 ***	0.36 ***
Ward's BMD (gcm ⁻²)	0.42 ***	0.49 ***	0.31 ***
Trochanteric BMD (gcm ⁻²)	0.49 ***	0.81 ***	0.49 ***
T-score	0.40 ***	0.51 ***	0.35 ***

* p<0.05, **p<0.01, ***p<0.001.

found between HW and maximum load ($r^2=0.27$, graph 9.1) In table 9.7 the correlations between DXA and mechanical testing is shown, all correlations were highly significant ($p<0.001$). The strongest correlation was found between maximum load and trochanteric BMD ($r^2=0.81$, fig 9.5). Table 9.8 shows the correlations between QCT parameters and mechanical testing. Except for FNAL, minimum CSA and minimum CSMI-Y all parameters showed a high correlation with maximum load. For QCT the strongest correlation was found between maximum load and trochanteric trabecular BMD ($r^2=0.54$, graph 9.2).

Table 9.8 - Linear regression correlations between QCT parameters and mechanical parameters (r²)

	Stiffness (kNm ⁻¹)	Maximum load (kN)	Energy Yield (mJ)
Total integral BMD ¹	0.27 *	0.45 ***	0.32 ***
Total cortical BMD	0.31 **	0.40 ***	0.36 ***
Total trabecular BMD	0.24 *	0.54 ***	0.28 **
Neck integral BMD	0.26 *	0.40 ***	0.22 **
Neck cortical BMD	0.34 *	0.39 ***	0.27 **
Neck trabecular BMD	0.18 *	0.41 ***	0.15 *
Troch. integral BMD	0.27 *	0.42 ***	0.33 ***
Troch. cortical BMD	0.32 **	0.38 ***	0.36 ***
Troch. trabecular BMD	0.31 ***	0.54 ***	0.22 *
FNAL (mm)	0.12	0.09	0.09
Minimum CSA (mm ²)	0.13 *	0.12 *	0.05
Minimal CSMI-X	0.09	0.33 ***	0.14 *
Minimal CSMI-Y	0.00	0.09	0.00

* p<0.05, ** p<0.01, ***p<0.001. ¹ all BMD measurements in mgcm⁻³, FNAL = Femur neck axis length.

Table 9.9 - Linear regression correlations between geometrical and DXA parameters measurements and maximum load (r²), in our study and previously reported data

	This study (n=35)	Maximum load (kN)		
		Bouxsein et al. (n=16) ⁶	Courtney et al. (n=17) ⁸	Cheng et al. (n=64) ⁷
PFAL (mm)	0.20 **	0.27*	. ¹	0.24**
NSA (°)	0.03 ^{NS}	.	.	0.02 ^{NS}
NW (mm)	0.10 **	.	.	0.22**
Neck BMD (gcm ⁻²)	0.61 ***	0.79***	0.92***	0.71***
Ward's BMD (gcm ⁻²)	0.49 ***	.	.	0.59***
Troch. BMD (gcm ⁻²)	0.81 ***	0.81***	0.73***	0.88***

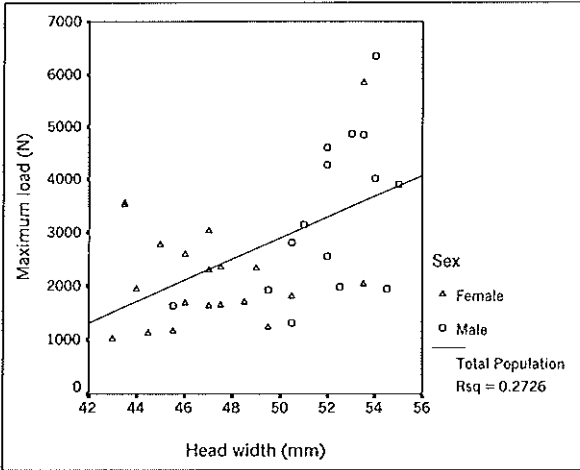
* p<0.05, **p<0.01, ***p<0.001, ^{NS} Not significant, ¹Not mentioned in the published data.

Table 9.10 - Linear regression correlations between QCT measurements and maximum load (r²), in our study and previously reported data

	Maximum load (kN)	
	This study (n=31)	Lang et al. (n=13) ²³
Tot intgl BMD (mgcm ⁻³)	0.45 ***	0.66 **
Tot trab BMD (mgcm ⁻³)	0.54 ***	0.81 **
Tot cort BMD (mgcm ⁻³)	0.40 ***	0.57 **
Neck intgl BMD (mgcm ⁻³)	0.40 ***	0.48 **
Neck trab BMD (mgcm ⁻³)	0.41 ***	0.56 **
Troch intgl BMD (mgcm ⁻³)	0.42 ***	0.67 **
Troch trab BMD (mgcm ⁻³)	0.54 ***	0.87 **

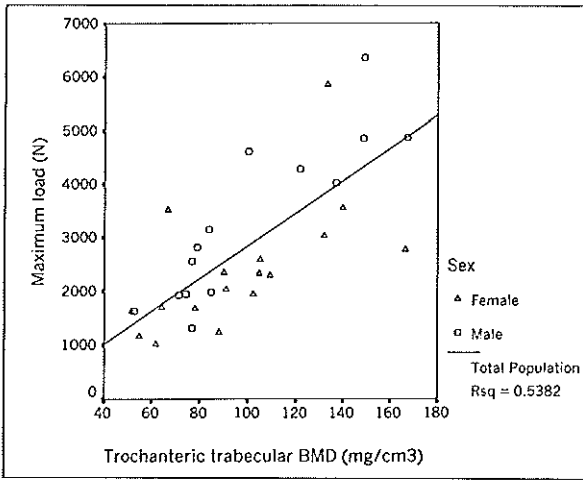
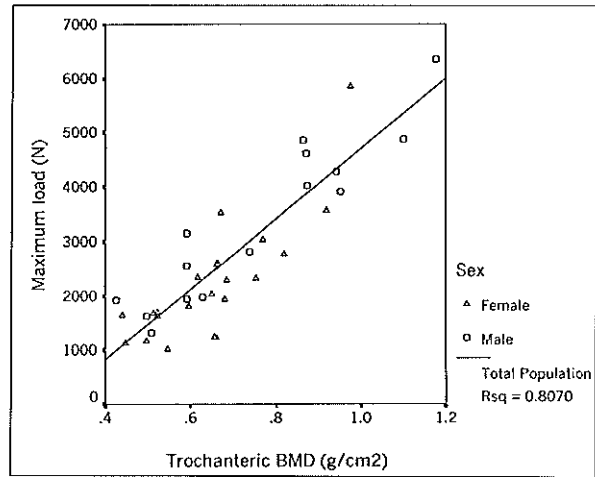
* p<0.05, **p<0.01, ***p<0.001, ^{NS} Not significant.

Tot = Total, Troch= trochanteric, intgl= integral, trab= trabecular, and cort= cortical.



Graph 9.1 - Scatter-plot of maximum load versus head width, as assessed on conventional radiographs

Graph 9.2 - Scatter-plot of maximum load versus trochanteric BMD, as assessed using DXA



Graph 9.3 - Scatter-plot of maximum load versus integral trochanteric BMD, as assessed using QCT

Stepwise regression showed that a combination of trochanteric BMD, as assessed with DXA, and minimum CSA yielded the highest correlation ($r^2=0.85$, $p<0.001$). Whereas trochanteric integral BMD, assessed with QCT, and minimum CSA showed a lower correlation ($r^2=0.67$, $p<0.001$). If only femoral neck or only trochanteric fractures were assessed separately trochanteric BMD, as assessed with DXA, had the strongest correlation in both groups, $r^2=0.78$ and $r^2=0.83$ respectively (both $p<0.001$).

9.4 Discussion

One of the aims of this study was to compare conventional radiography, DXA and QCT with respect to their ability to predict femoral strength. In our study the mean stiffness of the femora was 266 kNm^{-1} (SD 84 kNm^{-1}) which is significantly lower than values previously published, 1560 kNm^{-1} (SD 500 kNm^{-1})⁸. Our mean maximum load, 2451 N (SD 1209 N) also differs significantly from reported studies, where the mean loads range from 3440 N (SD 1330 N) to 3980 N (SD 160 N)^{7,8,18,19}. These differences can be partly explained by the high mean age (82.0 years) of the donors used in this study compared to the other studies (mean age range 69 to 76 years). However, we attribute the differences mainly to the fact that we used embalmed cadaver femora while other studies reported results on fresh cadaveric specimen. The mean energy absorption at the yield point was 10.92 J (SD 1.38 J), this is higher than values for energy absorption reported by Courtney et al., 5.5 J (SD 3.0 J)⁸. A possible explanation for this finding may be that embalming the femora makes them less brittle, therefore the displacement at maximum load could be higher than in fresh cadaver femora.

Geometry of the hip, in particularly the hip axis length, has recently gained considerable interest in epidemiological studies. In several studies, a longer hip axis length has shown to be positively correlated with hip fracture risk^{12,13,20}. In our study, in which we used parameters (i.e. PFAL, IFAL, FNAL) derived from the hip axis length, we could not confirm these results. An epidemiological study by Glüer et al. did not show a correlation between the femur axis length and hip fracture risk²¹. Significant positive correlations exists between maximum load and PFAL ($r^2=0.20$) and IFAL ($r^2=0.23$). This is in accordance with other in-vitro studies who also reported this contrasting finding^{7,18,22}. In our study the highest correlation between maximum load and a geometrical parameter was found for the head width ($r^2=0.27$) (graph 9.1). The Singh index showed a weak but significant correlation with maximum load ($r^2=0.18$). These two findings were also reported by Glüer et al. using data from an epidemiological study²¹.

Bone mineral density measurements are regularly performed using DXA and have shown a high correlation with in-vitro fracture strength^{7,8,18,19}. In our study we found a high correlation between maximum load and trochanteric BMD ($r^2=0.81$, graph 9.2) which was significantly better than for neck BMD

($r^2=0.61$). Even if femoral neck and trochanteric fractures were analysed separately, trochanteric BMD remained the single most significant predictor of femoral strength ($r^2=0.78$ and 0.83 respectively). These correlations correspond well with previously published data, as shown in table 9.9.

Volumetric QCT measurements showed, although slightly weaker, significant correlations with maximum load. The strongest correlation was found for total trabecular BMD and trochanteric trabecular BMD (graph 9.3), both $r^2=0.54$. The non significant correlation of FNAL with maximum load was, given the significant correlations for IFAL and PFAL, remarkable. The variance in the measurement of FNAL did not differ significantly from those of IFAL and PFAL. An explanation, based on our data, for this finding could not be given.

Recently Lang et al. published a study in which the volumetric QCT technique was presented ²³. In their study, with a smaller sample size ($n=13$) and a lower loading rate 0.5 mms^{-1} vs 2.0 mms^{-1} , the correlations between QCT parameters and maximum load were stronger. However, the trend in the correlations for both studies is comparable. In both studies trochanteric trabecular BMD had the strongest correlation with maximum load (table 9.10). The QCT data presented by Cheng et al. are not taken into consideration as they presented no volumetric QCT data ⁷.

Multiple stepwise forward regression showed that a combination of trochanteric BMD with minimum CSA yielded the highest correlation ($r^2=0.85$, $p<0.0001$).

An interesting finding is that DXA performs better than QCT in predicting femoral strength. Even when the QCT measurements were corrected for size, by means of a bivariate regression (BMD +min CSA), the strongest correlation for maximum load was not higher than $r^2=0.68$ for trochanteric trabecular BMD + min CSA.

A significant difference between our study design and those previously published, is the use of embalmed cadaver femora. One of the aims of this study was to investigate whether embalming influences biomechanical properties or correlations between radiological, densitometric and biomechanical parameters. Our results show that although the absolute biomechanical parameters demonstrate a significant difference compared to published studies, the correlations remain intact. This result, taking into account the small sample size, indicates that when correlations are the object of investigation in biomechanical studies, the use of embalmed cadaver material seems to be valid.

9.5 References

1. Gómez Alonso C 1994 Bone mineral density and geometric measurements as predictors of risk for hip fracture. In: Ring EJF, Elvins DM, Bhalte AK (eds.) Fourth Bath conference on osteoporosis and bone mineral measurement. British Institute of Radiology, Bath, pp 24.
2. Johnell O, Gullberg B, Kanis JA, Allander E, Elffors L, Dequeker J, Dilsen G, Gennari C, Lopez Vaz A, Lyritis G, Mazzuolo G, Miravet L, Passeri M, Perez Cano R, Rapado A, Ribot C 1995 Risk factors for hip fracture in European women: The MEDOS study. *J Bone Miner Res* 10(11):1802-15.
3. Melton III LJ 1993 Hip fractures: A worldwide problem today and tomorrow. *Bone* 14(suppl):1-8.
4. Poór G, Atkinson EJ, O'Fallon WM, Melton III LJ 1995 Predictors of hip fractures in elderly men. *J Bone Miner Res* 10(12):1900-7.
5. Cummings SR, Nevitt MC, Browner WS, Stone K, Fox KM, Ensrud KE, Cauley J, Black D, Vogt TM 1995 Risk factors for hip fracture in white women. *New Eng J Med* 332(12):767-73.
6. Bouxsein ML, Courtney AC, Hayes WC 1995 Ultrasound and densitometry of the calcaneus correlate with the failure loads of cadaveric femurs. *Calcif Tissue Int* 56:99-103.
7. Cheng XC, Lowet G, Boonen S, Nicholson PHF, Brys P, Nijs J, Dequeker J 1997 Assessment of strength of the proximal femur in vitro: Relationship to femoral bone mineral density and femoral geometry. *Bone* 20(3):213-8.
8. Courtney AC, Wachtel EF, Myers ER, Hayes WC 1995 Age-related reduction in the strength of the femur tested in a fall-loading configuration. *J Bone Joint Surg* 77-A(3):387-95.
9. Lotz JC, Hayes WC 1990 The use of quantitative computed tomography to estimate risk of fracture of the hip from fall. *J Bone Joint Surg* 72-A(5):689-700.
10. Nicholson PHF, Lowet G, Cheng XG, Boonen S, van der Perre G, Dequeker J 1996 Evaluation of bone mineral density and calcaneal ultrasound as predictors of femoral strength. In: vander Sloten J, Lowet G, van Audekercke R, van der Perre G (eds.) 10th conference of the European society of biomechanics, Leuven, Belgium, pp 74.
11. Nicholson PHF, Lowet G, Cheng XG, Boonen S, van der Perre G, Dequeker J 1997 Assessment of the strength of the proximal femur in vitro: Relationship with ultrasonic measurement of the calcaneus. *Bone* 20(3):219-24.
12. Boonen S, Koutri R, Dequeker J, Aerssens J, Lowet G, Nijs J, Verbeke G, Lesaffre E, Geusens P 1995 Measurement of femoral geometry in type I and type II osteoporosis: Differences in hip axis length consistent with heterogeneity in the pathogenesis of osteoporotic fractures. *J Bone Miner Res* 10(12):1908-12.
13. Faulkner KG, Cummings SR, Black D, Palermo L, Glüer CC, Genant HK 1993 Simple measurement of femoral geometry predicts hip fracture: The study of osteoporotic fractures. *J Bone Miner Res* 8(10):1211-7.
14. Rubin PJ, Leyvraz PF, Aubaniac JM, Argenson JN, Esteve P, de Roguin B 1992 The morphology of the proximal femur: A three-dimensional radiographic analysis. *J Bone Joint Surg* 74-B(1):28-32.
15. Fredensborg N, Nilsson BE 1977 Cortical index of the femoral neck. *Acta Radiol Diagnos* 18:492-6.

16. Singh M, Nagrath AR, Maini PS 1970 Changes in trabecular pattern of the upper end of the femur as an index of osteoporosis. *J Bone Joint Surg* 52-A(3):457-67.
17. Müller ME, Nazarian S, Koch P, Schatzker J 1990 The comprehensive classification of fractures of long bones. Springer-Verlag, Berlin Heidelberg, pp 116-27.
18. Bouxsein ML, Radloff SE 1997 Quantitative Ultrasound of the calcaneus reflects the mechanical properties of calcaneal trabecular bone. *J Bone Miner Res* 12(5):839-46.
19. Pinilla TP, Boardman KC, Bouxsein ML, Myers ER, Hayes WC 1996 Impact direction from fall influences the failure load of the proximal femur as much as age-related bone loss. *Calcif Tissue Int* 58:231-5.
20. Nakamura T, Turner CH, Yoshikawa T, Slemenda CW, Peacock M, Burr DB, Mizuno Y, Orimo H, Ouchi Y, Johnston Jr CC 1994 Do variations in hip geometry explain differences in hip fracture risk between Japanese and white Americans. *J Bone Miner Res* 9(7):1071-6.
21. Glüer CC, Cummings SR, Pressman A, Li J, Glüer K, Faulkner KG, Grampp S, Genant HK 1994 Prediction of hip fractures from pelvic radiographs: The study of osteoporotic fractures. *J Bone Miner Res* 9(5):671-7.
22. Karlsson KM, Sernbo I, Obrant KJ, Redlund-Johnell I, Johnell O 1996 Femoral neck geometry and radiographic signs of osteoporosis as predictors of hip fracture. *Bone* 18(4):327-30.
23. Lang TF, Keyak JH, Heitz MW, Augat P, Lu Y, Mathur A, Genant HK 1997 Volumetric quantitative computed tomography of the proximal femur: Precision and relation to bone strength. *Bone* 21(1):101-8.

Chapter 10

General discussion

"Tracking something" said Winnie-the-Pooh very mysteriously.
"Tracking what?" said Piglet, coming closer.
"That's just what I ask myself. I ask myself, what?".
"What do you think you'll answer?".
"I shall have to wait till I catch up with it" said Winnie-the-Pooh.

A.A. Milne

10.1 Introduction

In light of the rapidly increasing global problem of osteoporotic hip fractures, as stated in chapter 1, it is important to detect those at high risk of hip fractures at an early stage enabling preventive treatment. In 1994 a WHO study group stated that "The risk of fracture worldwide may be only partly explained by differences in bone density between communities. Data describing the relationship between fracture risk in specific sites and the distribution of bone mineral density (BMD) are required to clarify this"¹. Also, one can state that in order to predict hip fractures the basic mechanics of these fractures should at least be understood. In order to gain more knowledge of the mechanics of fracture and the relation with radiological and densitometric parameters a cadaver based study was undertaken. The aim of this dissertation is to address the following questions:

1. What are the mechanics of a hip fracture ?
2. Can we design a model that simulates falls leading to fractures of the hip ?
3. Can we assess the strength of the proximal femur with radiographic and densitometric (DXA and QCT) procedures ?

This final chapter will discuss the study design, the main results and the clinical implications. Suggestions for future research will be given.

10.2 Study design

The study design consisted of two parts, first a radiological and densitometric study of embalmed cadaver femora. Second a biomechanical study, in which a new device for dynamic biomechanical testing of femora is presented². The latter also focusses on the correlation between radiological and densitometric parameters on one side and biomechanical parameters on the other. Biomechanical parameters are obtained either using the new device or using a semi-static technique as published previously³⁻⁸.

The radiological evaluation consisted of:

- a) Conventional radiology which has gained renewed interest in the field of osteoporosis, prompted by recent publications of several excellent epidemiological studies assessing the relationship between geometry of the proximal femur and hip fracture risk⁹⁻²⁰. Especially the hip axis length has shown to be a good predictor of hip fracture risk^{11,12}. The use of direct magnification radiography (DIMA) is relatively novel²¹⁻²⁴. Geometry was measured using both conventional and DIMA radiography.
- b) Dual-energy X-ray absorptiometry is currently the most widely used technique for the detection of osteoporosis and by some even propagated as gold standard²⁵. Despite some technical problems DXA is capable of measuring bone mass in a short time with a high precision^{26,27}. The bone mass as measured with DXA has shown to be a predictor of hip fracture risk^{18,28-32}.
- c) Quantitative computed tomography is to date the only technique capable of measuring true volumetric bone density and separating trabecular and cortical bone³³⁻³⁵. Due to the intricate geometry of the hip there are no systems available to perform these measurements in a clinical setting³⁶. The technique presented in this dissertation has been developed at the Osteoporosis and Arthritis Research Group of the University of California, San Francisco, USA, and can be perceived as a pre-clinical system^{6,37,38}. This part of the study also focussed on the influence of scanning technique, sequential versus spiral, on BMD measurements.

The biomechanical analysis consisted of:

- a) Loading cadaveric femora in a true to life fashion, i.e. with a high loading speed and simulating muscular compression forces, using a new device. The design of this new loading device, presented in chapter seven was based on three assumptions were made; first, for a fall to result in a hip fracture it must be directed sideways³⁹. Second, the muscular component which also seems to be an important factor in fracture mechanics, should also be incorporated in the model⁴⁰. And third, the loading rate must be higher, in the order of 3 ms^{-1} as shown in

- an in-vivo study, than the 2 mms⁻¹ currently used in most semi-static in-vitro studies ^{41,42}. This device has been developed as part of this dissertation and is to our knowledge unique in the world ².
- b) Loading cadaveric femora in a semi-static fashion simulating a fall on the trochanter. The femur is loaded in an angle of 10° with respect to the horizontal and in 15° endo-rotation. With this technique the femora are loaded with a low loading speed and the muscular compression forces are not simulated. Although it clearly doesn't resemble in-vivo falls, this technique is currently the most widely used for in-vitro loading studies of the proximal femur ^{3-5,7,43}.

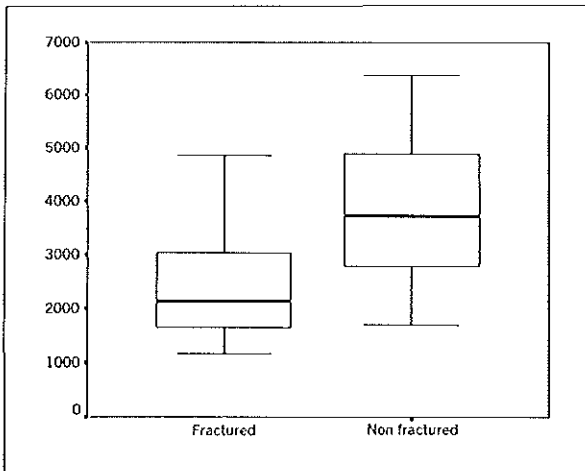
10.3 Main results

Geometrical measurements made on conventional and DIMA radiographs were compared in chapter three. Both techniques showed high inter- and intra-observer variance for the assessment of the Singh index. This high variance was also reported in a clinical study presented by Koot et al. ⁴⁴. Furthermore, this study showed that the use of DIMA had no additional value for the measurement of femoral geometry and as such this technique should not be advised for studies related to osteoporosis.

In chapter five we used a relatively new volumetric QCT technique of the hip, developed at the Osteoporosis and Arthritis Research Group, University of California, San Francisco, was used ^{6,37}. With the increased use of spiral CT, promoting higher patient comfort and shorter scanning times, it would be beneficial if this technique could also be used in quantitative CT. A previously published study suggests that, as spiral CT is more susceptible to partial volume effects, quantitative CT could be negatively influenced by that technique ⁴⁵. Our study however showed no significant differences in BMD values obtained using either technique, making the clinical use of spiral QCT more acceptable to both clinician and patient.

The new device presented in chapter seven is to our knowledge a unique approach to assess in-vitro femoral strength. This new technique mimics the aetiology of the sequences leading to a hip fracture ^{39,41,46}. It also realistically simulates the acetabulum, the muscles surrounding the femur, and the soft tissue overlying the trochanter major.

The new technique, which yields a dichotomous sample, fractured versus non-fractured femora, showed that total trabecular BMD, trochanteric trabecular BMD, minimum cross-sectional moment of inertia along the y-axis (all assessed using QCT) and PFAL (assessed on conventional radiographs) had the highest sensitivity and specificity for the prediction of femoral strength in a logistic regression model. The loading tests resulted in 13.5% (n=5) femoral neck, 43.2% (n=16) trochanteric, and 5.5% (n=2) subtrochanteric fractures. 37.8% (n=14) of the femora showed no fractures.



Graph 10.1 - Box-plot of maximum load of the contra lateral femur (chapter 9) versus the paired dichotomous fracture data (chapter 8).

This pattern, given the relative high age of our donors, resembles that as seen in a clinical setting, indicating that our technique does indeed emulate real life falls ^{47,48}.

To compare our sample of femora and to test the validity of the use of embalmed cadaver femora, we also performed

semi-static loading test used in many published studies ^{4-8,42,43}. The results of the semi-static technique showed that trochanteric BMD, as measured with DXA, had the highest correlation with maximum load ($r^2=0.81$, $p<0.001$). The QCT parameters showed significantly lower correlations.

After pairing the dichotomous fracture data (chapter 8) with the maximum load of the contra lateral femur (chapter 9) a significant difference was found for the maximum load between the fractured and non-fractured specimen ($p=0.015$, graph 10.1). This result provides further proof that our new technique is a valid method to assess bone strength.

The results of our study suggest that our new technique which emulates the aetiology of the sequences leading to a hip fracture and yields a fracture pattern as seen in a clinical setting, performs better than the semi-static techniques used previously. Furthermore the results suggest that bone density as well as geometrical parameters play a role in fracture prediction.

10.4 Discussion of main results

The first part of this paragraph is based on the outcome of the new dynamic study, as this seems to have the closest resemblance to the in-vivo situation. It is necessary to remember that this is an in-vitro study which only focusses on geometric and densitometric parameters. As not only those factors contribute to hip fracture risk, other factors such as mental state, muscle strength, concomitant disease, visual impairment and the surface on which the person falls are additional parameters which have to be considered in the in-vivo situation ⁴⁹. Furthermore bone architecture and inherent bone quality could play a role in fracture risk prediction. However, currently there are no methods available that can reliably describe the architecture or bone quality

with non-invasive techniques. Therefore they are beyond the scope of this dissertation.

The highest sensitivity and specificity was found for QCT parameters (appendix 8-A). This finding combined with the unique capability of QCT to separately assess trabecular and cortical bone, makes QCT a very interesting technique for the diagnosis of osteoporosis of the hip. As trabecular bone is more susceptible to metabolic changes, QCT could be also very valuable in the monitoring of therapeutic interventions^{50,51}. Volumetric QCT provides a 3D data set that gives the opportunity to measure additional geometrical parameter such as the minimum cross-sectional area, and the derived minimum cross-sectional moments of inertia. These parameters also showed a relatively high sensitivity and specificity in a logistic regression model.

QCT has a relatively low radiation dose; in a publication on hip QCT Cann et al. reported on the effective absorbed dose in a scanning protocol comparable to that suggested by Lang et al. for in-vivo studies^{6,52}. The effective dose reported was 40 μSv , which is low compared to a standard radiograph of one hip which is approximately 300 μSv (table 10.1)⁵³. A disadvantage is the limited availability of commercial software capable of hip QCT. Furthermore, no reference data are currently available.

The second best sensitivity and specificity for the prediction of femoral strength was found for a geometric parameter; proximal femur axis length, which is assessed on conventional radiographs. Given the wide availability of radiographic techniques and low cost of operation, this suggests that geometry measured on conventional radiographs is a promising technique to detect those at risk for hip fractures. However, before this technique can be introduced into a clinical setting it is of the utmost importance that normal data are gathered and cut-off points for hip fracture risk are determined. This would make it possible to express the data as either T- or Z-scores, which indicate the status of the individual patient. A disadvantage of conventional radiographs is the relative high radiation dose, which is 300 μSv for a targeted hip view and 1000 μSv for a pelvic view (table 10.1). In our study we used a correction for magnification so that true dimensions could be assessed. It has been shown that additional variability due to different magnification factors play an important role in the interpretation of geometrical parameters¹⁴. Therefore strict standardized operating

Table 10.1 - Effective doses and their equivalent natural radiation period^{52,64}.

Examination	Effective dose (μSv)	Approximate equivalent period of natural background radiation
X-hip (only one)	300	2 months
X-pelvis	1000	6 months
QCT-hip	40	1 week
DXA-hip	15	1 day

procedures with regard to patient placement and magnification are important⁵⁴. It is unlikely that the measurements of geometrical parameters could play a role in monitoring intervention studies. As such this technique seems to be more suitable as a simple screening tool.

DXA showed the highest sensitivity and specificity for trochanteric BMD (sensitivity 78.3% and specificity 64.3%); these values were less than those found in QCT and conventional radiography. However, this technique is widely used and relatively easy to perform. Recent improvements in system design have enhanced spatial resolution which gives DXA the potential of obtaining additional geometry measurements on these images. Reference data for hip BMD are widely available and it is likely that reference data for hip axis length will be available soon. The effective dose of this technique is in the order of approximately 15 μ Sv (table 10.1). A relative disadvantage is that DXA of the hip gives an integral measurement of the hip and therefore is comparably less sensitive to changes over time compared to QCT. An additional disadvantage is the influence of soft tissue on the measurements. Although the dual-energy technique corrects for the presence of soft tissue DXA has shown to be dependent on changes in weight and body changes²⁷. Both DXA and QCT are equally influenced by the fat marrow content in the proximal femur⁵⁵.

Our semi-static study showed similar results as previously published, a relative high correlation of trochanteric BMD with maximum load as well as significant correlations with geometrical parameters^{3,4,8,43,56}. The results of the semi-static loading study can not be directly compared to the dynamic study as the biomechanical principles are essentially different. The semi-static study uses force transduction whereas the dynamic model is based upon impulse moments. We feel that the dynamic test resembles more the impact of a fall on the hip than the semi-static techniques used previously. Our new device gives an outcome as seen in a clinical setting, where under comparable loading conditions some patients break their hip and some don't.

Both studies show that bone mineral density as well as geometrical parameters play a role in fracture mechanics. Our small sample size did not allow for definite conclusions concerning the combination of parameters in predicting femoral strength. It can be speculated however that because of the high correlations, sensitivity and specificity of bone mineral density measurements with fracture outcome or maximum load, the addition of any other parameter will contribute only little to the predictive power. In clinical practice where additional factors, such as discussed previously, as well as the normal biological distribution of all factors play a role, unravelling the contribution of all factors to fracture risk will be difficult.

10.5 Suggestions for future research

In this dissertation we have presented a new technique to perform in-vitro loading tests on cadaver femora. This technique has proven to be capable of generating fractures as seen in a clinical setting. Our conclusions are limited by the relatively small sample size, future studies using larger samples are required to confirm our findings. Furthermore these studies should also focus on the combination of parameters in predicting femoral strength.

As stated in the discussion of the main results, one of the factors not taken into account in this dissertation is bone architecture. The introduction of high resolution QCT could be an interesting aspect for future research⁵⁷⁻⁶⁰. Combination of BMD, geometry and bone architecture could well enhance the predictive power of QCT.

Our new device could also be used for studies into the effect of external hip protectors⁶¹⁻⁶³. The use of such protectors has been propagated to reduce the risk of hip fractures after a fall, by lowering the impact forces on the hip. With our device, which has shown to be capable of generating fractures, innovative research could be performed to further analyse and design external hip protectors.

10.6 References

1. WHO study group 1994 Assessment of fracture risk and it's application to screening for postmenopausal osteoporosis. WHO Technical reports series, Geneva.
2. van Rijn RR, Niesing R, Mulder BN, Grashuis JL 1996 Realistic hip fractures in vitro; a different approach. *Osteoporosis Int* 6(suppl 1):145.
3. Bouxsein ML, Courtney AC, Hayes WC 1995 Ultrasound and densitometry of the calcaneus correlate with the failure loads of cadaveric femurs. *Calcif Tissue Int* 56:99-103.
4. Cheng XC, Lowet G, Boonen S, Nicholson PHF, Brys P, Nijs J, Dequeker J 1997 Assessment of strength of the proximal femur in vitro: Relationship to femoral bone mineral density and femoral geometry. *Bone* 20(3):213-8.
5. Courtney AC, Wachtel EF, Myers ER, Hayes WC 1995 Age-related reduction in the strength of the femur tested in a fall-loading configuration. *J Bone Joint Surg* 77-A(3):387-95.
6. Lang TF, Keyak JH, Heitz MW, Augat P, Lu Y, Mathur A, Genant HK 1997 Volumetric quantitative computed tomography of the proximal femur: Precision and relation to bone strength. *Bone* 21(1):101-8.
7. Lotz JC, Hayes WC 1990 The use of quantitative computed tomography to estimate risk of fracture of the hip from fall. *J Bone Joint Surg* 72-A(5):689-700.
8. Pinilla TP, Boardman KC, Bouxsein ML, Myers ER, Hayes WC 1996 Impact direction from fall influences the failure load of the proximal femur as much as age-related bone loss. *Calcif Tissue Int* 58:231-5.
9. Beck TJ, Ruff CR, Mourtada FA, Shaffer RA, Maxwell-Williams K, Kao GL, Sartoris DJ, Brodine S 1996 Dual-energy X-ray absorptiometry derived structural geometry for stress fracture prediction in male U.S. marine corps recruits. *J Bone Miner Res* 11(5):645-53.
10. Boonen S, Koutri R, Dequeker J, Aerssens J, Lowet G, Nijs J, Verbeke G, Lesaffre E, Geusens P 1995 Measurement of femoral geometry in type I and type II osteoporosis: Differences in hip axis length consistent with heterogenicity in the pathogenesis of osteoporotic fractures. *J Bone Miner Res* 10(12):1908-12.
11. Faulkner KG, Cummings SR, Black D, Palermo L, Glüer CC, Genant HK 1993 Simple measurement of femoral geometry predicts hip fracture: The study of osteoporotic fractures. *J Bone Miner Res* 8(10):1211-7.
12. Faulkner KG, Mac Clung M, Cummings SR 1994 Automated evaluation of hip axis length for predicting hip fracture. *J Bone Miner Res* 9(7):1065-70.
13. Geusens P 1996 Geometric characteristics of the proximal femur and hip fracture risk. *Osteoporosis Int* 6(suppl 3):27-30.
14. Glüer CC, Cummings SR, Pressman A, Li J, Glüer K, Faulkner KG, Grampp S, Genant HK 1994 Prediction of hip fractures from pelvic radiographs: The study of osteoporotic fractures. *J Bone Miner Res* 9(5):671-7.
15. Gómez Alonso C 1994 Bone mineral density and geometric measurements as predictors of risk for hip fracture. In: Ring EJF, Elvins DM, Bhalke AK (eds.) Fourth Bath conference on osteoporosis and bone mineral measurement. British Institute of Radiology, Bath, pp 24.
16. Grampp S 1992 Korrelation von Knochenmasse, Knochengeometrie und Bruchfestigkeit am Schenkelhals [dissertation] Klinik für Radiologie, Nuklearmedizin und Physikalische Therapie. Freien Universität, Berlin, pp 94.

17. Mikhail MB, Vaswani AN, Aloia JF 1996 Racial differences in femoral dimensions and their relation to hip fracture. *Osteoporosis Int* 6:22-4.
18. Peacock M, Turner CH, Liu G, Manatunga AK, Timmerman L, Johnston jr CC 1995 Better discrimination of hip fracture using bone density, geometry and architecture. *Osteoporosis Int* 5:167-73.
19. Slis HW, van Daele PLA, Kuiper JW, Burger H, Algra D, Hofman A, Birkenhäger JC, Pols HAP 1995 The use of simple geometric measurements on standard pelvic X-rays in the prediction of hip fractures. *Osteoporosis Int* 5(4):311.
20. Yoshikawa T, Turner CH, Peacock M, Slemenda CW, Weaver CM, Teegarden D, Markwardt P, Burr DB 1994 Geometric studies of the femoral neck using dual-energy X-ray absorptiometry. *J Bone Miner Res* 9:1053-64.
21. Poulsen Nautrup C, Berens von Rautenfeld D 1991 Direktradiographischen Vergrößerung in der experimentellen Medizin. *Radiologe* 31:430-4.
22. Pruneau D, Faszold S, Sostarich D, Weinshilbaum K 1987 A practical approach to direct magnification radiography. *Radiol Technol* 59(2):121-7.
23. Reuther G, Krohnholz HL, Hüttenbrink KB 1991 Entwicklung und Perspektiven der medizinischen Vergrößerungsradiographie. *Radiologe* 31(9):403-6.
24. Schlossarek W, Wunderer S, Frühwald F 1987 Direkte Röntgenvergrößerung und ihre Aussagekraft bei Strukturänderungen im Spongiosabereich. *Fortschr Kiefer Gesichtschir* 32:14-6.
25. Netelenbos JC, Lips P 1996 Botdichtheidsmeting en de preventie van fracturen: Wie komen hiervoor in aanmerking? *Ned Tijdschr Geneesk* 140(20):1061-4.
26. Genant HK, Engelke K, Fuerst T, Glüer CC, Grampp S, Harris ST, Jergas M, Lang T, Majumdar S, Mathur A, Takada M 1996 Noninvasive assessment of bone mineral and structure: State of the art [review]. *J Bone Miner Res* 11(6):707-30.
27. Tothill P, Hannan WJ, Cowen S, Freeman CP 1997 Anomalies in the measurement of changes in total-body bone mineral by dual-energy X-ray absorptiometry during weight change. *J Bone Miner Res* 12(11):1908-21.
28. Burger H, van Daele PLA, van den Ouweland FA, Grobbee DE, Hofman A, van Kuijk C, Schütte HE, Birkenhäger JC, Pols HAP 1994 The association between age and bone mineral density in men and women aged 55 years and over: The Rotterdam study. *Bone Miner* 25:1-13.
29. Greenspan SL, Myers ER, Maitland LA, Kido TH, Krasnow MB, Hayes WC 1994 Trochanteric bone mineral density is associated with type of hip fracture in the elderly. *J Bone Miner Res* 9(12):1889-94.
30. Lunt M, Felsenberg D, Adams J, Benevolenskaya L, Cannata J, Dequeker J, Dodenhof D, Falch JA, Johnell O, Shaw K-T, Masaryk P, Pols H, Poor G, Reid D, Scheidt-Nave C, Weber K, Silman AJ, Reeve J 1997 Population-based geographic variations in DXA bone density in Europe: The EVOS study. *Osteoporosis Int* 7(3):175-89.
31. Mautalen C, Vega E, Gonzáles D, Carrilero P, Silberman F 1995 Ultrasound and dual X-ray absorptiometry in women with hip fracture. *Calcif Tissue Int* 57:165-8.
32. Stewart A, Reid DM, Porter RW 1994 Broadband ultrasound attenuation and dual energy X-ray absorptiometry in patients with hip fractures: Which technique discriminates fracture risk. *Calcif Tissue Int* 54:466-9.
33. Genant HK, Boyd D 1977 Quantitative bone mineral analysis using dual-energy computed tomography. *Invest Radiol* 12(6):545-51.

34. van Kuijk C 1991 Evaluation of postprocessing dual-energy quantitative computed tomography [dissertation] Department of Experimental Radiology. Erasmus University, Rotterdam, pp 115.
35. van Kuijk C, Genant HK 1993 Quantitative CT in osteoporosis. In: Thrall JA (ed.) Current practice in radiology. Mosby Year Book, St. Louis, pp 336-8.
36. Kuiper JW, van Kuijk C, Grashuis JL 1997 Distribution of trabecular and cortical bone related to geometry; a quantitative computed study of the femoral neck. *Invest Radiol* 32(2):83-9.
37. Lang T, Heitz M, Keyak J, Genant HK 1996 A 3D anatomic coordinate system for hip QCT. *Osteoporosis Int* 6(suppl 1):203.
38. van Rijn RR, Lang TF, Niesing R, Sniijders CJ, Schütte HE, van Kuijk C 1998 In vitro volumetric quantitative computed tomography of the proximal femur: Helical versus sequential 4th International Somatom plus CT scientific user conference, De Doelen, Rotterdam, the Netherlands.
39. Cummings SR, Nevitt MC 1989 A hypothesis: The cause of hip fractures. *J Geront* 44(4):M107-11.
40. Hirsch C, Frankel VH 1960 Analysis of forces producing fractures of the proximal end of the femur. *J Bone Joint Surg* 42-B(3):633-40.
41. van den Kroonenberg A 1995 Dynamic models of human falls for prediction of hip fracture risk [dissertation] Department of mechanical engineering. Massachusetts Institute of Technology, Boston.
42. Bouxsein ML, Boardman KC, Pinilla TP, Myers EM 1995 Ability of bone properties at the femur, forearm, and calcaneus to predict the structural capacity of the proximal femur during a sideways fall. *J Bone Miner Res* 10(suppl 1):178.
43. Nicholson PHF, Lowet G, Cheng XG, Boonen S, van der Perre G, Dequeker J 1997 Assessment of the strength of the proximal femur in vitro: Relationship with ultrasonic measurement of the calcaneus. *Bone* 20(3):219-24.
44. Koot VCM, Kesselaer SMMJ, Clevers GJ, de Hooge P, Weits T, van der Werken C 1996 Evaluation of the Singh index for measuring osteoporosis. *J Bone Joint Surg* 78B(5):831-4.
45. Horrocks JA, Speller RD 1994 Helical computed tomography: Where's the cut? *Br J Radiol* 67(793):107-11.
46. van den Kroonenberg AJ, Hayes WC, McMahon TA 1996 Hip impact velocities and body configurations for voluntary falls from standing height. *J Biomechanics* 29(6):807-11.
47. Kanis JA 1994 Osteoporosis. Blackwell Science Ltd., Oxford, pp 254.
48. Karagas MR, Lu-Yao GL, Barrett JA, Beach ML, Baron JA 1996 Heterogeneity of hip fracture: Age, race, sex, and geographic patterns of femoral neck and trochanter fractures among the US elderly. *Am J Epidemiol* 143:677-82.
49. Brocklehurst JC, Exton-Smith AN, Lempert Barber SM, Hunt LP, Palmer MK 1978 Fracture of the femur in old age: A two-centre study of associated clinical factors and the cause of fall. *Age Ageing* 7:7-15.
50. Berning B, van Kuijk C, Kuiper JW, Coelingh Bennink HJT, Kicovic PM, Fauser BCJM 1996 Effect of two doses of Tibolone on trabecular and cortical bone loss in early postmenopausal women: A two-year randomized, placebo-controlled study. *Bone* 19(4):395-9.

51. Reinbold WD, Wannennmacher M, Hodapp N, Adler CP 1989 Osteodensitometry of vertebral metastases after radiotherapy using quantitative computed tomography. *Skeletal Radiol* 18:517-21.
52. Cann C, Sanches S, Arnaud C, Roe B, del Puerto G, Pierini E 1996 3D QCT BMD of the hip; regional comparison with DXA. *J Biomed Mater Res* 11:5479.
53. Kalender WA 1992 Effective dose values in bone mineral measurement by photon absorptiometry and computed tomography. *Osteoporosis Int* 2:82-7.
54. van Bodegom JW, Kuiper JW, van Rijn RR, van Kuijk C, Zwamborn AW, Grashuis JL 1998 Vertebral dimensions: Influence of X-ray technique and patient size on measurements. *Calcif Tissue Int* 62(3):214-8.
55. Kuiper JW, van Kuijk C, Slis H, Grashuis JL, Schütte HE 1996 Influences of surrounding soft tissue and bone of the pelvis on quantitative CT measurements of the femoral neck. *Osteoporosis Int* 6(suppl 1):183.
56. Nicholson PHF, Lowet G, Cheng XG, Boonen S, van der Perre G, Dequeker J 1996 Evaluation of bone mineral density and calcaneal ultrasound as predictors of femoral strength. In: vander Sloten J, Lowet G, van Audekercke R, van der Perre G (eds.) 10th conference of the European society of biomechanics, Leuven, Belgium, pp 74.
57. Engelke K, Kalender W 1998 Beyond bone densitometry: Assessment of bone architecture by x-ray computed tomography at various levels of resolution. In: Genant HK, Gugliemi G, Jergas M (eds.) *Bone densitometry and osteoporosis*, 1 ed. Springer, Berlin, pp 602.
58. Feldkamp LA, Goldstein SA, Parfitt AM, Jesion G, Kleerekoper M 1989 The direct examination of three-dimensional bone architecture in vitro by computed tomography. *J Bone Miner Res* 4(1):3-11.
59. Goldstein SA, Goulet R, McCubbrey D 1993 Measurement and significance of three-dimensional architecture at the mechanical integrity of trabecular bone (review). *Calcif Tissue Int* 53(suppl 1):S127-32.
60. Link TM, Majumdar S, Lin JC, Newitt D, Augat P, Ouyang X, Mathur A, Genant HK 1998 A comparative study of trabecular bone properties in the spine and femur using high resolution MRI and CT. *J Bone Miner Res* 13(1):122-32.
61. Parkari J, Kannus P, Heikkilä J, Poutala J, Sievänen H, Vuori I 1995 Energy-shunting external hip protector attenuates the peak femoral impact force below the theoretical fracture threshold: An in vitro biomechanical study under falling conditions of the elderly. *J Bone Miner Res* 10(10):1437-42.
62. Lauritzen JB, Hindso K, Sonne-Holm S, Pedersen MM, Lund B 1996 Effect of hip protectors in falls on the hip. *Osteoporosis Int* 6(suppl 1):95.
63. Okuizumi H, Harada A 1997 Effects of trochanteric padding system on femoral neck under simulated fall. *J Bone Miner Res* 12(suppl 1):169.
64. The Royal College of Radiologists 1993 Making the best use of a department of clinical radiology, 2 ed. The Royal College of Radiologists, London, pp 72.

Summary

Osteoporosis is a very common skeletal disease. In 1994 the world health organization gave the following definition of osteoporosis: 'osteoporosis is a disease characterised by low bone mass and micro-architectural deterioration of bone tissue, leading to enhanced bone fragility and a consequent increase in fracture risk'. The most serious outcome of osteoporosis is a fracture of the hip. In day to day practice the term hip fracture is used for fractures of the proximal femur, i.e. the upper end of the thighbone. This fracture mainly occurs in Caucasian females aged 70 year and over (in all more than 90% of all hip fractures occur in this group). The consequences of these fractures are serious, with a reported mortality (death resulting from the hip fracture) rate of approximately 25% and a morbidity (disease resulting from a hip fracture) rate of approximately 30%. Besides these medical aspects there's also an important socioeconomic aspect. A recent study has shown that in 1993 the cost for hip fractures in the Netherlands amounted to 362 million Dutch guilders. In light of the expected increase of the ageing population in the near future, osteoporosis is an important and serious health threat. It is therefore of the utmost importance to detect those at high risk for hip fractures at an early stage. In order to succeed it is necessary to get familiarized with the relationship between radiologic and densitometric parameters and the strength of the proximal femur. This is the basic question to be addressed in the study presented in this dissertation.

Chapter one describes hip fractures and osteoporosis from a historical, social and medical perspective. Furthermore the microscopic anatomy of bone and macroscopic anatomy of the hip are briefly discussed. This introductory chapter is concluded by stating the aim of this study.

Chapter two discusses the different classification systems of fractures of the proximal femur furthermore the choice for the classification system used in this study is discussed.

Chapter three focusses on measurements of geometrical parameters of the proximal femur as performed on embalmed human cadaver femora. These measurements were done using conventional and direct magnification (DIMA) radiography. Several epidemiological studies have shown that, geometrical parameters have a predictive power for fracture risk.

Dual-energy x-ray absorptiometry (DXA) measurements are presented in chapter four. Currently DXA is the most widely used technique for the early detection of osteoporosis and monitoring of therapeutic interventions.

Chapter five describes the measurements performed with quantitative computed tomography (QCT). These measurements were performed in

cooperation with the Osteoporosis and Arthritis Research Group of the university of California, San Francisco, USA. Due to the intricate geometry of the proximal femur QCT measurements of this region are not used in a clinical setting. The technique used in this dissertation is however a predecessor of a technique which could well be introduced in a clinical setting.

Chapter six describes the basics of biomechanics in general and biomechanics of the hip during stance and fall in more detail.

Chapter seven starts with a historic overview of the semi-static biomechanical tests previously published. Using these examples the necessity of a new technique is demonstrated. This new technique is presented and the theories behind this design are discussed.

Chapter eight correlates measurements performed with the new technique, presented in chapter seven, with radiologic and densitometric parameters presented in chapters three through five. From this study several parameters with a predictive power emerged. The data presented in this chapter also led to the conclusion that our new design was able to generate fractures as seen in a clinical setting.

In chapter nine a semi-static loading technique, which is used in most recent publications, is used as a comparison with the new technique and to check the validity of data obtained using embalmed material. This chapter showed that the use of embalmed cadaver specimen for studies into the correlation between radiographic and densitometric parameters and biomechanical parameters is valid, although absolute biomechanical parameters differed significantly to those presented in preciously published studies.

In the final chapter of this dissertation the main findings and clinical implications are discussed and suggestions for future research are given. The main conclusion of this study supports the idea that both geometry and bone mineral density have predictive power for hip fractures.

Samenvatting

Osteoporose is de meest voorkomende afwijking aan het skelet. In 1994 werd deze ziekte door de Wereld Gezondheidsorganisatie als volgt gedefinieerd: 'Osteoporose is een ziekte die gekenmerkt wordt een lage bot massa en micro-architecturale veranderingen, leidend tot een toename in breukgevoeligheid en een daar aan gerelateerde verhoging van de kans op fracturen'. De ernstigste verschijningsvorm van osteoporose is de gebroken heup (heupfractuur), in het dagelijkse taalgebruik wordt met een heupfractuur een breuk van het bovenste deel van het bovenbeen, het proximale femur, bedoeld. Deze fractuur komt in overgrote meerderheid (>90% van alle heupfracturen) voor bij blanke vrouwen boven de 70 jaar. De gevolgen van deze fracturen zijn zeer ernstig, er is sprake van een mortaliteit (overlijden ten gevolge van de heupfractuur) in ongeveer 25% van alle patiënten en in de morbiditeit (ziekte of blijvend gebrek ten gevolge van de heupfractuur) in ongeveer 30%. Naast deze gevolgen voor de volksgezondheid is er ook een belangrijk economisch aspect. In een recent Nederlands onderzoek is berekend dat in 1993 de totale kosten voor heupfracturen, behandeling en nazorg, 362 miljoen gulden bedroegen. Met het oog op de toenemende vergrijzing is dit probleem dus in toenemende mate een zeer belangrijk en ernstig ziekte beeld. Dit maakt het noodzakelijk om in een vroeg stadium die personen, die een verhoogd risico hebben voor een heupfractuur, op te sporen. Hiervoor is het noodzakelijk dat er een beter inzicht verkregen wordt in de relatie tussen breukgevoeligheid en de radiologische en bot densitometrische (de bepaling van de hoeveelheid kalk in het skelet) parameters van de heup. Deze vraagstelling is dan ook het onderwerp van deze studie, waarin naast radiologie ook biomechanica een prominente rol speelt. Hiervoor is een in-vitro (een simulatie van de werkelijkheid) studie opgezet waarbij gebruik gemaakt wordt van gebalsemd kadaver materiaal.

In hoofdstuk 1 wordt een overzicht gegeven van de geschiedenis van en medische en socio-economische gevolgen van heupfracturen. Verder wordt een overzicht gegeven van de microscopische anatomie van bot en de macroscopische anatomie van het proximale femur. Dit inleidende hoofdstuk wordt besloten met het uiteenzetten van de doelstellingen van dit proefschrift.

Hoofdstuk 2 behandelt de classificatie van fracturen van het proximale femur en wordt de keuze voor de in deze studie toegepaste classificatie gemotiveerd.

In hoofdstuk 3 worden de metingen van de geometrie van het proximale femur besproken. Hiervoor wordt gebruik gemaakt van, met behulp van conventionele en 'direct magnification' radiografie. Enige geometrische

maten blijken namelijk uit epidemiologisch onderzoek een voorspellende waarde te hebben ten aanzien van heupfracturen.

Hoofdstuk 4 behandelt metingen met behulp van dual-energy X-ray absorptiometry (DXA). Deze techniek is momenteel de meest toegepaste techniek voor de bepaling van de bot massa.

In hoofdstuk 5 worden metingen gepresenteerd die verricht zijn met quantitative CT (QCT). Deze metingen zijn in samenwerking met de 'Osteoporosis and Arthritis Research Group' in San Francisco verwerkt. Metingen met QCT van het proximale femur zijn tot nu toe, door de ingewikkelde architectuur van het proximale femur, nog niet toepasbaar in een klinische omgeving. De hier toegepaste techniek kan echter beschouwd worden als voorstadium van een systeem dat wel klinisch inzetbaar is.

Hoofdstuk 6 behandelt basale biomechanica en meer in detail de biomechanica van de heup in stand en tijdens een val.

In hoofdstuk 7 wordt een kort historisch overzicht van biomechanische proeven op het proximale femur gegeven. Aan de hand hiervan wordt uiteengezet waarvoor het noodzakelijk is een nieuwe techniek te introduceren. Deze nieuwe techniek en de theorie achter het ontwerp worden vervolgens in detail behandeld.

Hoofdstuk 8 behandelt de correlatie van metingen verricht met de nieuwe techniek en de radiologische en densitometrische parameters gepresenteerd in hoofdstukken 3, 4 en 5. Uit dit deel van de studie komen enkele voorspellende parameters naar voren. De gegevens gepresenteerd in dit hoofdstuk leiden tot de conclusie dat ons nieuwe ontwerp in staat is om fracturen, zoals die gezien worden in de kliniek, te genereren.

In hoofdstuk 9 wordt een semi-statische belastingstechniek, vergelijkbaar met die in de meeste recente publicaties, gebruikt als een vergelijkingsmethode ten opzichte van ons nieuwe ontwerp. Tevens wordt de validiteit van het gebruik van gebalsemd kadaver materiaal getest. Uit de gegevens getoond in dit hoofdstuk kan worden geconcludeerd, dat als het doel van het onderzoek de correlatie tussen biomechanische parameters en radiologische en densitometrische parameters is, gebalsemd kadaver materiaal gebruikt kan worden.

Het afsluitende hoofdstuk bespreekt de belangrijkste bevindingen van dit onderzoek en geeft suggesties voor toekomstig onderzoek. De belangrijkste bevindingen in dit onderzoek ondersteunen de gedachte dat zowel geometrie als botdichtheid een belangrijke rol spelen in het voorspellen van heupfracturen.

Publications and presentations

Publications and presentations based on studies described in this dissertation.

Chapter 1

1. Entius CAC, van Rijn RR, Holstege JC, Stoeckart R, Zwamborn AW 1997 Correlating sheet plastinated slices, computed tomography images and magnetic resonance images of the pelvic girdle: A teaching tool. *Acta Anatomica* 158:44-7.
2. van Rijn RR, Lequin MH, van Kuijk C 1998 Botdensitometrie; een overzicht voor de medicus practicus. *Patient Care* 25(1):9-16.

Chapter 5

3. van Rijn RR, Lang TF, Niesing R, Snijders CJ, Schütte HE, van Kuijk C 1998 In vitro volumetric quantitative computed tomography of the proximal femur: helical versus sequential. 4th International Somatom plus CT scientific user conference, De Doelen, Rotterdam, the Netherlands.

Chapter 7

4. van Rijn RR, Niesing R, Mulder BN, Grashuis JL 1996 Realistic hip fracture in vitro; a different approach. *Osteoporosis Int* 6(suppl 1):145.
5. van Rijn RR, Niesing R, Mulder BN, Grashuis JL 1996 Generating in vitro fractures of the hip; a novel technique [multi-media 'World Wide Web' presentation]. 10th Conference of the European society of biomechanics, Leuven, Belgium, pp 381.

Chapter 8

6. van Rijn RR, Niesing R, Lang TF, Schütte HE, Snijders CJ, van Kuijk C 1998 In-vitro dynamic loading of the proximal femur: fracture resistance depends on bone mineral density and geometry. European congress on osteoporosis, Berlin, Germany.
7. van Rijn RR, Niesing R, Lang TF, Schütte HE, Snijders CJ, van Kuijk C 1998 In-vitro dynamic loading of the proximal femur: bone mineral density and geometry predict fracture resistance. **submitted**.

Chapter 9

8. van Rijn RR, Niesing R, van der Drift LTH, Sterk J, Schütte HE, van Kuijk C 1997 Ability of geometry to predict in vitro fracture strength of the proximal femur. *J Bone Miner Res* 12(Suppl 1):495.
9. van Rijn RR, Niesing R, Lang TF, Mulder PGM, Schütte HE, Snijders CJ, van Kuijk C 1998 Geometry and bone mineral density predict in-vitro failure loads in embalmed femora. **submitted**.

Other publications and presentations related to the field of bone densitometry:

1. Lequin MH, van Rijn RR, Robben SGF, Keinan DD, van Kuijk C 1997 Quantitative Ultrasound of the tibia: precision in a pediatric population. *Osteoporosis Int* 7(3):300.
2. Lequin MH, van Rijn RR, Robben SGF, Meradji M, van Kuijk C 1997 Validering van echografische botdensitometrie in een pediatrische populatie. *Radiologen dagen, Veldhoven, the Netherlands*.
3. Lequin MH, van Rijn RR, Robben SGF, Keinan DD, van Kuijk C 1997 Quantitative ultrasound bone densitometry of the tibia: preliminary results in a pediatric population. *Osteoporosis Int* 7(suppl 2):14.
4. Lequin MH, van Rijn RR, Robben SGF, Hop W.C.J., Dijkhuis S, Fijten MMEG, Meijer LAW, van Kuijk C 1998 Evaluation of short-term precision for tibial ultrasonometry. *Calcif Tissue Int* **In press**.
5. Lequin MH, van Rijn RR, Robben SGF, Keinan DD, van Kuijk C 1998 Pediatric ultrasound bone assessment of the tibia: normative Caucasian data European Society of Pediatric Radiology, Rhodos.
6. Lequin MH, van Rijn RR, Robben SGF, Keinan DD, van Kuijk C 1998 Quantitative ultrasound bone assessment of the tibia normative data for a pediatric, 6 to 19 years Caucasian population. *J Clin Densito* 1(1):102-3
7. van Bodegom JW, Kuiper JW, van Rijn RR, van Kuijk C, Zwamborn AW, Grashuis JL 1998 Vertebral dimensions: influence of X-ray technique and patient size on measurements. *Calcif Tissue Int* 62(3):214-8.
8. van Rijn RR, Lequin MH, van Leeuwen WJ, van Kuijk C 1998 Normal values for radiographic absorptiometry of the phalanx in Caucasian children; aged 6 to 19 years. **Submitted**.
9. Veenland JF, Link TM, van Rijn RR, Grashuis JL, Gelsema ES 1996 Reproducibility of texture features in femur radiographs Intern. Workshop trabecular bone texture analysis on radiographs, Orleans (Fr.).

Dankwoord

Toen ik vier jaar geleden begon aan mijn promotie onderzoek, wist ik nog niet wat mij precies te wachten stond en hoeveel ik wel niet aan anderen te danken zou hebben. Hierbij doel ik niet alleen op steun die direct verband houdt met het verrichten van onderzoek. Een ieder die mij kent en mijn onderzoek een beetje gevolgd heeft weet dat er, zoals bij elke onderzoeker, in de afgelopen jaren ups en downs zijn geweest. Het zijn vooral die laatste momenten, die ik voor ogen heb als ik spreek over dankbaar zijn voor hulp. Zonder alle mensen die mij geholpen, gesteund en bij tijd en wijle achter de kont hebben aangezetten was er naar alle waarschijnlijkheid nu geen boekje geweest. Hoewel ik van mening ben dat het aandeel van een ieder belangrijk is geweest wil ik toch graag van de gelegenheid gebruik maken om enige mensen speciaal te bedanken. Mocht blijken dat ik aan het eind van mijn dankwoord iemand heb overgeslagen, wijt dat dan aan mijn vergeetachtigheid er is zeker geen kwade zin mee bedoeld.

Beste Kees, cornelis.vankuijk@oarg.ucsf.edu, hoewel vele duizenden kilometers ver weg, was en ben jij dankzij e-mail, fax en telefoon die begeleider die elke AIO zichzelf toewenst. Altijd constructief en opbeurend, maar bij tijd en wijle ook zeer streng edoch rechtvaardig (O, ja? Is dat zo? poeh poeh!). Jij zorgde ervoor dat ik een klein deel van mijn onderzoek in San Francisco kon volbrengen en er zo een extra dimensie aan toevoegde. Jouw enthousiasme voor research, zowel fundamenteel (dit onderzoek) als klinisch (de 'Myriad' studie), hebben ervoor gezorgd dat deze AIO periode zeer leerzaam en vruchtbaar is geweest.

Professor Schütte, u dank ik voor uw steun gedurende mijn AIO periode en de kans die u mij gegeven heeft om via deze weg de opleiding tot radioloog te beginnen.

Professor Snijders, daar waar anderen, inclusief de promovendus zelf, bij tijd en wijlen twijfelden over het succes van dit onderzoek bleef u altijd aanstekelijk optimistisch. Als ik het even niet meer zag zitten was een gesprek bij u voldoende om weer positief tegen het onderzoek aan te kijken. Hierbij kan ook Ria niet vergeten worden die met koffie, thee en altijd een lach de besprekingen omlijstte.

Ruud Niesing, jou ben ik veel dank verschuldigd voor de vele uren die je de afgelopen jaren in mijn onderzoek hebt gestoken en het begrip dat je toonde voor mijn gebrek aan fysica kennis.

Heel veel dank ben ik verschuldigd aan de medewerkers van de afdeling experimentele radiologie. Zij zijn degene met wie ik voor kortere of langere tijd optrok en die het bestaan van een AIO veraangamen. Beste Andries, Caroline, Wibeke, Elena en Hein dank voor jullie gezelligheid en hulp in de afgelopen jaren. Ik hoop nog vaak boven te komen en in een gezellige omgeving samen te kunnen werken. Wibeke ook bedankt voor de hulp bij alle röntgenfoto's die zijn gemaakt. Andries en Teun dank ik voor al het

grafische werk 'nog even een diaatje, een poster of een tekening' dat zij in de afgelopen jaren verricht hebben.

Veel plezier heb ik ook beleefd aan de tijd die ik besteedde achter de CT's van zowel het 'Dijkzigt' als het 'Sophia'. De enthousiaste medewerking van alle laboranten is heel waardevol. Ik zal jullie in de toekomst nog regelmatig ontmoeten, en hoop dat gedurende mijn opleiding de samenwerking net zo goed blijft verlopen.

Op de afdeling anatomie zijn er twee personen die mij heel veel werk uit handen hebben genomen, Kees Entius en Jan Velkers. Veel van het, laten we eerlijk zijn, niet altijd even leuke preparateerwerk hebben zij mij uit handen genomen. Ik wil jullie hiervoor hartelijk bedanken hopelijk kan ik bij toekomstig onderzoek nog vaak bij jullie aan de deur kloppen.

Voor alle uren werk die zijn gaan zitten in het maken en modificeren van de bottenkraker en alle andere kleine klusjes die in de loop van dit onderzoek zijn voorgekomen, dank ik J. Aartsen, A. Brouwer, A. Burggraaf, G. Heuvelsland, G. Maas, B. Mulder, A. den Ouden, A. Schot en A. Vlasveld (CID) en C. Goedegebuur (BNT). J. de Vries van het CDAI dank ik voor het aanpassen van het MKR meetsysteem.

Voor mijn werkzaamheden op de afdeling werktuigbouw van de Technische Universiteit Delft wil ik graag Ir. L.T.H. v/d Drift en Ir. J. Sterk danken.

Thomas Link en de afdeling radiologie van de 'Universität Klinik Münster', bedank ik voor de hulp bij en het gebruik van de DIMA opstelling.

Voor het DXA onderzoek wil ik graag Jopie Hensen en de afdeling nucleaire geneeskunde bedanken.

General Electric Nederland, in het bijzonder dhr. P.M. van Kordelaar en dhr. J. Klement, wil ik bedanken voor het omzetten van de QCT data van OD naar DAT.

De 'Vereniging Trustfund Erasmus Universiteit Rotterdam' dank ik voor de subsidie die een stage in Amerika mogelijk maakte.

A special word of thanks goes to Tom Lang who helped with my work on the QCT data. Without his software and work, my time spent on the CT would have been in vane. I would also like to thank all of the people working at the Osteoporosis and Arthritis Research Group, for making me feel at home and for making my stays in San Francisco memorable. Prof. H.K. Genant is especially thanked for his hospitality at the department as well as at his house.

Nu is het tijd om diegene die altijd op de achtergrond zijn gebleven te danken.

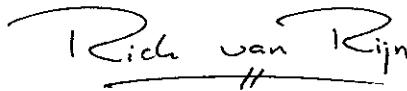
Beste Elly, Elsemiek en Annemaartje bedankt voor jullie gastvrijheid gedurende mijn verblijf in San Francisco, het was heel 'cool'.

Remco 'Bro' bedankt voor de tijd die je gestoken hebt in de lay-out van dit proefschrift. Het visuele aspect, zeker voor een radioloog in spé, is natuurlijk heel belangrijk. Ook wil ik je danken dat je mijn paranimf wilde zijn, en hiervoor speciaal naar de kapper ging.

Beste Martijn, bedankt dat ik zo vaak bij je kon klagen over hoe slecht het leven van een AIO wel niet is. Ik ben dan ook heel blij dat je mijn paranimf wilde zijn.

Beste Rosalie en Cyp om met G. Bomans te spreken 'en dan gij, dierbare familieleden, aan wie dit proefschrift is toegewijd, zou ik u vergeten? Dat nooit. Ook gij hebt, ofschoon het geen uwer helder voor den geest stond waar ik mee bezig was, uw steentje bij gedragen. De zorg, waarmee ge de uit uw midden voortgekomen promovendus hebt omringd, kan hier niet in den brede worden beschreven. Ik weet: gij zult dit werk, nu het eindelijk voltooid voor u ligt, lezen en veel zal u daarin niet duidelijk zijn. Maar weest overtuigd, dat het zonder u niet geschreven zou zijn' (Thomas Robert Spoon, werken III).

Tot slot wil ik de, voor mij, belangrijkste persoon bedanken. Lieve Melanie, jij hebt heel wat moeten verduren voor mijn promotie onderzoek. Ik zou je het liefste willen beloven dat het van nu af aan rustiger zal worden, maar met de opleiding tot radioloog en daarnaast het doen van onderzoek zal het daar wel niet echt van komen.

Rich van Rijn

